NASA-CR-190608

College of Engineering
Virginia Polytechnic Institute and State University
Blacksburg, Virginia 24061

August 1992

VPI-E-92-21
CCMS-92-24

Structural Analysis and Design of Geodesically Stiffened Composite Panels with Variable Stiffener Distribution

B. Grall[1]
Z. Gürdal[2]

Performance period:
September 1990 - May 1992

Grant NAG-1-643

Prepared for: Aircraft Structuers Branch
                   NASA Langley Research Center
                   Hampton, VA 23665-5225

---

[1] Graduate Student, Department of Engineering Science and Mechanics, Virginia Polytechnic Institute and State University

[2] Associate Professor, Department of Engineering Science and Mechanics Virginia Polytechnic Institute and State University

i

Abstract

A computationally efficient analysis is developed to predict the critical buckling loads of geodesically stiffened composite panels under in-plane loading. The analysis procedure accounts for the contribution of the in-plane extensional and out-of-plane bending stiffnesses of the stiffeners through the use of Lagrange multipliers technique in an energy method solution. The analysis is used to understand the effect of various stiffener deformation modes on the buckling load and to determine skin deformation patterns of geodesically stiffened panels under various load combinations.

The analysis routines are then coupled with the numerical optimizer ADS to create a package for the design of minimum-mass stiffened panels, subject to constraints on buckling of the panel assembly and material strength failure. Material failure in the skin and stiffeners is estimated using a maximum strain criterion. The design variables that can be used for optimization include thickness of the skin laminate, stiffener thickness and height, and positions of straight stiffeners. Applied loads are uniaxial compression, pure shear, and combined compression-shear.

Acknowledgements

Table of Contents

List of Illustrations

List of Tables

1.0 Introduction

One of the most important considerations in designing aircraft and aerospace vehicles is weight. By reducing the weight of an aircraft, it is possible to increase the flight range or increase the payload. The structural frame of an aircraft generally represents a large percentage of its weight and, therefore, it is important to choose the lightest but adequate material and structural configurations to minimize the frame weight. Imposing additional requirements such as constraints on the durability and the cost makes the design problem even more challenging.

With the introduction of high performance composite materials and advanced manufacturing processes over the past few decades, it is possible to use composite materials for light-weight primary load carrying structures such as the fuselage of an aircraft. Filament winding and tow-placement techniques now permit manufacturing of cylindrical (Figure 1) and flat (Figure 2 and Figure 3) components with complex stiffening arrangements in a short enough time to be applied in various industries cost effectively. Panels that have a grid of stiffeners with a prescribed uniform pattern, such as the geodesically stiffened panels, are promising structural components since they permit low cost fabrication through automated manufacturing techniques and have superior response characteristics under combined loadings. Moreover, by going to different stiffening arrangements, the response of these panels can be tailored to meet various design requirements.

INNOVATIVE FABRICATION CONCEPT

Built-up Structure

Integrated Structure
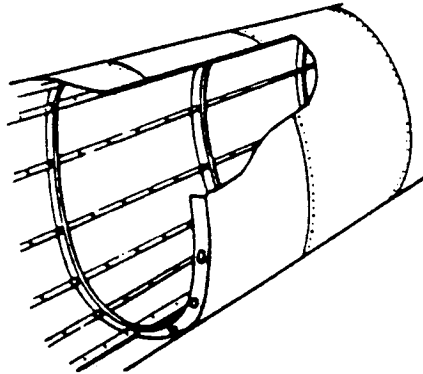
- Highly labor intensive
- Large number of parts
- Large number of fasteners
- High structural assembly costs
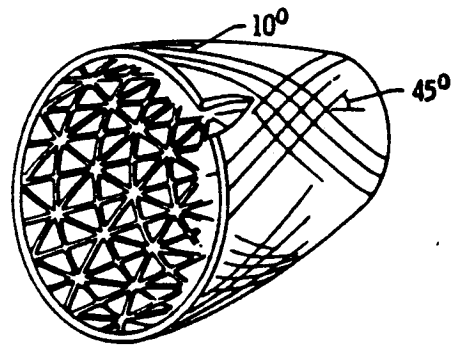
- Highly automated fabrication
- Integral stiffened cocured design
- Low cost finished structure

Figure 1. Filament wound geodesically stiffened fuselage concept: [After FREEMAN[1]]

SKIN PANEL
INTEGRALLY STIFFENED
(PULTRUSION)

INTERMEDIATE
TRUSS SPAR
(PULTRUSION)

FRONT AND REAR SPAR
FILAMENT WOUND
GEODESIC STIFFENED

ONE PIECE
SPAR ASSY
(GR/EP)
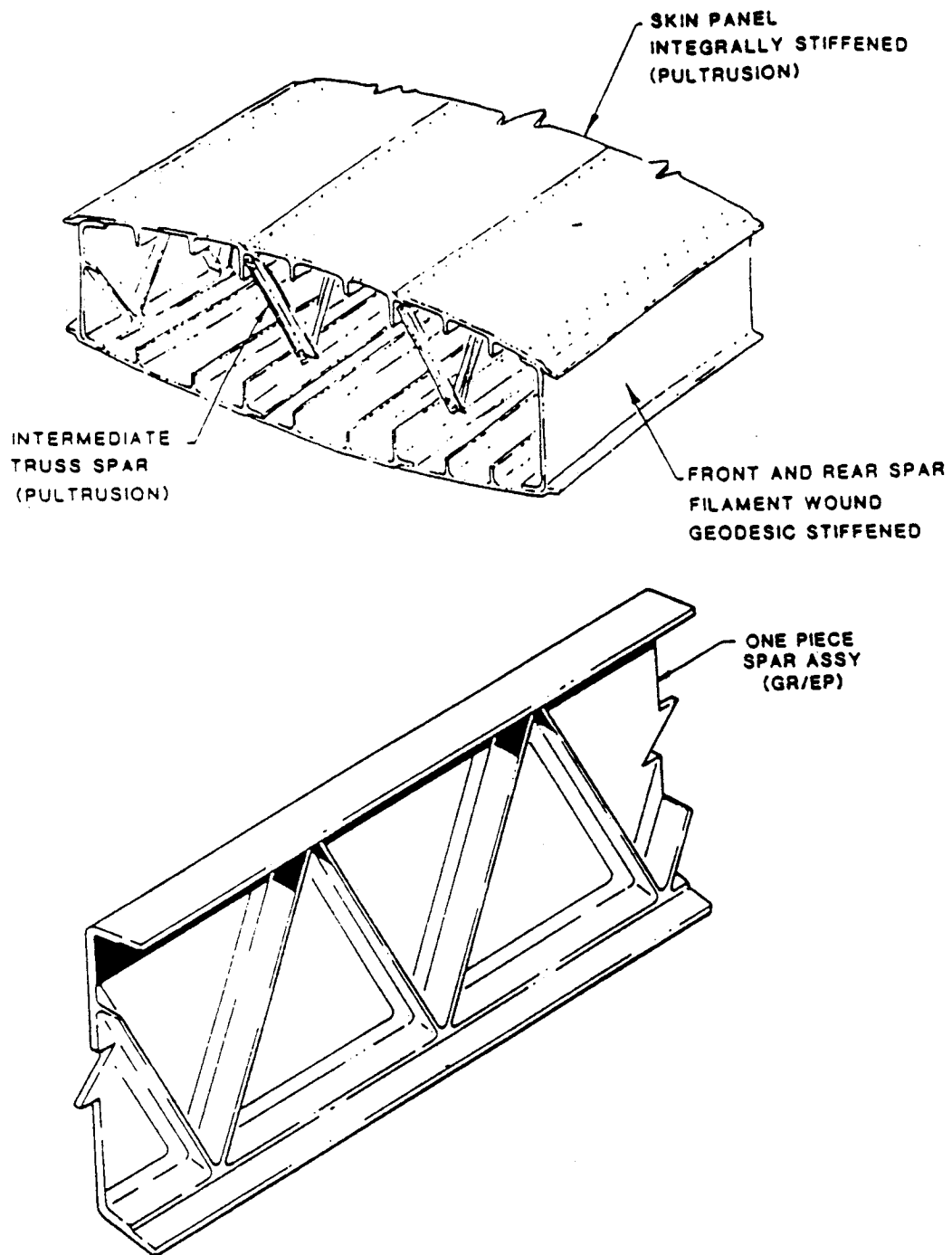
Figure 2.   Wing box assembly with geodesically stiffened spar: [After BARRIE, et al[2]]

WOVEN FIBER FORM
(1 AT EACH
INTERSECTION)

STIFFENER WRAP
(TYP)

SIDE RAIL
(REMOVEABLE)

SECTION A-A

1. INSTALL WOVEN FIBER
   FORMS AND STIFFENER
   WRAPS IN MANDREL-
   LOCATE SIDE RAIL.
2. WIND UNIDIRECTIONAL
   STIFFENERS AND CAP
   REINFORCING.
3. REMOVE SIDE RAIL.
4. FILAMENT WIND SPAR
   ASSY.

FILAMENT WINDING
MANDREL

GR/EP
TOOLING

STIFFENERS
WOUND INTO
GROOVES IN
MANDREL

SPARS WOUND
IN PAIRS

WINDING PATTERN FOR
STIFFENERS

Figure 3. Geodesically stiffened spar fabrication method: [After BARRIE, et al[2]]

A promising application of geodesically stiffened panels are the wing rib panels in large transport aircraft. There are typically a large number of such components and, therefore, the weight saving can be substantial. Wing ribs are used to separate the upper and lower skins of the wing (Figure 4). Due to aerodynamic loads, engine forces, loads due to the fuel stored in the wing, etc., the wing is subject to a complicated combination of axial, bending and twisting forces. The bending of the wing causes axial compressive loading of the rib while the twisting results in shear loading (Figure 5). Geodesically stiffened panels present some superior properties in compression and shear, and this is why they are likely to be used in this particular application.

Analysis of stiffened panels with a complex grid pattern can be quite difficult. During the optimization of such panels different computational techniques can be used for the analysis. For example, the finite element method coupled with an optimizer (see Ref. 4) is often used for the purposes of analysis. However, the use of the finite element method can become prohibitively expensive due to the large number of analyses that are needed for an optimization run. Also using the positions of the stiffeners as design variables would require expensive remeshing of the structure (at least one per call to the optimizer), and therefore, can be used only in cases for which the design cost is not a real constraint. Another alternative is to use analytical techniques, such as the energy method, coupled with an optimizer.

Application of the energy method to buckling analysis of flat unstiffened panels is commonly used for geometry and boundary conditions where the buckled shape of the panel can be approximated by a Fourier series. The values of the coefficients of the series corresponding to the actual shape are calculated by minimizing the total potential energy. In the case of panels stiffened by discrete plate-like stiffeners, a similar approach can be used. In this case, in addition to the skin deformations, the assumed form of the stiffener deformations can be expressed in Fourier series. The mode shape and the load at buckling can be determined by minimizing the total potential energy of the entire system while maintaining certain compatibility conditions between the deformation of skin and the stiffeners. Such an approach has recently been used in Ref. 5 to determine buckling loads of grid stiffened panels. In Ref. 5, the stiffeners are modeled as beams, and only the effect of

Wing

Skin

Spar

Rib
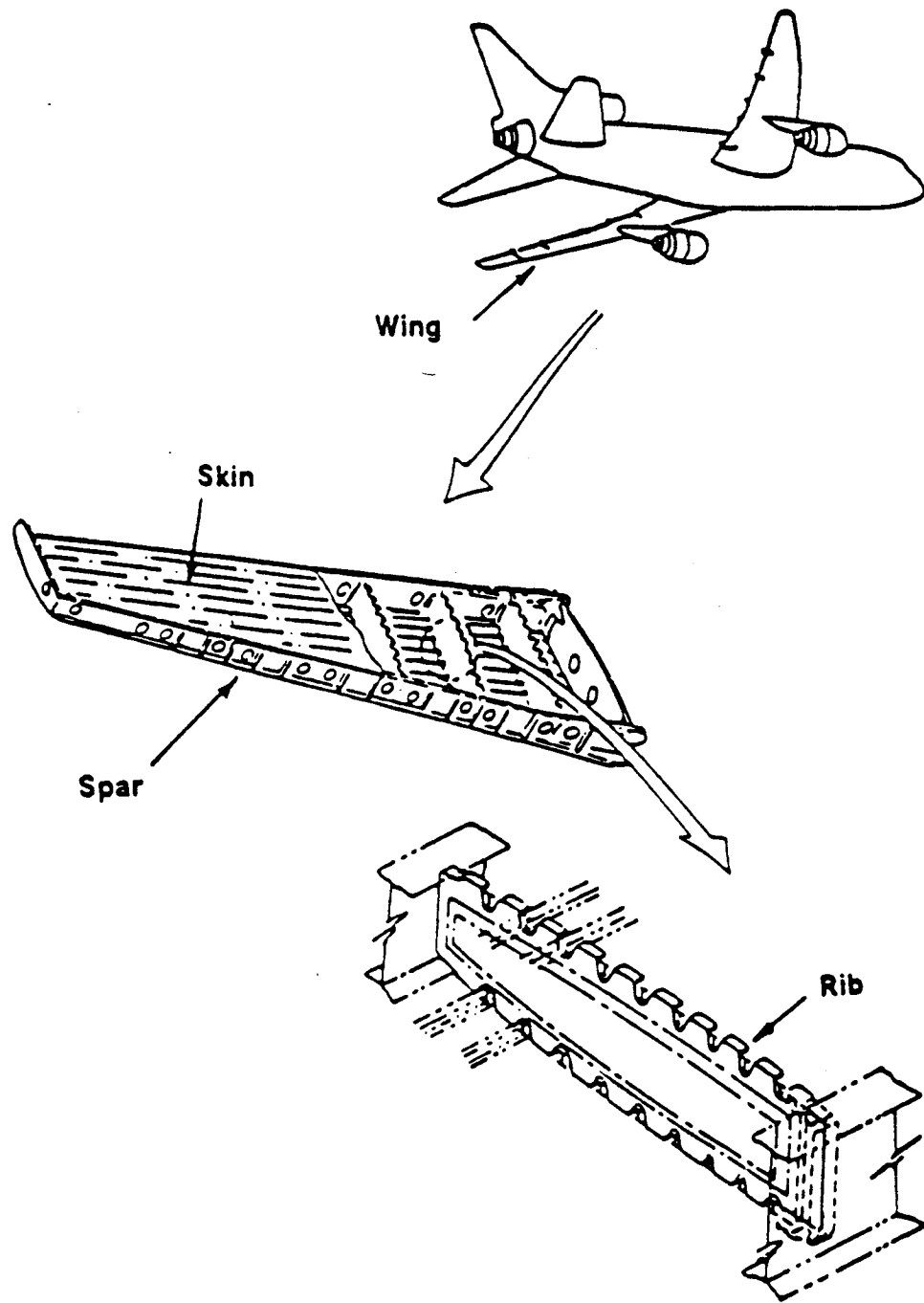
Figure 4. General wing structure diagram: [After SWANSON[3]]
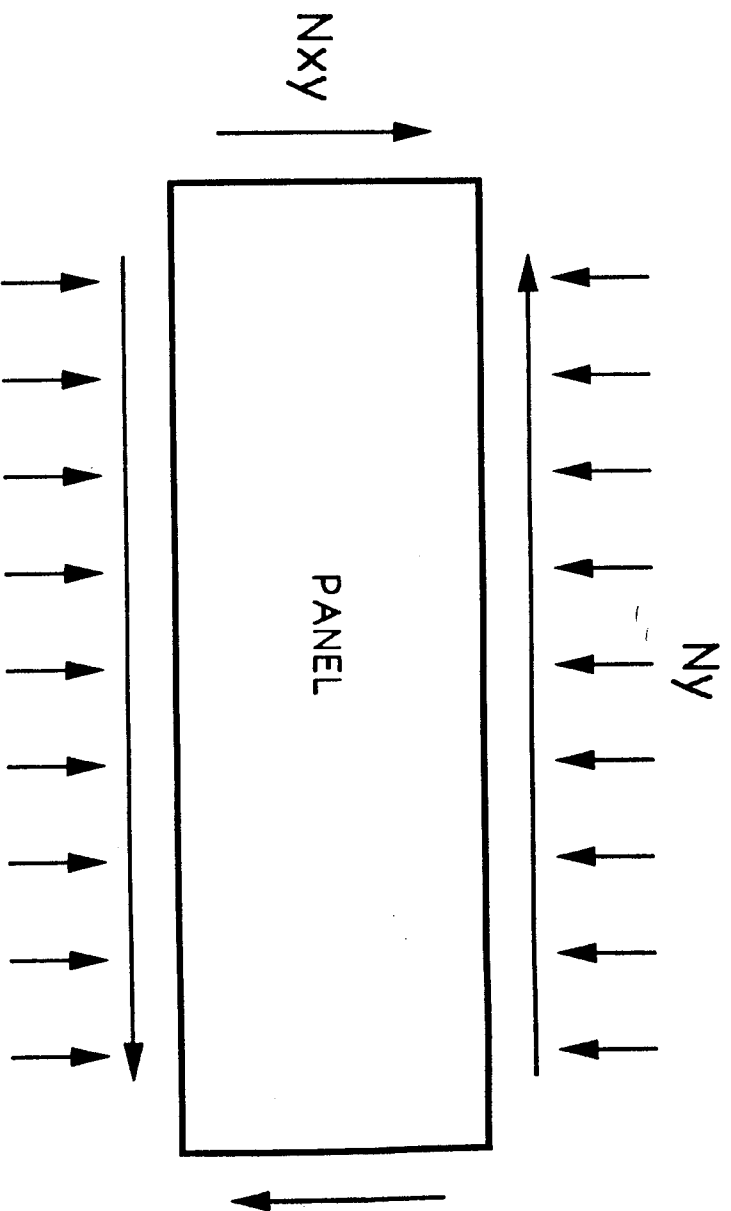
Figure 5. Loading on a wing rib

the bending stiffnesses of the stiffeners in the direction perpendicular to the skin is considered. Continuity of the skin and the stiffener deformations at selected locations along the length of the stiffeners are then imposed via the Lagrange Multiplier technique.

The objectives of the present work are twofold. First, an improvement in the analysis procedure described in Ref. 5 is sought by assuming the stiffeners to be modeled as plate elements and by including the out-of-plane deformation of the stiffeners as a new degree of freedom. This additional degree of freedom requires that the continuity of the rotations between the skin and the stiffeners at the base of the stiffeners be maintained during the analysis procedure. The second objective of the present work is to expand the design configurations studied earlier by allowing the stiffener locations to be design variables, such that a more optimal configurations under various loadings can be obtained.

2.0   Design Problem Formulation

The purpose of this section is to present the wing rib geometry and to state all the assumptions and restrictions about the panel.

In section 2.1 the geometry of the ribs is introduced, and the material for the skin and the stiffeners is specified. In section 2.2 the design variables that will be used for the analysis and the optimization are presented. Finally, in section 2.3 a brief introduction of the analysis/optimization tool is given.

2.1 Geodesically Stiffened Wing Rib Panels

2.1.1 A global view of the panels

The rib is modeled as a rectangular panel 80 inches wide in the wing chord direction and 28 inches high in the wing thickness direction. The panel incorporates a skin and a grid of stiffeners placed symmetrically on both sides of the skin.

There are three kinds of stiffening arrangements: a panel can be longitudinally stiffened, diagonally stiffened, or cross stiffened (Figure 6). To simplify the description of these stiffening arrangements, the concept of cells is introduced (Figure 7).

The skin is symmetrically laminated, balanced, and is made of AS4/3502 Graphite-Epoxy with typical properties given in Table 1.

Table 1. AS4/3502 Graphite-Epoxy Material Properties

Elastic Properties:

Longitudinal Modulus	$E_1 = 18.5 \times 10^6$ lbf/in^2
Transverse Modulus	$E_2 = 1.64 \times 10^6$ lbf/in^2
In-Plane Shear Modulus	$G_{12} = 0.87 \times 10^6$ lbf/in^2
Transverse Shear Modulus	$G_{23} = 0.54 \times 10^6$ lbf/in^2
In-Plane Poisson's Ratio	$\nu_{12} = 0.30$

Strength Properties:

Longitudinal Tensile Strain Allowable	$\varepsilon_1^t = 0.0090$
Longitudinal Compressive Strain Allowable	$\varepsilon_1^c = 0.0080$
Transverse Tensile Strain Allowable	$\varepsilon_2^t = 0.0055$
Transverse Compressive Strain Allowable	$\varepsilon_2^c = 0.0290$
Shear Strain Allowable	$\gamma_{12} = 0.0250$

Physical Properties:

Mass Density	$\rho = 0.057$ lbm/in^3
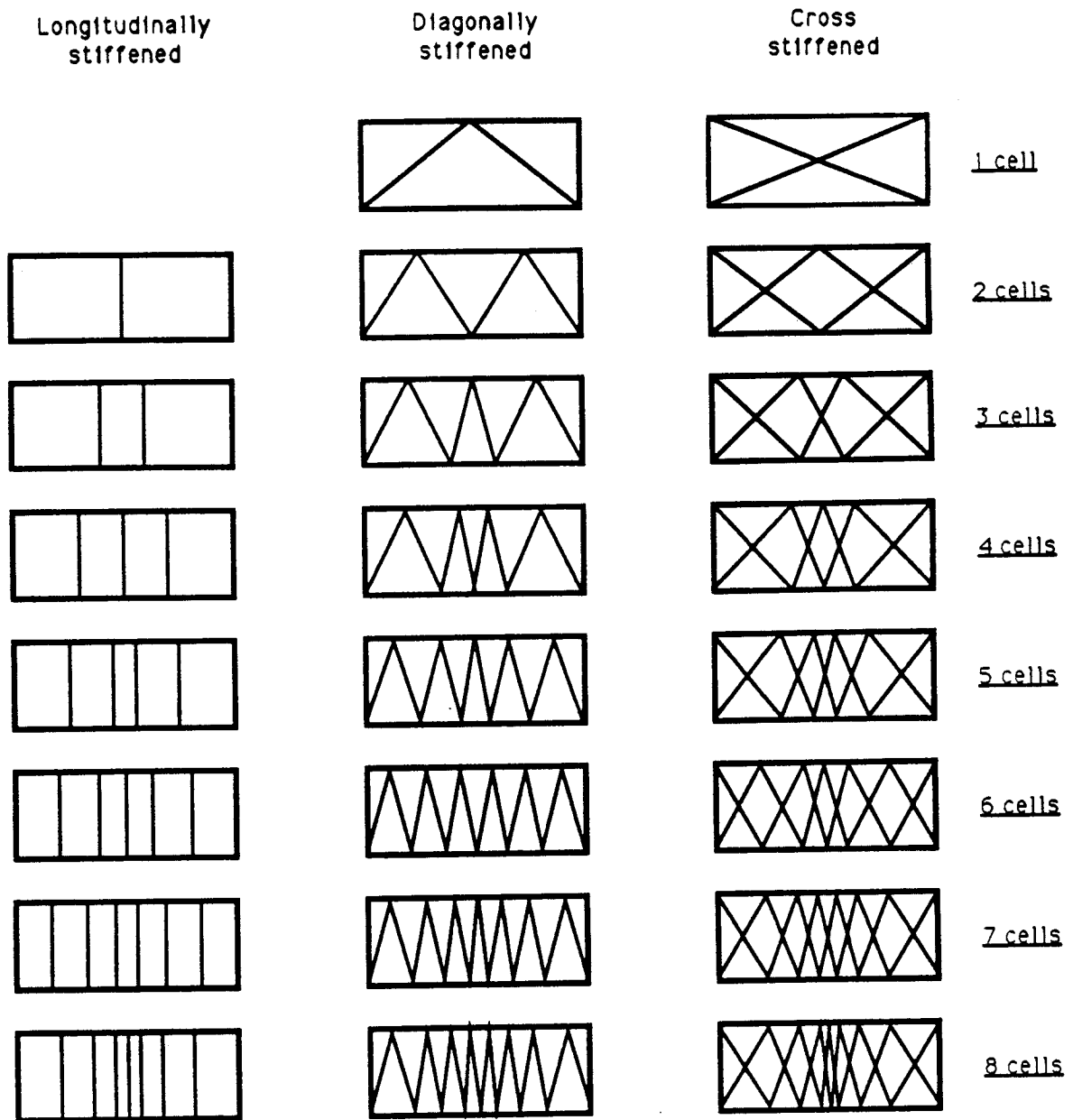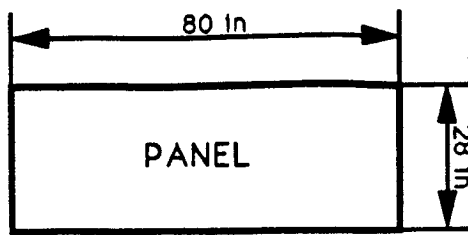
Figure 6. Panel configurations

Longitudinally stiffened cell   Diagonally stiffened cell   cross stiffened cell

The three basic cells

cell #1   cell #2   cell #3   cell #4   cell #5   cell #6
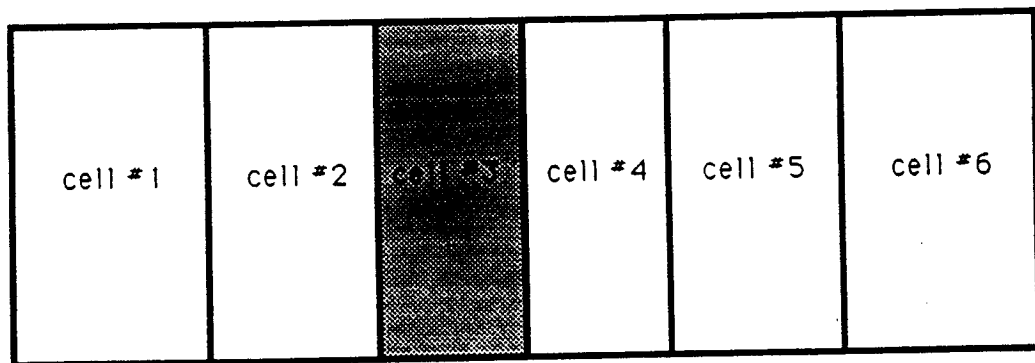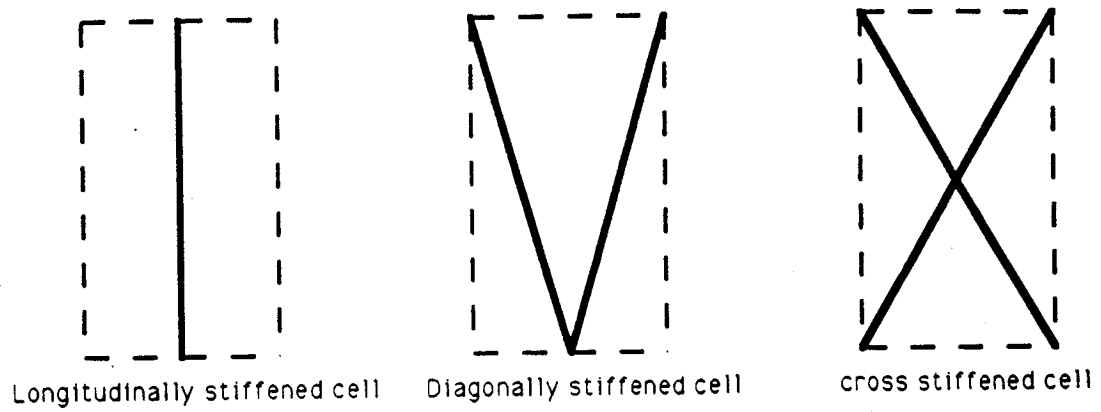
Figure 7. The cells

The stiffeners are located on both sides of the skin, symmetrical about the midplane of the skin laminate and are made of unidirectional AS4/3502 Graphite-Epoxy or are symmetrically laminated and balanced (Figure 8). Oblique stiffeners occur by pairs oriented at equal but opposite angles with respect to the panel axis.

2.1.2 Assumptions for the panel configuration

In this sub-section, the assumptions used for the panel configuration are explained.

First, both the skin and the grid of stiffeners are set to be symmetric about the midplane of the skin. In order to justify such a choice, the following facts are recalled:

1. A symmetrically laminated plate does not exhibit bending-extension coupling.

2. Moreover, by placing the stiffeners symmetrically on both sides of the skin, the panel bending-extension coupling is eliminated.

3. A linear prebuckling equilibrium state is more realistic in the absence of bending-extension coupling.

4. Only out-of-plane displacements participate in the buckling mode if the stiffened panel remains in-plane during stable equilibrium.

Thus, for a symmetric panel the in-plane and out-of-plane deformations will be uncoupled so that its buckling can be studied by considering the out-of-plane deflection w only. Moreover, based on these assumptions the linear theory can be used to determine the internal load distribution in the skin.

Secondly, the skin layup is balanced and oblique stiffeners occur in pairs oriented at equal but opposite angles with respect to the skin axis. This construction avoids the in-plane extension-shear coupling, which may not be desirable in the case of wing ribs.

Symmetric, balanced laminated Skin

Symmetric, balanced laminated Stiffener
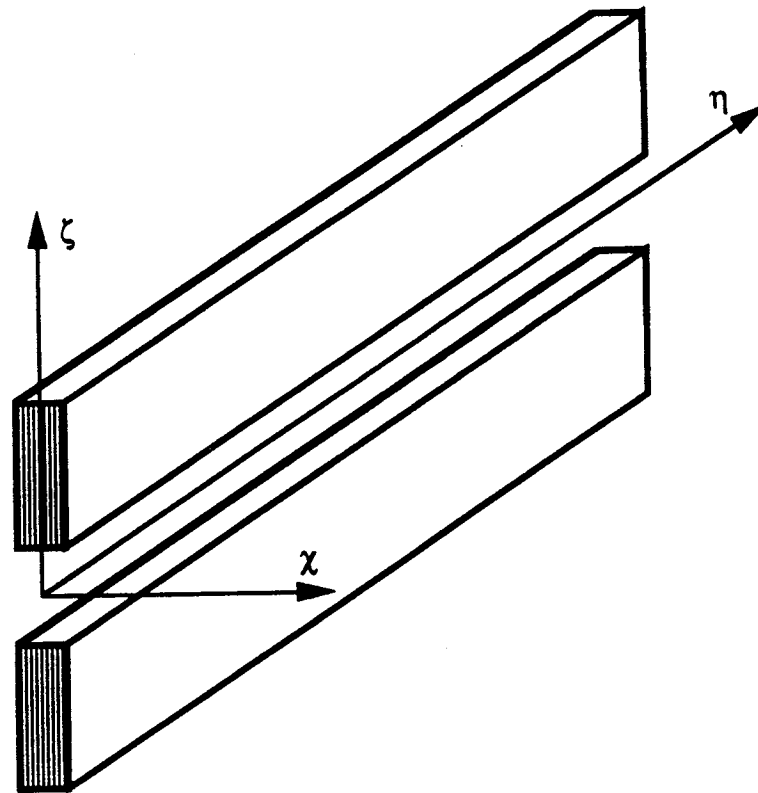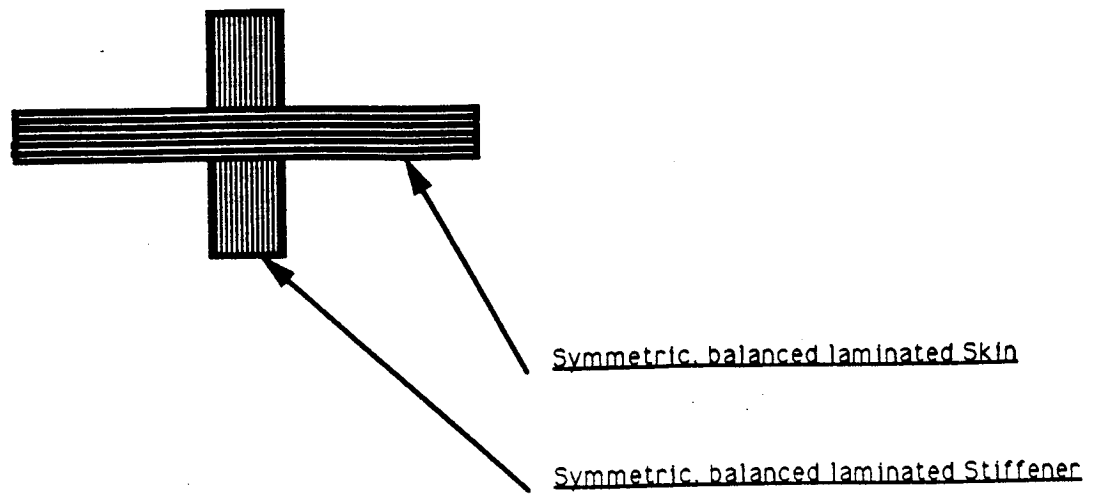
Figure 8. The stiffener

Thirdly, the stiffeners are symmetrically laminated and balanced respectively to avoid bending-extension coupling ($B_{ij} = 0$) and in-plane extension in-plane shear coupling ($A_{16} = A_{26} = 0$).

Fourthly, like in the previous study[5], the effect of bending-twisting coupling terms D_{16}, D_{26} is ignored for both the skin and the stiffeners; this simplifies the analysis. However, it is well known that the presence of these terms can account for a considerable drop in the buckling load and sensitivity to the direction of applied shear load. For this reason this analysis is used for specially orthotropic laminates for which $D_{16} = D_{26} = 0$.

Finally, it is assumed that when the panel is loaded by uniform end shortening the spars are rigid enough to restrain the panel deformation to zero ($\varepsilon_x = 0$, $N_x \neq 0$).

2.2 Design Variables And Constraints

2.2.1 Design variables

The design variables are the parameters that will be changed to optimize the panel. During this study, the design variables are taken to be the stiffener height and thickness, the skin thickness, and the cell distribution. The number of additional variables needed to define the cell distribution depends on the number of cells and is equal to the number of independent cell widths that are needed to fully define the symmetric cell distribution (it is the number of degrees of freedom of the cell distribution). Figure 9 shows the cells for which the width is a design variable. These cells are shaded in the figure. The following table (Table 2) gives the number of additional variables needed to take into account the cell distribution during the design. For example, a seven cell panel requires three new design variables.
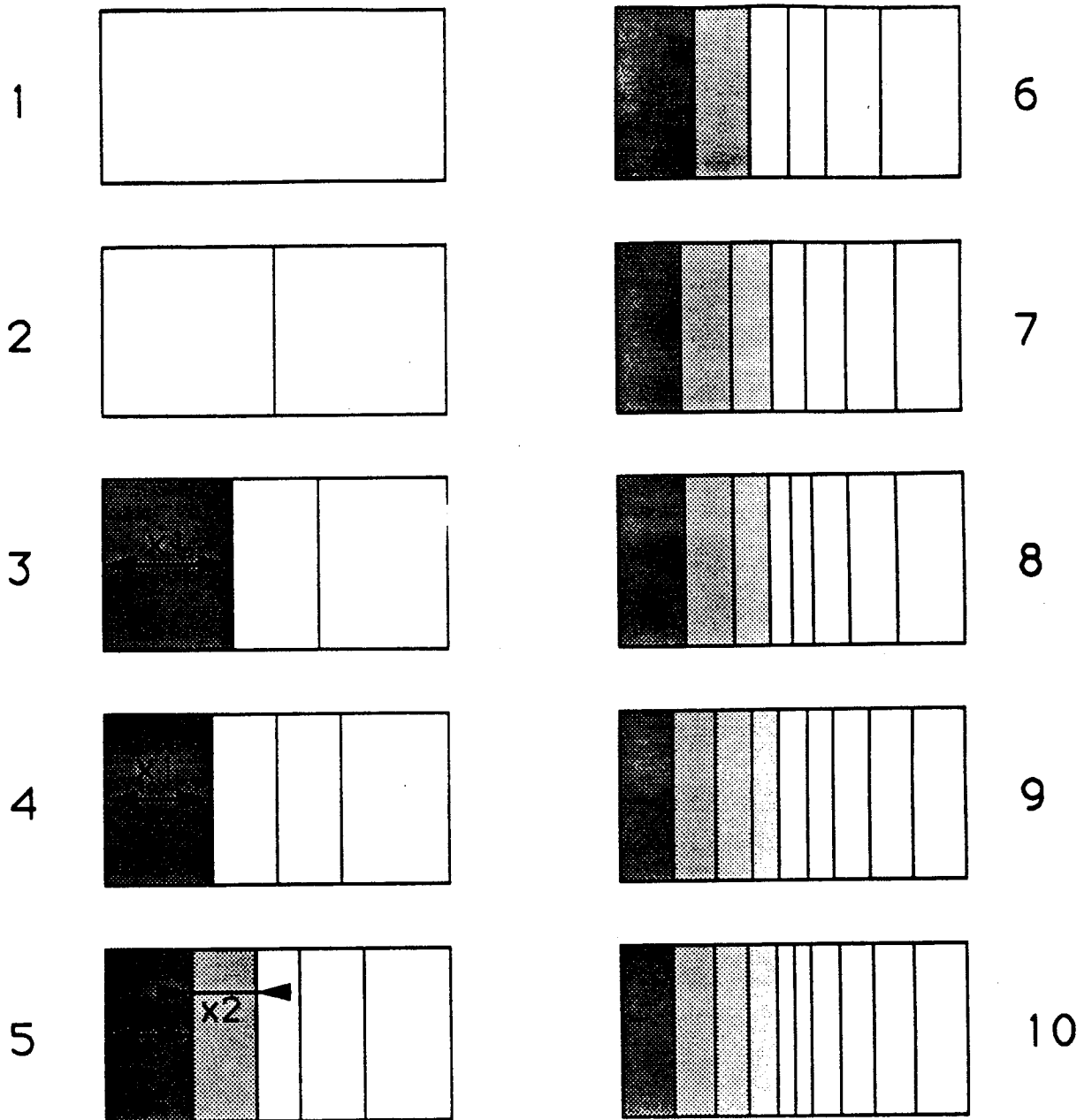
Figure 9.   The cells for which the width is a new design variable

Table 2. Number of additional design variables

Number of cells	Number of new variables
1	0
2	0
3	1
4	1
5	2
6	2
7	3
8	3
9	4
10	4

2.2.2 Constraints.

The constraints that are used for this study include

1. The panel buckling constraint,

2. Material failure constraint,

3. In case of cell-width design variables constraints for linking the design variables.

In the analysis conducted by Phillips[5], the buckling of the skin and the buckling of the stiffeners in their own out-of-plane direction were studied separately. As will be presented in the next chapter, one of the major improvements of this study over the one presented in Ref. 5 is the removal of the separate panel and stiffener buckling analysis used by Phillips. Because equations governing the buckling of the panel are modified to include the stiffeners as plate elements, the panel buckling

constraint can include both the skin and stiffener buckling together as an assemblage.

2.3 Overview Of The Analysis/Optimization

A computerized code can be used for the preliminary design of grid stiffened flat panels. The computer code developed in this work has two main parts: the optimizer and the analysis. The optimizer and analysis are called by the main program in an iterative procedure.

1. The optimizer decides how to change the design variables based on the constraints, the objective function value, and their derivatives with respect to the design variables.

2. The analysis then uses the design variables to evaluate the new constraints and the new objective function (e.g., the panel weight).

This procedure, as represented in Figure 10, is repeated until a design is reached for which the objective function is minimized and all the constraints are satisfied.

As was mentioned in the introduction, the analysis could be done with a finite element code, but it would be computationally too expensive. Thus, instead of using the Finite Element Method a method that involves both the Energy Method and the Lagrange Multiplier Technique is used.

2.3.1 The optimizer

The optimization code ADS[6] is used as a "black box" to which the analysis subroutine gives the constraints and objective function values, and from which the modified values of the design variables are obtained.
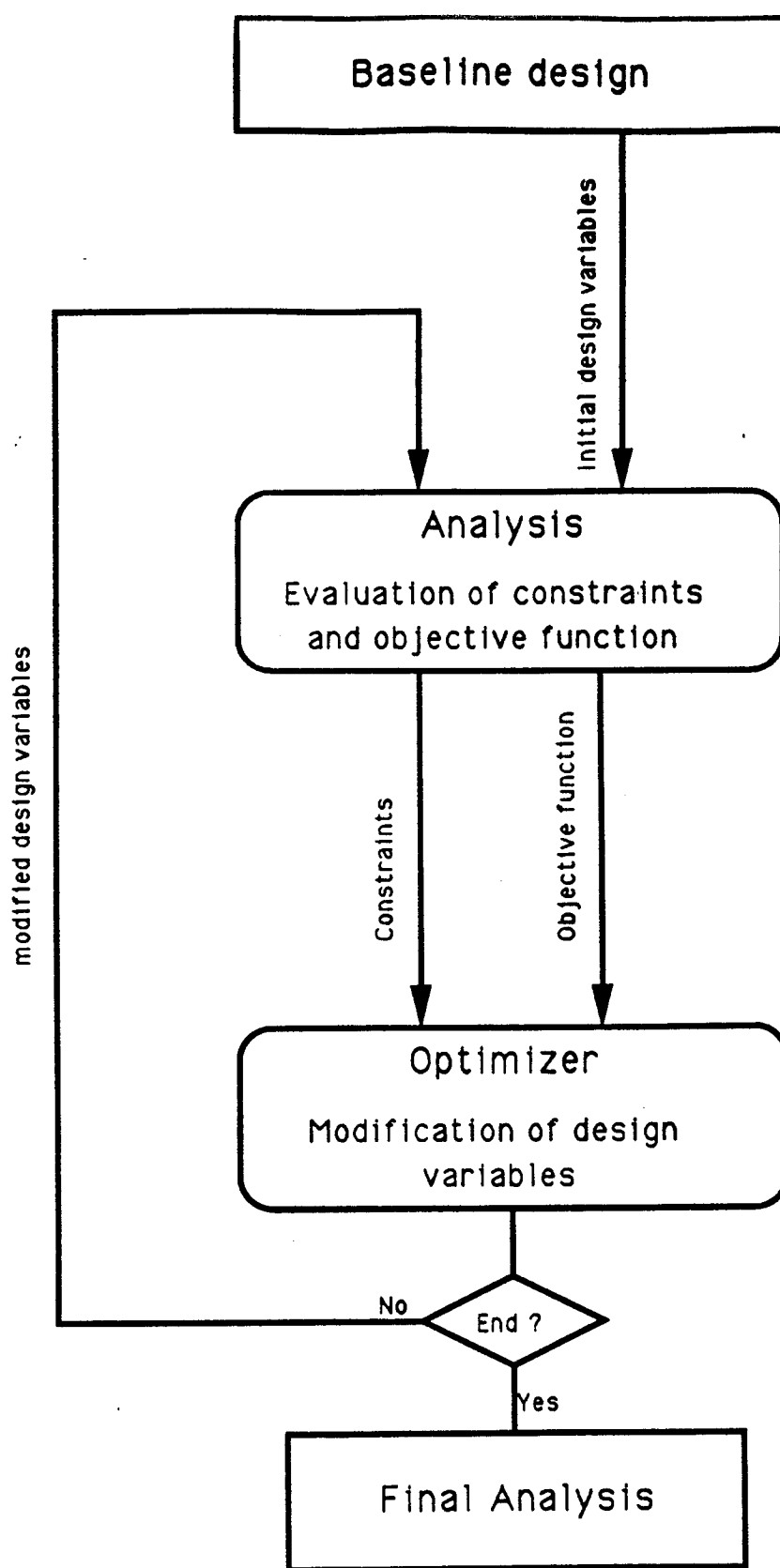
Figure 10. The optimization scenario

ADS is a Fortran optimization program for solution of nonlinear constrained problems. It is designed to be used as a subroutine in a Fortran code. ADS offers many selections for the strategy, the optimizer, and the one-dimensional search used in optimization. Selection of these options depends upon the problem to be solved. The ADS manual suggests the following combination of options for problems with mildly nonlinear objective function and constraints, and problems in which only a few constraints are active. Based on the previous authors (Ref. 5) experience, the present problem fits into this description, and the following options are employed:

1. The strategy can be either Sequential Convex Programming or Sequential quadratic programming.

2. The optimizer is the modified method of feasible directions for constrained minimization.

3. The appropriate one-dimensional search is such that the minimum of a constrained function is found by first finding the bounds and then by using a polynomial interpolation.

2.3.2   The analysis

The energy method is used to find the total potential energy of the panel for displacements of the skin or the stiffeners expressed in terms of Fourier series. Then, with the use of Lagrange multipliers, this energy is minimized subject to the constraints that enforce the compatibility of the skin and stiffener deformations. As will be shown, a generalized discrete eigenvalue problem is obtained. The smallest eigenvalue of this problem corresponds to the critical buckling load of the panel, and its corresponding eigenvector corresponds to the buckling mode shape.

3.0 Analysis Development

The method used to analyze grid stiffened flat panels under in-plane loading is described in this chapter. In the first section, the assumptions corresponding to this analysis are stated. In section 3.2 the load distribution analysis is established. Then, in the section 3.3 the stability equations of the panel are derived.

3.1 Fundamental Assumptions For The Analysis

The first assumption of this analysis is that the panel deformations prior to buckling are small enough to allow the application of the principle of superposition of displacements under the action of multiple external loads.

Secondly, an appropriate prebuckling equilibrium analysis is employed to estimate the load distribution in the elements of the wing ribs.. Interaction of the prebuckling deformations of the skin and the stiffeners are ignored.

Micro-mechanic complications at the stiffener intersection points, stress concentration in the corners between the skin and the stiffener and imperfections due to the manufacturing related issues, such as resin rich and resin starved regions resulting from filament winding, are ignored. Briefly, the wing rib is composed of perfectly uniform plates connected to each other. The load is assumed to be uniform in the skin and the stiffeners, and unidirectional in the stiffeners.

Thirdly, it is assumed that the plates are thin enough to neglect transverse shear effects and to apply the classical lamination theory for both the skin and the stiffeners.

Finally, the panel is loaded by uniform end shortening and it is assumed that the panel strains are spatially uniform. Moreover the spars are supposed to be rigid enough to ensure $\varepsilon_x = 0$ (X is the long axis of the panel). In the case of shear, the strains ε_x and ε_y are set to zero and loading is introduced through uniform shear strain γ_{xy}.

3.2 Load Distribution Analysis In Prebuckling

This part of the analysis is divided into three steps. First, the panel strain vector is computed. Then, using the constitutive equations the loads carried by the skin and the stiffening cells are derived. Finally, using adequate geometry transformations, the longitudinal load in each stiffener is computed.

Since the cell distribution is not uniform and the panel is loaded by uniform end shortening, the applied load is not uniform along the long edges of the panel. For this reason, the panel average compressive (or shear) stress resultant is defined as the ratio of the total compressive (or shear) load over the width of the panel.

3.2.1 Panel strains

The total applied compressive load P and the shear load S are distributed among the skin and the different cells by assuming uniform end shortening of the panel.

For longitudinally stiffened panels the panel strains are the same independent of the cell distribution. Therefore, the load distribution for a longitudinally stiffened panel is obtained using the previous analysis[5] developed for uniform cell distribution. For diagonally stiffened and cross-stiffened panels with non-uniform cell distribution some changes have to be made.

3.2.1.1 Skin constitutive equations

The constitutive equations of a general laminate is

$$
\left\{ \begin{matrix} N^s \\ M^s \end{matrix} \right\} = \left[\begin{matrix} A^s & B^s \\ B^s & D^s \end{matrix} \right] \left\{ \begin{matrix} \varepsilon \\ \kappa \end{matrix} \right\} \; , \tag{1}
$$

where $\{N^s\}$ is the vector of in-plane stress resultants, $\{M^s\}$ is the vector of moment resultants, $\{\varepsilon\}$ is the vector of midplane in-plane strains, $\{\kappa\}$ is the vector of curvatures, and the superscript s stands for skin (the skin of the stiffened panel). Since the skin laminate is assumed to be symmetric, there is no coupling between in-plane extension and out-of-plane bending. Therefore, the constitutive equations corresponding to the in-plane stress resultants and strains are written as

$$
\left\{ \begin{matrix} N_x{}^s \\ N_y{}^s \\ N_{xy}{}^s \end{matrix} \right\} = \left[\begin{matrix} A_{11}^s & A_{12}^s & A_{16}^s \\ A_{12}^s & A_{22}^s & A_{26}^s \\ A_{16}^s & A_{26}^s & A_{66}^s \end{matrix} \right] \left\{ \begin{matrix} \varepsilon_x \\ \varepsilon_y \\ \gamma_{xy} \end{matrix} \right\} \; . \tag{2}
$$

Moreover, the skin laminate is assumed to be a balanced laminate. As a result, the constitutive equations can be simplified further:

$$\left\{ \begin{array}{c} N_x^s \\ N_y^s \\ N_{xy}^s \end{array} \right\} = \left[\begin{array}{ccc} A_{11}^s & A_{12}^s & 0 \\ A_{12}^s & A_{22}^s & 0 \\ 0 & 0 & A_{66}^s \end{array} \right] \left\{ \begin{array}{c} \varepsilon_x \\ \varepsilon_y \\ \gamma_{xy} \end{array} \right\} . \tag{3}$$

3.2.1.2 Stiffening cell constitutive equations

The constitutive equations of a regular grid of stiffening arrangement were derived by Phillips and Gurdal[5]. For a cross-stiffened panel or a diagonally stiffened panel the constitutive equations of a stiffening cell are given by

$$\left\{ \begin{array}{c} N_x^r \\ N_y^r \\ N_{xy}^r \end{array} \right\} = \left[\begin{array}{ccc} A_{11}^r & A_{12}^r & 0 \\ A_{21}^r & A_{22}^r & 0 \\ 0 & 0 & A_{66}^r \end{array} \right] \left\{ \begin{array}{c} \varepsilon_x \\ \varepsilon_y \\ \gamma_{xy} \end{array} \right\} , \tag{4}$$

where the superscript r stands for stiffening arrangement and the A^r terms are given by

$$\begin{aligned} A_{11}^r &= \frac{2AE_\ell}{b} c^3 & A_{12}^r &= \frac{2AE_\ell}{b} cs^2 \\ A_{21}^r &= \frac{2AE_\ell}{L} sc^2 & A_{22}^r &= \frac{2AE_\ell}{L} s^3 \\ A_{66}^r &= \frac{2AE_\ell}{b} cs^2 \end{aligned} \tag{5}$$

with

E_ℓ : axial elastic modulus of the stiffeners

A : cross sectional area of the stiffeners

L : cell width

b : panel height

ϕ : $arctan\left(\dfrac{b}{L}\right)$

Analysis Development

$$c = \cos \phi$$

$$s = \sin \phi$$

In the case of laminated stiffeners, AE_r is replaced by $A_{11}^{rib} H^{rib}$ where A_{11}^{rib} is the in-plane stiffness of the laminate along the η axis of the rib (Figure 11), and H^{rib} is the stiffener height.

These constitutive equations change from one cell to another and will only be used to compute the load carried by a single stiffening cell. The in-plane force resultants for the skin and the cells are presented in Figure 12.

The load carried by the stiffening cell (see Figure 13) is given by

$$
\begin{aligned}
F_x^r &= N_{xi}^r b \\
F_y^r &= N_{yi}^r L \\
F_{xy}^{r\,h} &= N_{xyi}^r L \\
F_{xy}^{r\,v} &= N_{xyi}^r b
\end{aligned}
\tag{6}
$$

3.2.1.3 Global strains

First, only the compressive load P is considered. This load is carried by the stiffening cells and the skin. Since $\varepsilon_x = 0$, the constitutive equations yield

$$
P = (A_{22}^s a + \sum_{i=1}^{nc} A_{22i}^r L_i) \varepsilon_y^P ,
\tag{7}
$$

or
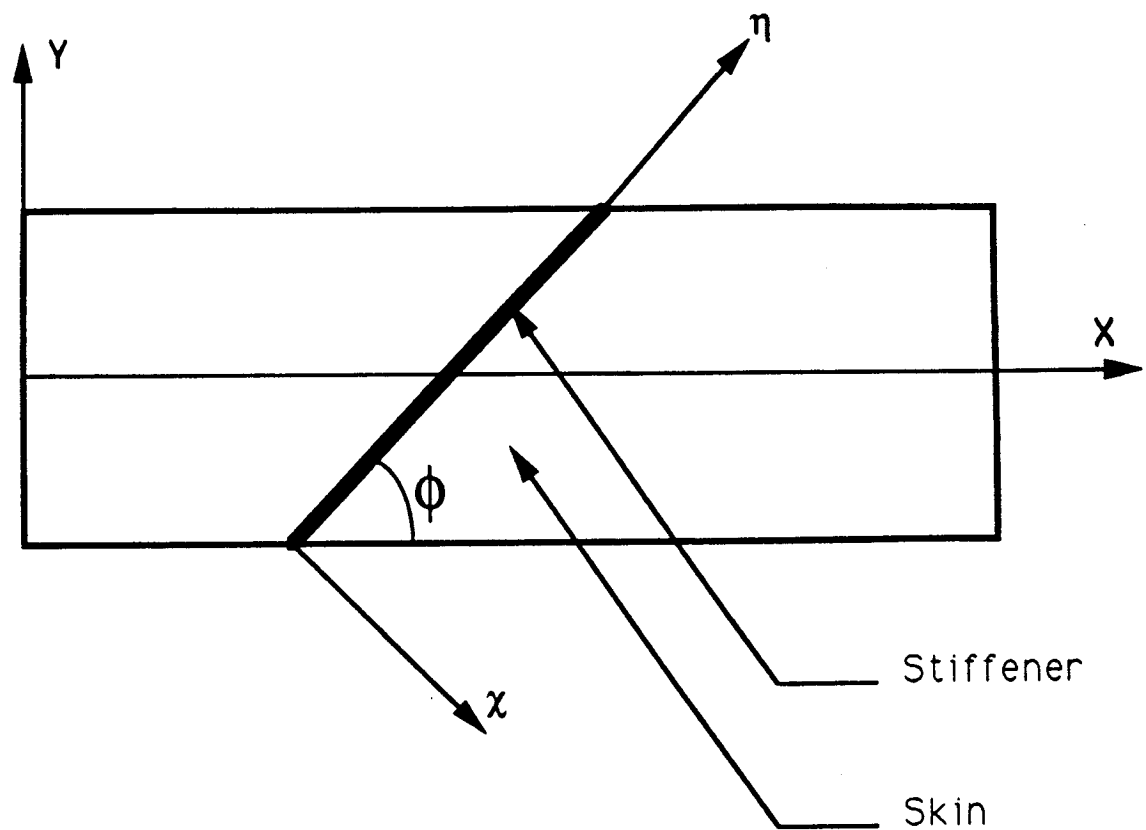
Figure 11. The axis of the stiffener
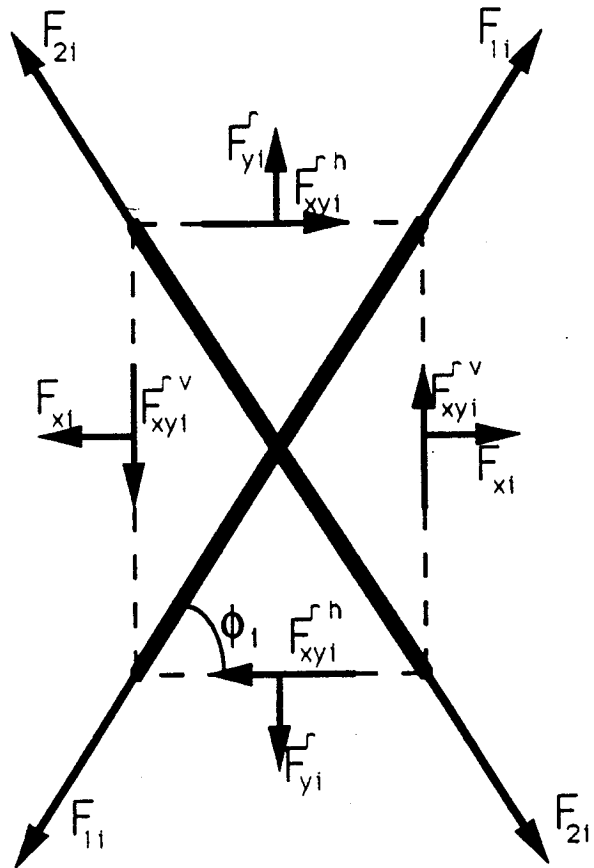
Figure 12. In-plane force resultants for the skin and the stiffeners
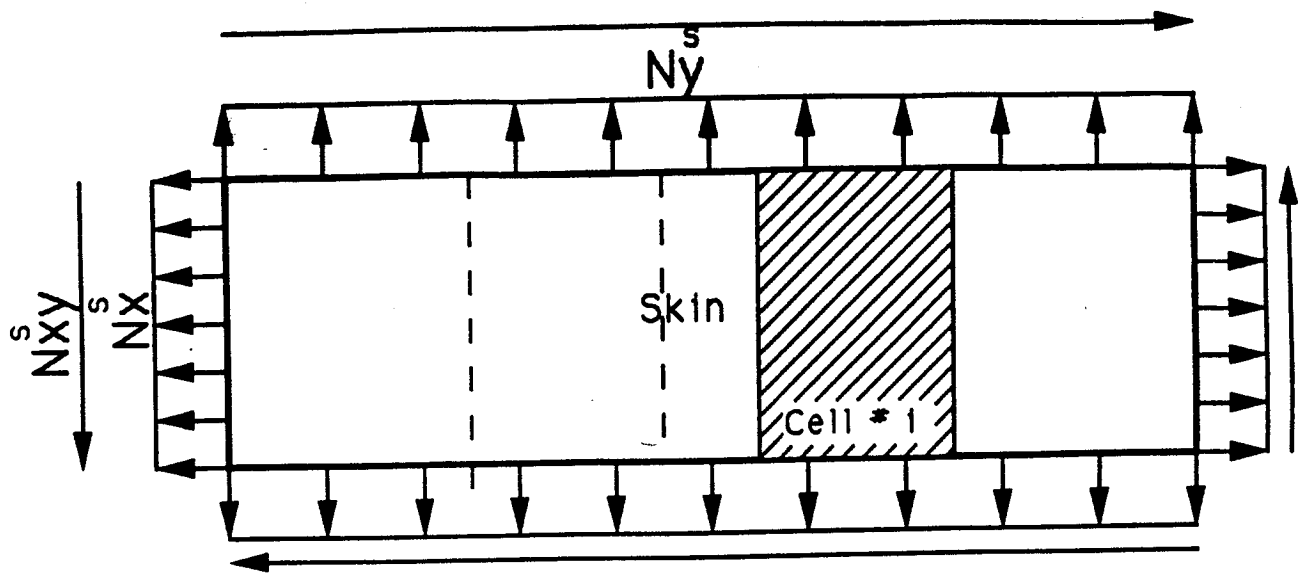
Skin loading
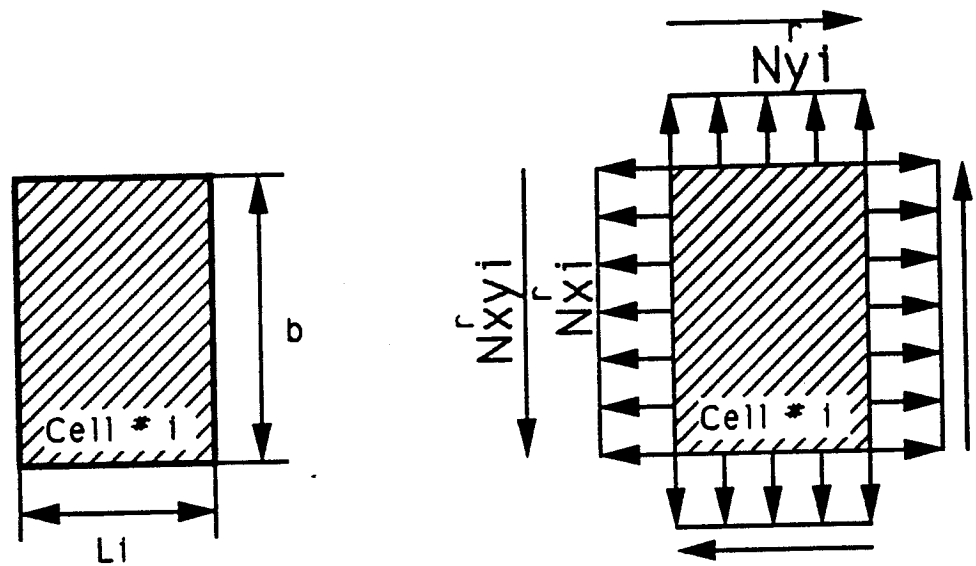
Stiffening cell loading

Figure 13. The cell loading

$$\varepsilon_y^P = \frac{P}{A_{22}^s\, a + \sum_{i=1}^{nc} A_{22i}^r\, l_i} \quad , \tag{8}$$

where the index i stands for the stiffened cell number, l_i is the width of the cell number i, a is the panel width, ε_y^P is the panel strain due to the compressive load P, and nc is the number of cells.

Now, only the shear load is taken into account. Using a methodology similar to compression loading analysis yields a shear strain

$$\gamma_{xy}^S = \frac{S}{A_{66}^s\, a + \sum_{i=1}^{nc} A_{66i}^r\, l_i} \quad , \tag{9}$$

where S corresponds to the total shear load.

3.2.2 Load distribution

Using the principle of superposition, when both compressive and shear loading are applied to the panel, the strains are given by

$$\varepsilon_x = 0 \qquad \varepsilon_y = \varepsilon_y^P \qquad \gamma_{xy} = \gamma_{xy}^S \quad . \tag{10}$$

and the stress resultant vector in the skin can now be obtained from the skin constitutive equations

$$\left\{ \begin{array}{c} N_x^s \\ N_y^s \\ N_{xy}^s \end{array} \right\} = \left\{ \begin{array}{c} A_{12}^s\, \varepsilon_y^P \\ A_{22}^s\, \varepsilon_y^P \\ A_{66}^s\, \gamma_{xy}^S \end{array} \right\} \quad . \tag{11}$$

This stress resultant vector in the skin is uniform.

The load carried by the ith cell is obtained from the stiffened cell constitutive equation and equation (6) as

$$
\begin{matrix}
F^r_{xi} & A^r_{12i}\, b\, \varepsilon^P_y \\[4pt]
\left\{ \begin{array}{c} F^r_{yi} \\ F^{r\,h}_{xyi} \end{array} \right\} = \left\{ \begin{array}{c} A^r_{22i}\, l_{\cdot i}\, \varepsilon^P_y \\ A^r_{66i}\, l_{\cdot i}\, \gamma^S_{xy} \end{array} \right\} \\[10pt]
F^{r\,v}_{xyi} & A^r_{66i}\, b\, \gamma^S_{xy}
\end{matrix}
\qquad (12)
$$

Using the same geometric transformations defined in Ref. 5, the longitudinal load carried by the two stiffeners in the ith cell is given by

$$
F_{1i} = \frac{F^r_{yi}}{2\,\sin\phi_i} + \frac{F^{r\,h}_{xyi}}{2\,\cos\phi_i} \qquad\qquad F_{2i} = \frac{F^r_{yi}}{2\,\sin\phi_i} - \frac{F^{r\,h}_{xyi}}{2\,\cos\phi_i} \qquad (13)
$$

3.3 Instability Analysis Of Geodesically Stiffened Panels

In this section, the buckling analysis of grid stiffened flat panels is established.

The two main modes of failure of a geodesically stiffened panel are a material strength failure and buckling. In order to design an optimum wing rib, these two modes have to be studied. The material failure analysis of the panel is done by the systematic application of a maximum strain criterion to the skin and the stiffeners, for any panel configuration. The remaining mode is due to an instability of the panel under external loads. Once the critical loading is reached the effect is buckling failure of the panel.

In this part, an analysis tool is developed to determine the critical loads of geodesically stiffened panels. For this purpose the Rayleigh-Ritz method is coupled with the Lagrange multiplier technique to obtain a constrained system on which a stability analysis is performed.

3.3.1 The Rayleigh-Ritz method

The Rayleigh-Ritz method is based on energy methods and is widely used for the buckling, bending and vibrations of beams and plates. This approximate solution method is useful in the case of problems for which the differential equations are too complicated to solve.

3.3.1.1 The energy method

The total potential energy is defined as the sum of the strain energy stored in the body added to the potential energy of the external forces (equal to minus their work)

$$\Pi(u, v, w) = U + V \; , \tag{14}$$

where u,v,w are the displacements in the x,y,z directions and U and V are the strain energy and the potential energy of the applied external forces, respectively.

A state of stable equilibrium of a body is then defined by the two following requirements:

1. The total potential energy has a stationary value or[7]

$$\Pi(u, v, w) = U + V = Stationary\, value \; . \tag{15}$$

2. The total potential energy is minimum.

Analysis Development

3.3.1.2 The Rayleigh-Ritz method

In the Rayleigh-Ritz method, the additional displacements due to buckling (u,v,w) are expressed in the form of a finite series. For example, in the case of a plate problem the three additional displacements can be expressed as

$$u = \sum_{m=1}^{M} \sum_{k=1}^{K} A_{mk} U_{mk}(x,y)$$

$$v = \sum_{p=1}^{P} \sum_{q=1}^{Q} B_{pq} V_{pq}(x,y) \qquad , \qquad (16)$$

$$w = \sum_{r=1}^{R} \sum_{s=1}^{S} C_{rs} W_{rs}(x,y)$$

where U_{mk}, V_{pq}, W_{rs} are called shape functions and A_{mk}, B_{pq}, C_{rs} are the undetermined coefficients.

The shape functions should be chosen carefully, the general guideline for their selection is the following :

1. Each one of the shape functions must satisfy the essential boundary conditions.

2. In order to simplify the analysis, they should be chosen, if possible, to be in the separation of variables form:

$$F(x_1, x_2, ..., x_N) = F_1(x_1) F_2(x_2) ... F_N(x_N) \qquad (17)$$

3. To reduce the number of terms in the series, and hence reduce the order of the system to be solved, the shape functions should also be chosen to correspond as closely to the actual deformed shape of the body as possible. For example, in the case of free oscillations of a spring, a well known function ($\sin \omega t$) is a perfect shape function, performing much better than would a polynomial function of time.

Substituting Eq.(16) for the buckling displacements into the second variation of Π (i.e., $\delta^2\Pi$), the Trefftz criterion ($\delta(\delta^2\pi) = 0$) is the variational statement for the buckling:

$$
\begin{aligned}
\frac{\partial \delta^2\Pi}{\partial A_{mk}} &= 0 & & \begin{aligned} m &= 1, 2, \ldots, M \\ k &= 1, 2, \ldots, K \end{aligned} \\
\frac{\partial \delta^2\Pi}{\partial B_{pq}} &= 0 & & \begin{aligned} p &= 1, 2, \ldots, P \\ q &= 1, 2, \ldots, Q \end{aligned} \\
\frac{\partial \delta^2\Pi}{\partial C_{rs}} &= 0 & & \begin{aligned} r &= 1, 2, \ldots, R \\ s &= 1, 2, \ldots, S \end{aligned}
\end{aligned}
\tag{18}
$$

This set of linear simultaneous equations represents the stability condition for the problem.

3.3.2 The Lagrange multiplier technique

This method represents a powerful tool for the minimization of a functional subject to constraints on its variables.

Let π be the functional to minimize

$$\pi = \pi(x_1, x_2, \ldots, x_N) \quad , \tag{19}$$

subject to the following J constraints:

$$
\begin{aligned}
C_1(x_1, x_2, \ldots, x_N) &= 0 \\
C_2(x_1, x_2, \ldots, x_N) &= 0 \\
&\vdots \\
C_J(x_1, x_2, \ldots, x_N) &= 0
\end{aligned}
\tag{20}
$$

The following function L, called the Lagrangian, is built

Analysis Development

$$L(x, y) = \Pi(x) + y_1 C_1(x) + y_2 C_2(x) + \cdots + y_J C_J(x)$$

$$= \Pi(x) + \sum_{j=1}^{J} y_j C_j(x) \qquad , \qquad (21)$$

where x and y_j are, respectively, the vector of the variables $x_1, x_2, \ldots, x_N$ and the Lagrange multipliers. Note that there is exactly one Lagrange multiplier per constraint.

Stationarity of the second variation of Π subjected to the J constraints requires the $N + J$ conditions

$$\frac{\partial L(x, y)}{\partial x_n} = 0 \qquad n = 1, 2, \ldots, N$$

$$\frac{\partial L(x, y)}{\partial y_j} = 0 \qquad j = 1, 2, \ldots, J \qquad (22)$$

Recalling equation (21), this can also be written as

$$\frac{\partial \delta^2 \Pi(x)}{\partial x_n} + \sum_{j=1}^{J} y_j \frac{\partial C_j(x)}{\partial x_n} = 0 \qquad n = 1, 2, \ldots, N$$

$$C_j(x) = 0 \qquad j = 1, 2, \ldots, J \qquad (23)$$

which represents a set of $(N + J)$ simultaneous equations in the $(N + J)$ unknowns x and y.

3.3.3 Buckling of geodesically stiffened panels

In the present analysis, the Lagrange multiplier method is applied to the stability analysis of geodesically stiffened panels. The functional that is used is the second variation of the total potential energy of the panel, which is the sum of the total potential energies of the skin and stiffeners. The total potential energies of the skin and stiffeners are derived in terms of independent shape

functions. Likewise, constraints that enforce the continuity of the deformations of the skin and stiffeners are written in those terms. Certain derivatives are then used to obtain the set of equations that governs the entire system.

More specifically, the Lagrange multiplier method is used to ensure the compatibility of the out-of-plane deformation of the skin, w_{skin}, with the transverse in-plane deformation pattern of the stiffeners, and the compatibility of the skin and stiffener rotations along the stiffener line of attachment. This is achieved by imposing constraints at a finite number of points (collocation) along the stiffener axes. Then, the second variation of the total potential energy is made stationary subject to the all the constraints simultaneously.

There are five main parts in this section:

1.   Derivation of the second variation of the total potential energy of the skin.

2.   Derivation of the second variation of the total potential energy of the stiffeners.

3.   Constraint 1 : flexural contribution of the stiffeners.

4.   Constraint 2 : continuity of skin and stiffener rotations.

5.   Connections and final eigenvalue system.

3.3.3.1   *Skin total potential energy*

In order to explain all the future choices, recall here the main assumptions that were made about the skin. The skin laminate was chosen to be symmetric about the midplane ($B_{ij} = 0$), balanced ($A_{16} = A_{26} = 0$), and specially orthotropic ($D_{16} = D_{26} = 0$). The anisotropic coupling effects are neglected[5] and the panel is subjected to uniform in-plane forces only.

Whitney[7] gives a complete derivation of the strain energy of a laminated plate. Since the skin is balanced, symmetric and specially orthotropic, this energy can be simplified by discarding the terms

which are multipliers of $A_{16}, A_{26}, B_{ij}, D_{16}, D_{26}$. Moreover, since the strain energy is uncoupled, the strain energy due to in-plane displacements is considered as an arbitrary constant[7]. The second variation of the strain energy is

$$\delta^2 U = \frac{1}{2} \int_0^a \int_0^b \left[D_{11}(w_{,xx})^2 + 2D_{12}(w_{,xx})(w_{,yy}) + D_{22}(w_{,yy})^2 + 4D_{66}(w_{,xy})^2 \right] dx\, dy \quad , \qquad (24)$$

where (see Figure 14) a is the skin width in the x direction, b is the height in the y direction, D_{ij} are the bending stiffnesses, and w is the skin out-of-plane deflection due to buckling.

The second variation of the potential energy of the external in-plane forces is given by

$$\delta^2 V = -\frac{1}{2} \int_0^a \int_0^b \left[N_x(w_{,x})^2 + 2N_{xy}(w_{,x})(w_{,y}) + N_y(w_{,y})^2 \right] dx\, dy \quad , \qquad (25)$$

where N_x, N_{xy}, N_y are the applied loads in prebuckling equilibrium.

The second variation of the total potential energy of the skin is defined as

$$\delta^2 \pi_{skin} = \delta^2 U + \delta^2 V \quad . \qquad (26)$$

The shape function for the out-of-plane deflection must be chosen to satisfy all the kinematic boundary conditions, which are those of a simply supported plate:

$$\begin{aligned} w &= 0 \text{ at } x = 0, a \\ w &= 0 \text{ at } y = 0, b \end{aligned} \qquad (27)$$

The following shape function seems to be adequate for such a problem.

$$w(x,y) = \sum_{m=1}^{M} \sum_{n=1}^{N} A_{mn} \sin \frac{m\pi x}{a} \sin \frac{n\pi y}{b} \qquad \begin{aligned} 0 &\leq x \leq a \\ 0 &\leq y \leq b \end{aligned} \qquad (28)$$

Moreover, the chosen shape function satisfies the mechanical boundary conditions as well:

$$M_x = -(D_{11}w,_{xx} + D_{12}w,_{yy}) = 0 \text{ at } x = 0, a$$
$$M_y = -(D_{12}w,_{xx} + D_{22}w,_{yy}) = 0 \text{ at } y = 0, b$$

(29)

Using this shape function and introducing a common multiplicative factor λ extracted from the applied load (proportional loading) defined by

$$N_x = \lambda \overline{N_x}$$
$$N_y = \lambda \overline{N_y} \quad ,$$
$$N_{xy} = \lambda \overline{N_{xy}}$$

(30)

the following expression for the second variation of the total potential energy of the skin can be obtained (Phillips and Gurdal[5]):

$$\delta^2 \pi_{skin} = \delta^2 U + \delta^2 V$$
$$\delta^2 U = \sum_{m=1}^{M} \sum_{n=1}^{N} A_{mn}^2 P^{mn}$$
$$\delta^2 V = -\lambda \left\{ \sum_{m=1}^{M} \sum_{n=1}^{N} A_{mn}^2 R^{mn} + \sum_{m=1}^{M} \sum_{n=1}^{N} \sum_{p=1}^{M} \sum_{q=1}^{N} A_{mn} A_{pq} S^{mnpq} \right\}$$

(31)

where

$$P^{mn} = \frac{\pi^4 ab}{8} \left[D_{11} \left(\frac{m}{a} \right)^4 + 2(D_{12} + 2D_{66}) \left(\frac{mn}{ab} \right)^2 + D_{22} \left(\frac{n}{b} \right)^4 \right]$$

$$R^{mn} = \frac{\pi^2 ab}{8} \left[\overline{N_x} \left(\frac{m}{a} \right)^2 + \overline{N_y} \left(\frac{n}{b} \right)^2 \right]$$

$$S^{mnpq} = \left[\begin{array}{ll} \overline{N_{xy}} \dfrac{4mnpq}{(p^2 - m^2)(n^2 - q^2)}, & (m+p) \text{ and } (n+q) \text{ odd} \\ \\ 0, & \text{otherwise} \end{array} \right]$$

Analysis Development

3.3.3.2 *Stiffener potential energy*

Instead of considering the stiffeners as beams as was done in the previous study[5], they are considered here to be plates. In the previous study deformation of the stiffeners in their out-of-plane direction was not taken into account; only flexural deformation in the out-of-plane direction to the skin was included. Since the previously obtained optimum designs are composed of stiffeners with heights 15 to 20 times larger than their thicknesses (see Ref.5), the beam assumption may not be valid.

Let η be the longitudinal axis of the stiffener, ζ its transverse axis, χ its out-of-plane axis, and u,v,w their corresponding displacements. Assuming that cross-sectional planes remain plane and normal to the stiffener axis as the stiffener bends in its own plane[8] ,

$$u(\eta, \zeta) = u_o(\eta) - \zeta \frac{\partial v_o(\eta)}{\partial \eta} \quad . \tag{32}$$

Moreover, for small displacements it is assumed that

$$v(\eta, \zeta) = v_o(\eta) \quad , \tag{33}$$

where u_o, v_o are the displacements at $\zeta = \chi = 0$, i.e., the base of the stiffener.

Complete derivation of the strain energy of a general laminated plate, starting with the Kirchhoff displacement-strain relations, is given by Whitney[7] . In the case of a symmetric, balanced and specially orthotropic plate, the second variation of the strain energy is given by

$$\delta^2 U = \frac{1}{2} \int_0^L \left\{ \int_{-H-\frac{\tau_s}{2}}^{-\frac{\tau_s}{2}} + \int_{\frac{\tau_s}{2}}^{H+\frac{\tau_s}{2}} \begin{bmatrix} A_{11}(u_{,\eta})^2 + 2A_{12}u_{,\eta}v_{,\zeta} + \\ \\ A_{22}(v_{,\zeta})^2 + A_{66}(u_{,\zeta} + v_{,\eta})^2 \end{bmatrix} d\zeta \right\} d\eta$$

$$+ \frac{1}{2} \int_0^L \left\{ \int_{-H-\frac{\tau_s}{2}}^{-\frac{\tau_s}{2}} + \int_{\frac{\tau_s}{2}}^{H+\frac{\tau_s}{2}} \begin{bmatrix} D_{11}(w_{,\eta\eta})^2 + 2D_{12}(w_{,\eta\eta})(w_{,\zeta\zeta}) + \\ \\ D_{22}(w_{,\zeta\zeta})^2 + 4D_{66}(w_{,\eta\zeta})^2 \end{bmatrix} d\zeta \right\} d\eta$$

(34)

where L, H, τ_s are the length and the height of the stiffener, and the thickness of the skin, respectively (Figure 14), and u,v,w are the additional displacements due to buckling.

Substituting Eqs. (32) and (33) into Eq. (34) the second variation of the strain energy reduces to

$$\delta^2 U = \frac{1}{2} \int_0^L \left\{ \int_{-H-\frac{\tau_s}{2}}^{-\frac{\tau_s}{2}} + \int_{\frac{\tau_s}{2}}^{H+\frac{\tau_s}{2}} \left[A_{11}(u_{o,\eta}^2 + \zeta^2 v_{o,\eta\eta}^2 - 2\zeta\, u_{o,\eta}\, v_{o,\eta\eta}) \right] d\zeta \right\} d\eta$$

$$+ \frac{1}{2} \int_0^L \left\{ \int_{-H-\frac{\tau_s}{2}}^{-\frac{\tau_s}{2}} + \int_{\frac{\tau_s}{2}}^{H+\frac{\tau_s}{2}} \begin{bmatrix} D_{11}(w_{,\eta\eta})^2 + 2D_{12}(w_{,\eta\eta})(w_{,\zeta\zeta}) + \\ \\ D_{22}(w_{,\zeta\zeta})^2 + 4D_{66}(w_{,\eta\zeta})^2 \end{bmatrix} d\zeta \right\} d\eta$$

(35)

The term $-2\zeta\, u_{o,\eta}\, v_{o,\eta}$ in Eq.(35) is odd with respect to ζ and, therefore, vanishes during the integration. Moreover, the term $A_{11}u_{o,\eta}^2$ is independent of ζ or χ coordinates, and can be considered an arbitrary constant during out-of-plane or in-plane bending. Thus, the final form of the second variation of the strain energy of the stiffeners reduces to

$$\delta^2 U = \frac{1}{2} \int_0^L \left\{ \int_{-H-\frac{\tau_s}{2}}^{-\frac{\tau_s}{2}} + \int_{\frac{\tau_s}{2}}^{H+\frac{\tau_s}{2}} \left[A_{11}\zeta^2 v_{o,\eta\eta}^2 \right] d\zeta \right\} d\eta$$

$$+ \frac{1}{2} \int_0^L \left\{ \int_{-H-\frac{\tau_s}{2}}^{-\frac{\tau_s}{2}} + \int_{\frac{\tau_s}{2}}^{H+\frac{\tau_s}{2}} \begin{bmatrix} D_{11}(w_{,\eta\eta})^2 + 2D_{12}(w_{,\eta\eta})(w_{,\zeta\zeta}) + \\ \\ D_{22}(w_{,\zeta\zeta})^2 + 4D_{66}(w_{,\eta\zeta})^2 \end{bmatrix} d\zeta \right\} d\eta$$

(36)
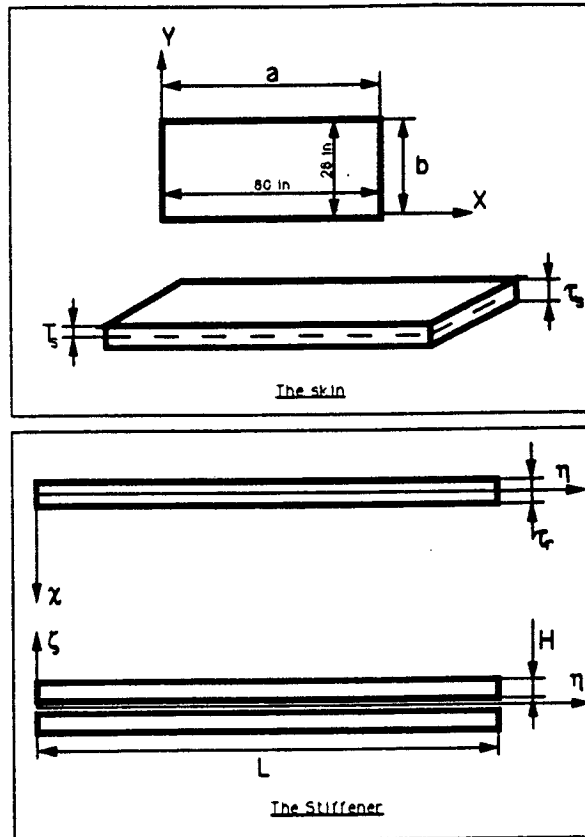
Figure 14. The dimensions. Definitions.

At this point, two kinds of terms appear in Eq. (36) : some of the terms are related to the in-plane bending, and others are due to the out-of-plane bending of the stiffeners. Small displacement theory permits us to write the total strain energy of the stiffeners as the sum of the two contributions.

In the case of a stiffener made of unidirectional material oriented along the longitudinal axis, it is possible to rewrite the second variation of the in-plane energy term as

$$\frac{1}{2}\int_0^L \left\{ \int_{-H-\frac{\tau_s}{2}}^{-\frac{\tau_s}{2}} + \int_{\frac{\tau_s}{2}}^{H+\frac{\tau_s}{2}} [A_{11}\zeta^2 v_{o,\eta\eta}^2]d\zeta \right\} d\eta = \frac{E_l I_l}{2}\int_0^L [v_{o,\eta\eta}^2]d\eta \quad , \tag{37}$$

with

$$I_l = 2\left[\frac{\tau_r H^3}{12} + \tau_r H \left(\frac{H}{2} + \frac{\tau_s}{2} \right)^2 \right] \quad ,$$

where τ_s, τ_r are the skin and stiffener thicknesses, and I_l and E_l are the moment of inertia and the longitudinal elastic modulus of the stiffener, respectively. The in-plane part of the energy expression is the same as the one used in Ref. 5.

Potential energy of the uniform axial loading N applied along short edges of the stiffener is derived next. N is defined as the ratio of the load carried by the stiffener (given by Eq. (13)) over the stiffener height $(2H)$. The expression of the additional end shortening $s(\zeta)$ due to the buckling displacements v,w is given by[8]

$$s(\zeta) = -\frac{1}{2}\int_0^L \left(\frac{\partial w}{\partial \eta} \right)^2 d\eta - \frac{1}{2}\int_0^L \left(\frac{\partial v_o}{\partial \eta} \right)^2 d\eta \quad , \tag{38}$$

where $w = w(\eta, \zeta)$, $v_o = v_o(\eta)$ are the additional displacements due to buckling. Therefore, the second variation of the potential energy of the applied load is

$$\delta^2 V = - W(N) = - \left\{ \int_{-H-\frac{\tau_s}{2}}^{-\frac{\tau_s}{2}} + \int_{\frac{\tau_s}{2}}^{H+\frac{\tau_s}{2}} s(\zeta) N \ d\zeta \right\}$$

$$= N \left\{ \int_{-H-\frac{\tau_s}{2}}^{-\frac{\tau_s}{2}} + \int_{\frac{\tau_s}{2}}^{H+\frac{\tau_s}{2}} \left[-\frac{1}{2} \int_0^{L} \left(\frac{\partial w}{\partial \eta} \right)^2 - \left(\frac{\partial v_o}{\partial \eta} \right)^2 d\eta \right] d\zeta \right\}$$

(39)

We now define the shape functions for the stiffener additional in-plane and out-of-plane deformations due to buckling, $v_o(\eta)$ and $w(\eta, \zeta)$, respectively. Note that the stiffener in-plane deformation $v_o(\eta)$ is to be connected to the out-of-plane deformation of the skin, which is described by a double Fourier series:

$$w(x,y) = \sum_{m=1}^{M} \sum_{n=1}^{N} A_{mn} \sin \frac{m\pi x}{a} \sin \frac{n\pi y}{b} \qquad \begin{matrix} 0 \le x \le a \\ 0 \le y \le b \end{matrix}$$

(40)

We also assume a simple Fourier series to describe $v_o(\eta)$ of the stiffener

$$v_o(\eta) = \sum_{k=1}^{K} B_k \sin \frac{k\pi \eta}{L} \qquad 0 \le \eta \le L \ ,$$

(41)

where B_k are the undetermined coefficients. This shape function satisfies the geometric boundary conditions at the ends of the stiffeners:

$$\begin{matrix} v_o = 0 & \text{at} & \eta = 0 \\ v_o = 0 & \text{at} & \eta = L \end{matrix}$$

(42)

The shape function for the stiffener out-of-plane deformation pattern is more complicated. The stiffeners are attached to the skin along their longitudinal axis, and their out-of-plane deformation corresponds to the in-plane-deformation of the skin. In this study, the contribution of the in-plane deformations of the skin is ignored. Therefore, it is assumed that $w = 0$ at $\zeta = 0$ for all η. The other

long edge of the stiffeners is free, and the two short edges are assumed to be simply supported. The following shape function satisfies these boundary conditions:

$$w(\eta, \zeta) = \sum_{l=1}^{L} \sum_{k=1}^{K'} C_{lk} \zeta^l \sin \frac{k\pi\eta}{L} \qquad \begin{array}{c} 0 \leq \eta \leq L \\ -H - \frac{\tau_s}{2} \leq \zeta \leq H + \frac{\tau_s}{2} \end{array}, \qquad (43)$$

where C_{lk} are the undetermined coefficients. For a panel that has I number of stiffeners, the shape functions have to be re-indexed to indicate the stiffener number, $v_{oi}(\eta)$ and $w_i(\eta, \zeta)$, where the un-determined shape coefficients for the displacements $v_{oi}(\eta)$ and $w_i(\eta, \zeta)$ are B_{ik} and C_{ilk}, respectively. The length of the ith stiffener is L_i, where $i = 1,...,I$. The expression for the second variation of the total potential energy of the stiffeners is the sum of the total energies of all the stiffeners:

$$\delta^2 \pi_{grid} = \sum_{i=1}^{I} \delta^2 \pi_{stiffener\ i} \qquad (44)$$

The derivation of each $\delta^2 \pi_{stiffener\ i}$ is done by placing the shape functions into the equations (36), (39), and (44). This leads to

$$\delta^2 \pi_{stiffener\ i} = U^i_{flexural} + U^i_{bending11} + U^i_{bending12} + U^i_{bending22} + U^i_{bending66} + V^i_{loading}, \qquad (45)$$

with

$$U^i_{flexural} = \frac{\pi^4 E_i I_i}{4 L_i^3} \sum_{k=1}^{K} k^4 B_{ik}^2$$

$$U^i_{bending11} = \frac{D_{11}\pi^4}{2L_i^3} \sum_{l=1}^{L} \sum_{p=1}^{L} \sum_{k=1}^{K'} \left\{ C_{ilk} C_{ipk} \frac{k^4}{l+p+1} \left[(T_s + H)^{l+p+1} - T_s^{l+p+1} \right] \eta_l^p \right\}$$

$$U^i_{bending12} = -\frac{D_{12}\pi^2}{L_i} \sum_{l=1}^{L} \sum_{p=1}^{L} \sum_{k=1}^{K'} \left\{ C_{ilk} C_{ipk} k^2 p(p-1) \frac{1}{l+p-1} \left[(T_s + H)^{l+p-1} - T_s^{l+p-1} \right] \eta_l^p \right\}$$

$$U^i_{bending22} = \frac{D_{22} L_i}{2} \sum_{l=1}^{L} \sum_{p=1}^{L} \sum_{k=1}^{K'} \left\{ C_{ilk} C_{ipk} \, lp(l-1)(p-1) \frac{1}{l+p-3} \left[(T_s + H)^{l+p-3} - T_s^{l+p-3} \right] \eta_l^p \right\}$$

$$U^i_{bending66} = \frac{2D_{66}\pi^2}{L_i} \sum_{l=1}^{L} \sum_{p=1}^{L} \sum_{k=1}^{K'} \left\{ C_{ilk} C_{ipk} \, lp \frac{k^2}{l+p-1} \left[(T_s + H)^{l+p-1} - T_s^{l+p-1} \right] \eta_l^p \right\}$$

$$V^i_{loading} = -\frac{\lambda \overline{N}_i \pi^2}{2 I_i} \left[\sum_{l=1}^{L} \sum_{p=1}^{L} \sum_{k=1}^{K'} \left\{ C_{ilk} C_{ipk} \frac{k^2}{l+p+1} \left[(T_s + H)^{l+p+1} - T_s^{l+p+1} \right] \eta_l^p \right\} + H \sum_{k=1}^{K} B_{ik}^2 k^2 \right]$$

where

$$\eta_l^p = \frac{(1 + (-1)^{l+p})}{2} \, ,$$

$$T_s = \frac{\tau_s}{2}$$

(46)

and $l + p \geq 4$ in the summation for $U_{bending22}$.

3.3.3.3 Second variation of the total energy of the panel

The total energy of the panel is the sum of the total potential energies of the skin and the stiffeners.

The second variation of the panel total energy is given as follows:

$$\delta^2 \pi_{panel} = \delta^2 \pi_{skin} + \delta^2 \pi_{grid}$$
$$= U_{skin} + V_{skin} + U_{grid} + V_{grid}$$

(47)

Analysis Development

Substituting the expressions of second variation of the energies, derived in Eqs. (31) and (45), into

Eq. (47) gives

$$\delta^2 \pi_{panel} = U_{skin} + V_{skin} + U_{grid} + V_{grid}$$

$$U_{skin} = \sum_{m=1}^{M} \sum_{n=1}^{N} A_{mn}^2 P^{mn}$$

$$V_{skin} = -\lambda \left[\sum_{m=1}^{M} \sum_{n=1}^{N} A_{mn}^2 R^{mn} + \sum_{m=1}^{M} \sum_{n=1}^{N} \sum_{p=1}^{M} \sum_{q=1}^{N} A_{mn} A_{pq} S^{mnpq} \right] ,$$

(48)

$$U_{grid} = \sum_{i=1}^{I} \sum_{l=1}^{L} \sum_{p=1}^{L} \sum_{k=1}^{K'} C_{ilk} C_{ipk} U^{ilkp} + \sum_{i=1}^{I} \sum_{k=1}^{K} B_{ik}^2 Q^{ik}$$

$$V_{grid} = -\lambda \left[\sum_{i=1}^{I} \sum_{l=1}^{L} \sum_{p=1}^{L} \sum_{k=1}^{K'} C_{ilk} C_{ipk} V^{ilkp} + \sum_{i=1}^{I} \sum_{k=1}^{K} B_{ik}^2 T^{ik} \right]$$

Analysis Development

where the different coefficients are given by the following expressions,

$$P^{mn} = \frac{\pi^4 ab}{8}\left[D_{11}\left(\frac{m}{a}\right)^4 + 2(D_{12} + 2D_{66})\left(\frac{mn}{ab}\right)^2 + D_{22}\left(\frac{n}{b}\right)^4 \right]$$

$$Q^{ik} = \frac{\pi^4 E_i I_s}{4L_i^3} k^4$$

$$R^{mn} = \frac{\pi^2 ab}{8}\left[\overline{N_x}^P\left(\frac{m}{a}\right)^2 + \overline{N_y}^P\left(\frac{n}{b}\right)^2 \right]$$

$$S^{mnpq} = \left[\begin{array}{ll} \overline{N_{xy}}^P \dfrac{4mnpq}{(p^2 - m^2)(n^2 - q^2)}, & (m+p) \text{ and } (n+q) \text{ odd} \\[2ex] 0, & \text{otherwise} \end{array} \right]$$

$$T^{ik} = \frac{\pi^2 k^2 H}{2I_i} \overline{N_i}$$

$$U^{ilkp} = U_{11}^{ilkp} + U_{12}^{ilkp} + U_{22}^{ilkp} + U_{66}^{ilkp}$$

$$U_{11}^{ilkp} = \frac{D_{11}\pi^4}{2L_i^3} \frac{k^4}{l+p+1}\left[(T_s + H)^{l+p+1} - T_s^{l+p+1} \right]\eta_l^p$$

$$U_{12}^{ilkp} = -\frac{D_{12}\pi^2}{L_i} k^2 p(p-1) \frac{1}{l+p-1}\left[(T_s + H)^{l+p-1} - T_s^{l+p-1} \right]\eta_l^p$$

$$U_{22}^{ilkp} = \frac{D_{22}L_i}{2} lp(l-1)(p-1) \frac{1}{l+p-3}\left[(T_s + H)^{l+p-3} - T_s^{l+p-3} \right]\eta_l^p$$

$$U_{66}^{ilkp} = \frac{2D_{66}\pi^2}{L_i} lp \frac{k^2}{l+p-1}\left[(T_s + H)^{l+p-1} - T_s^{l+p-1} \right]\eta_l^p$$

$$V^{ilkp} = \frac{\overline{N_i}\pi^2}{2I_i} \frac{k^2}{l+p+1}\left[(T_s + H)^{l+p+1} - T_s^{l+p+1} \right]\eta_l^p$$

$$\eta_l^p = \frac{(1 + (-1)^{l+p})}{2}$$

and $l + p \geq 4$ in the summation for the term U_{22}^{ilkp}. The λ is the load factor defined as

$$N_x^P = \lambda \overline{N_x}^P \quad N_y^P = \lambda \overline{N_y}^P \quad N_{xy}^P = \lambda \overline{N_{xy}}^P \quad N_i = \lambda \overline{N_i} \ . \tag{49}$$

Note that the only unknowns in Eqs. (48) are the Fourier coefficients, all other coefficients are

specified in terms of the material properties, geometry, and load coefficients.

3.3.3.4 First constraint : continuity of skin and stiffener bending displacements

This constraint enforces the condition that the out-of-plane deformation of the skin w_{skin} has to be equal to the in-plane transverse deflection of the stiffeners v_{oi}. The constraint is enforced at a finite number of points located on the stiffener axes (Figure 15).

Let x,y,z be the axes of the skin and η,ζ,χ the axes of a stiffener :

x,η are the longitudinal axes of the skin and the stiffener

y,ζ are the transverse axes of the skin and the stiffener

z,χ are the out-of-plane axes of the skin and the stiffener.

On each of the I stiffeners, there are J constraint points, located at the coordinates $(\eta_{ij}, 0, 0)$ for the stiffeners and $(x_{ij}, y_{ij}, 0)$ for the skin. Using the shape functions, this constraint can be expressed as

$$g_{ij} = \sum_{m=1}^{M} \sum_{n=1}^{N} A_{mn} \sin \frac{m\pi}{a} x_{ij} \sin \frac{n\pi}{b} y_{ij} - \sum_{k=1}^{K} B_{ik} \sin \frac{k\pi}{I_i} \eta_{ij} = 0 \qquad \begin{array}{l} i = 1, 2, \dots, I \\ j = 1, 2, \dots, J \end{array} \qquad (50)$$

This constraint is exactly the same as the one used in the previous work[5].

3.3.3.5 Second constraint : Continuity of the skin and stiffener rotations

This constraint is included to ensure the continuity of rotation between the skin and the stiffeners at the base of the stiffeners (along the η axis (Figure 16)). It ensures that right angles between the stiffeners and the skin are maintained.
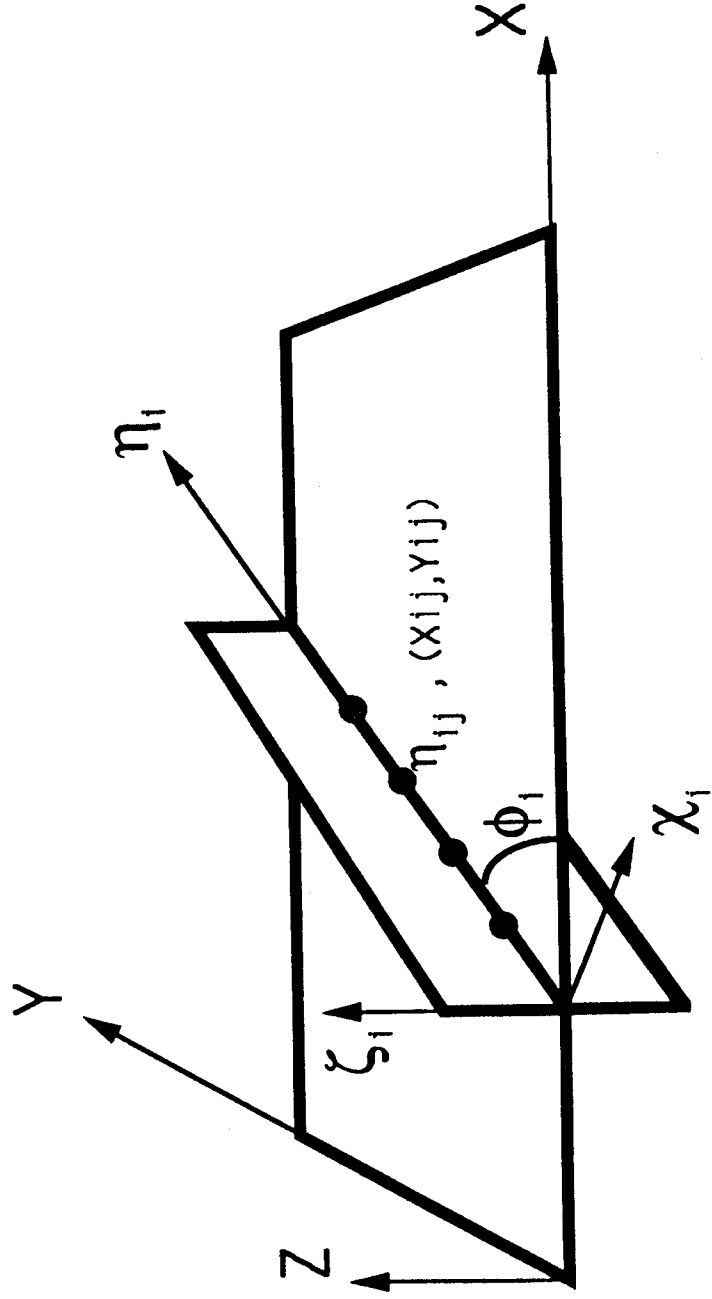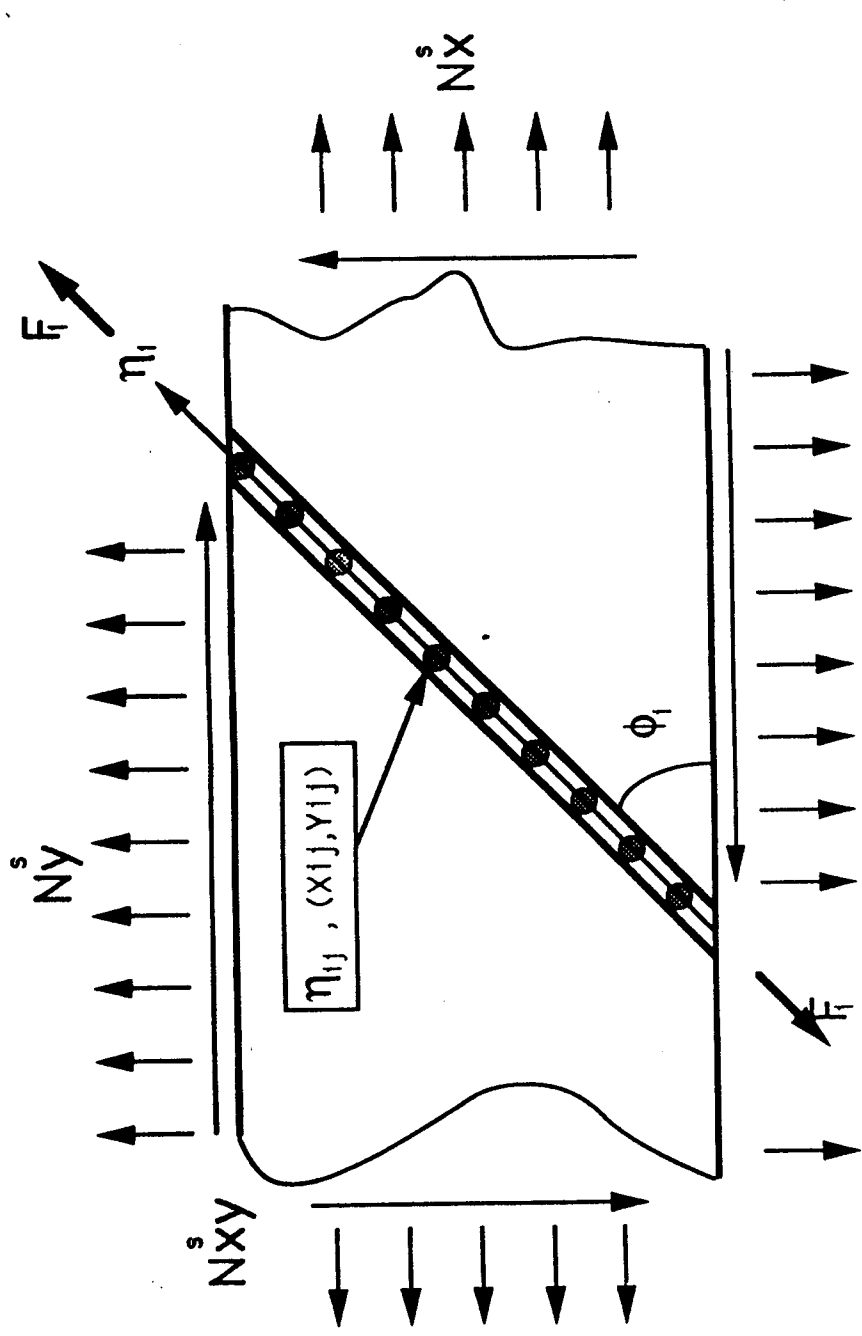
Figure 15. Location of the constraint points for both constraints

Analysis Development
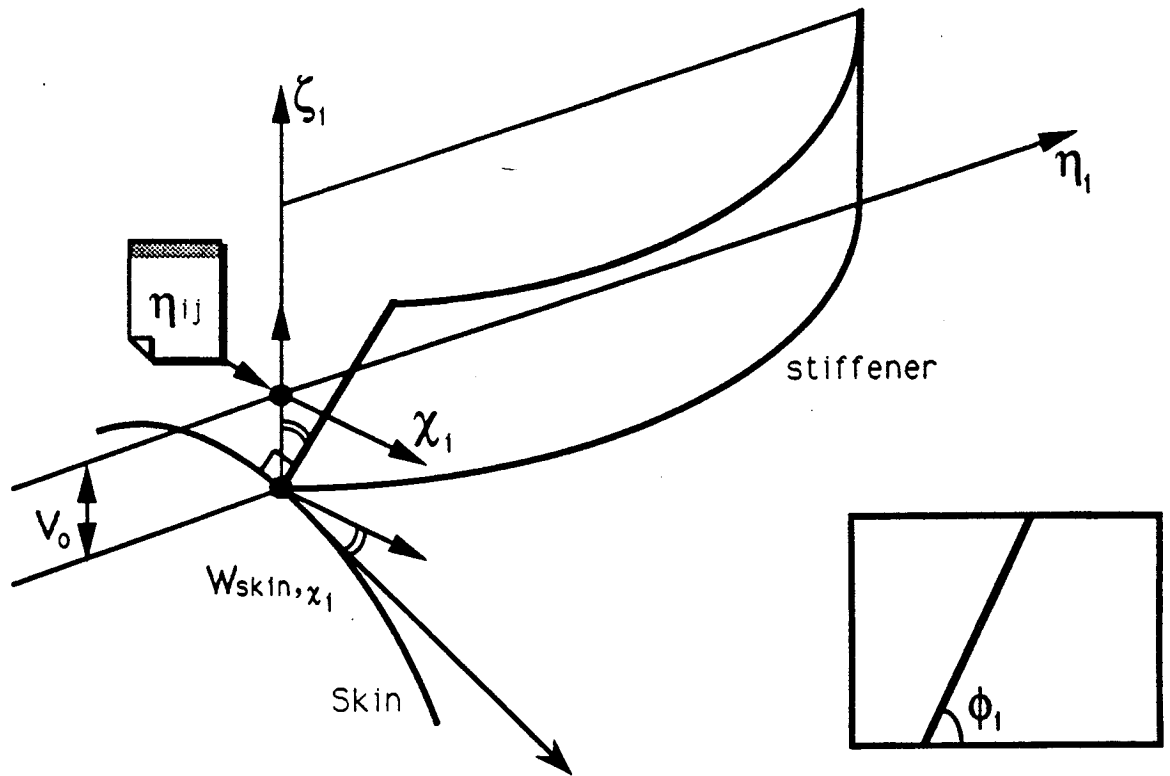
Figure 16.   Second constraint. Rotation of the skin and stiffener at the constraint points

The effect of the out-of-plane bending stiffnesses of the stiffeners on the panel buckling load is rendered by the application of this constraint. The terminology "rotational contribution" will be used to describe this effect.

ϕ_i is defined as the angle between the stiffener i and the x axis of the skin. The slope of the deflection of the skin in the direction of the χ axis is obtained by using the chain rule differentiation

$$\frac{\partial}{\partial \chi} = \frac{\partial x}{\partial \chi} \frac{\partial}{\partial x} + \frac{\partial y}{\partial \chi} \frac{\partial}{\partial y} \quad , \tag{51}$$

where

$$\frac{\partial x}{\partial \chi} = \sin \phi_i$$

$$\frac{\partial y}{\partial \chi} = -\cos \phi_i$$

Using the shape function for w_{skin} in Eq. (29), the slope of the skin deflection with respect to a stiffener axis χ_i is given by

$$\frac{\partial w_{skin}}{\partial \chi_i} = \sum_{m=1}^{M} \sum_{n=1}^{N} A_{mn} \left[\sin \phi_i \frac{m\pi}{a} \cos \frac{m\pi x}{a} \sin \frac{n\pi y}{b} - \cos \phi_i \frac{n\pi}{b} \sin \frac{m\pi x}{a} \cos \frac{n\pi y}{b} \right] \quad . \tag{52}$$

Using the first derivative of the shape function associated with the out-of-plane deformation of the stiffeners, with respect to the ζ axis (evaluated at $\zeta = 0$), the constraint can be expressed as

$$h_{ij} = \frac{\partial w_{skin}}{\partial \chi_i} (x_{ij}, y_{ij}) + \frac{\partial w_{stiff}^i}{\partial \zeta_i} (\eta_{ij}, 0) = 0 \quad , \tag{53}$$

or as

$$h_{ij} = \sum_{m=1}^{M} \sum_{n=1}^{N} A_{mn} \left[\sin \phi_i \, \frac{m\pi}{a} \cos \frac{m\pi x_{ij}}{a} \sin \frac{n\pi y_{ij}}{b} - \cos \phi_i \, \frac{n\pi}{b} \sin \frac{m\pi x_{ij}}{a} \cos \frac{n\pi y_{ij}}{b} \right]$$
$$+ \sum_{k=1}^{K'} C_{i1k} \sin \frac{k\pi}{L_i} \, \eta_{ij} = 0 \tag{54}$$

3.3.3.6 Final System of Equations

The Lagrangian of the system is built as following:

$$L = \delta^2 \pi + \sum_{i=1}^{I} \sum_{j=1}^{J} \mu_{ij} g_{ij} + \sum_{i=1}^{I} \sum_{j=1}^{J} v_{ij} h_{ij} \tag{55}$$

where μ_{ij}, v_{ij} are the Lagrange multipliers associated with the constraints g_{ij}, h_{ij}.

The solution of the problem is given by the set of equations

$$\frac{\partial L}{\partial A_{mn}} = 0 \qquad \begin{aligned} m &= 1, 2, \dots, M \\ n &= 1, 2, \dots, N \end{aligned}$$

$$\frac{\partial L}{\partial B_{ik}} = 0 \qquad \begin{aligned} i &= 1, 2, \dots, I \\ k &= 1, 2, \dots, K \end{aligned}$$

$$\frac{\partial L}{\partial C_{ilk}} = 0 \qquad \begin{aligned} i &= 1, 2, \dots, I \\ k &= 1, 2, \dots, K' \\ l &= 1, 2, \dots, L \end{aligned} , \tag{56}$$

$$\frac{\partial L}{\partial \mu_{ij}} = 0 \qquad \begin{aligned} i &= 1, 2, \dots, I \\ j &= 1, 2, \dots, J \end{aligned}$$

$$\frac{\partial L}{\partial v_{ij}} = 0 \qquad \begin{aligned} i &= 1, 2, \dots, I \\ j &= 1, 2, \dots, J \end{aligned}$$

which represent $(MN + IK + ILK' + 2IJ)$ equations in $(MN + IK + ILK' + 2IJ)$ unknowns. In expended form they are

Analysis Development

$m = 1, 2, ..., M$
$n = 1, 2, ..., N$

$$2A_{mn}P^{mn} + \sum_{i=1}^{I}\sum_{j=1}^{J} \mu_{ij}\left[\sin\frac{m\pi}{a}x_{ij}\sin\frac{n\pi}{b}y_{ij}\right]$$

$$+ \sum_{i=1}^{I}\sum_{j=1}^{J} v_{ij}\left\{-\sin\phi_i\frac{m\pi}{a}\cos\frac{m\pi x_{ij}}{a}\sin\frac{n\pi y_{ij}}{b} + \cos\phi_i\frac{n\pi}{b}\sin\frac{m\pi x_{ij}}{a}\cos\frac{n\pi y_{ij}}{b}\right\}$$

$$-\lambda\left\{2A_{mn}R^{mn} + 2\sum_{p=1}^{M}\sum_{q=1}^{N}A_{pq}S^{mnpq}\right\} = 0$$

$i = 1, 2, ..., I$
$k = 1, 2, ..., K$

$$\left[2B_{ik}Q^{ik} + \sum_{j=1}^{J}\mu_{ij}\left[-\sin\frac{k\pi}{L_i}\eta_{ij}\right] - \lambda\{2B_{ik}T^{ik}\}\right] = 0$$

$i = 1, 2, ..., I$
$l = 1, 2, ..., L$
$k = 1, 2, ..., K'$

$$\left[2\sum_{p=1}^{L}C_{ipk}U_{ilkp} - \sum_{j=1}^{J}v_{ij}\left[\sin\frac{k\pi}{L_i}\eta_{ij}\delta_1^l\right] + \sum_{t=1}^{T}\left[\zeta_{it}^l\sin\frac{k\pi}{2}\eta_{ij}\delta_1^l - \zeta_{it}\sin\frac{k\pi}{2}\delta_1^l\right] = 2\lambda\sum_{p=1}^{L}C_{ipk}V_{ilkp}\right]$$

$i = 1, 2, ..., I$
$j = 1, 2, ..., J$

$$\left[\sum_{m=1}^{M}\sum_{n=1}^{N}A_{mn}\sin\frac{m\pi}{a}x_{ij}\sin\frac{n\pi}{b}y_{ij} - \sum_{k=1}^{K}B_{ik}\sin\frac{k\pi}{L_i}\eta_{ij} = 0\right]$$

$i = 1, 2, ..., I$
$j = 1, 2, ..., J$

$$\left[\sum_{m=1}^{M}\sum_{n=1}^{N}A_{mn}\left[-\sin\phi_i\frac{m\pi}{a}\cos\frac{m\pi x_{ij}}{a}\sin\frac{n\pi y_{ij}}{b} + \cos\phi_i\frac{n\pi}{b}\sin\frac{m\pi x_{ij}}{a}\cos\frac{n\pi y_{ij}}{b}\right]\right.$$

$$\left. + \sum_{k=1}^{K'}C_{i1k}\sin\frac{k\pi}{L_i}\eta_{ij} = 0\right]$$

This is a generalized eigenvalue problem: the eigenvalue of the problem is λ and the eigenvector is composed of the undetermined A_{mn}, B_{ik}, C_{ilk}, μ_{ij}, v_{ij}. The problem can be written in the following matrix form:

$$
\begin{bmatrix}
[K_{11}] & [0] & [0] & [K_{14}] & [K_{15}] \\
[0] & [K_{22}] & [0] & [K_{24}] & [0] \\
[0] & [0] & [K_{33}] & [0] & [K_{35}] \\
[K_{41}] & [K_{42}] & [0] & [0] & [0] \\
[K_{51}] & [0] & [K_{53}] & [0] & [0]
\end{bmatrix}
\begin{Bmatrix}
\{A\} \\ \{B\} \\ \{C\} \\ \{\mu\} \\ \{v\}
\end{Bmatrix}
= \lambda
\begin{bmatrix}
[M_{11}] & [0] & [0] & [0] & [0] \\
[0] & [M_{22}] & [0] & [0] & [0] \\
[0] & [0] & [M_{33}] & [0] & [0] \\
[0] & [0] & [0] & [0] & [0] \\
[0] & [0] & [0] & [0] & [0]
\end{bmatrix}
\begin{Bmatrix}
\{A\} \\ \{B\} \\ \{C\} \\ \{\mu\} \\ \{v\}
\end{Bmatrix}
\tag{58}
$$

In order to reduce the order, and hence the computer running time, a condensation is used. By setting $J = K$, which sets the number of terms in the in-plane deflection series of the stiffener to be equal to the number of constraint points, it is possible to invert $[K_{24}]$ and $[K_{42}]$, and eliminate $\{\mu_{ij}\}$ and $\{B_{ik}\}$ before calling the eigenvalue solver. Using the second and the fourth "lines" $\{\mu\}$ and $\{B\}$ are written in terms of the other unknowns:

$$
\{\mu\} = [K_{24}]^{-1}\{\lambda[M_{22}]\{B\} - [K_{22}]\{B\}\}
$$
$$
\{B\} = -[k_{42}]^{-1}[K_{41}]\{A\}
\tag{59}
$$

The system is then reduced to the following one, which is much smaller than Eq.(58).

$$
\begin{bmatrix}
[K^*] & [0] & [K_{15}] \\
[0] & [K_{33}] & [K_{35}] \\
[K_{51}] & [K_{53}] & [0]
\end{bmatrix}
\begin{Bmatrix}
\{A\} \\ \{C\} \\ \{v\}
\end{Bmatrix}
= \lambda
\begin{bmatrix}
[M^*] & [0] & [0] \\
[0] & [M_{33}] & [0] \\
[0] & [0] & [0]
\end{bmatrix}
\begin{Bmatrix}
\{A\} \\ \{C\} \\ \{v\}
\end{Bmatrix}
\tag{60}
$$

where

$$
[K^*] = [K_{11}] + [K_{14}][K_{24}]^{-1}[K_{22}][K_{42}]^{-1}[K_{41}]
$$
$$
[M^*] = [M_{11}] + [K_{14}][K_{24}]^{-1}[M_{22}][K_{42}]^{-1}[K_{41}]
\tag{61}
$$

No other reduction of the system is possible, but a modification can be done. The eigenvalue solver reduces the left hand side matrix to upper Hessenberg form and the right hand side matrix to upper triangular form. To minimize the number of operations needed for this step, it may be helpful to re-order the terms inside the matrices and the vectors:

$$
\begin{bmatrix} [K^*] & [K_{15}] & [0] \\ [K_{51}] & [0] & [K_{53}] \\ [0] & [K_{35}] & [K_{33}] \end{bmatrix} \begin{bmatrix} \{A\} \\ \{v\} \\ \{C\} \end{bmatrix} = \lambda \begin{bmatrix} [M^*] & [0] & [0] \\ [0] & [0] & [0] \\ [0] & [0] & [M_{33}] \end{bmatrix} \begin{bmatrix} \{A\} \\ \{v\} \\ \{C\} \end{bmatrix} \tag{62}
$$

The order of the system is given by

$$ Order = MN + IK + IK'L \; , \tag{63} $$

where

1. $M \times N$ is the number of terms used in the skin deflection series

2. I is the number of stiffeners

3. K is both the number of constraint point per stiffener or the number of terms used in the series describing the in-plane deflection of the stiffener.

4. $K'L$ is the number of terms used in the out-of-plane deflection series of the stiffeners.

For a panel composed of numerous cells, the order increases very rapidly to a point where the precision of the computer used might be a problem. A typical example is a 5 cell cross stiffened panel ($I = 10$), with $K = 13$, $K' = 6$, $L = 6$, $M = 17$, $N = 9$. The order is 643, while the same problem without the constraints number 2 would have an order of only 153 (if $M = 17, N = 9$).

4.0 Verification and Examples

A new computerized design code was developed based on the analysis derived in Chapter 3. The purpose of this chapter is to analyze some results of the new code in order to verify its accuracy, and to compare the new analysis with the previous ones.

A shorthand coding defined in this section is useful later on. This coding gives a quick description of a panel and its loading, and is defined as

$$I_{geom} \quad C\, n_{cell} \quad C\, lc \quad S\, sl \quad , \tag{64}$$

where I_{geom} stands for the type of stiffening geometry (2 for longitudinally,3 for diagonally and 4 for cross stiffened panels), n_{cell} stands for the number of cells, 10^{lc} lbf/in is the average compression stress resultant applied to the panel, and 10^{ls} lbf/in is the average shear stress resultant applied to the panel. For example, for an 8 cell cross-stiffened panel loaded by 1000 lbf/in in compression and 100 lbf/in in shear, the shorthand coding is 4C8C3S2.

4.1 Partial Verification Of The New Analysis

In order to check the analysis, some of its parts are isolated and studied independently.

There are two parts in this section. First, the analysis corresponding to the buckling of the stiffeners is compared with the analysis of Stoll[9], which is already verified. Second, some new results are compared to the results obtained in the previous study[5].

4.1.1 Stiffener buckling

In the set of equations (57), it is possible to isolate the equations corresponding to the buckling of a single stiffener which is simply supported on its short edges and longitudinal axis while free on its long edges.

$$
\begin{aligned}
& l = 1, 2, \dots, L \\
& k = 1, 2, \dots, K' \\
& \left[\sum_{p=1}^{L} C_{ipk} U_{illkp} = \lambda \sum_{p=1}^{L} C_{ipk} V_{illkp} \right]
\end{aligned}
\tag{65}
$$

This set of equations corresponds to the buckling of the ith stiffener. All the participating terms were previously defined. Using this set of equations, a Fortran code was written to compute the buckling load of stiffeners with various dimensions. The results were compared with those obtained using the code developed by Stoll[9] which includes shear effects. For stiffeners with small thickness compared to their width ($\tau_r \leq \frac{H}{5}$) the computed buckling load was within 3% of the value computed in Ref.9. Thus, for thin stiffeners the present analysis is sufficient to calculutate the buckling load of the stiffeners, and the transverse shear contribution does not need to be taken into account.

The accuracy of the program with constraint on the rotation of the stiffener can also be checked. By imposing a zero deflection of the skin everywhere, the constraint will set the rotation of the stiffener to zero at the constraint points, which is close to clamped boundary conditions along the stiffener longitudinal axis. The present analysis was then compared successfully to a buckling analysis for an isotropic stiffener for which one long edge is free, the other is clamped, and the two short edges are simply supported.

4.1.2 Partial verification with the previous analysis

The stability equation of the panel as a whole (see Eq. (62)) is rewritten for convenience:

$$
\begin{bmatrix}
[K^*] & [K_{15}] & [0] \\
[K_{51}] & [0] & [K_{53}] \\
[0] & [K_{35}] & [K_{33}]
\end{bmatrix}
\begin{bmatrix}
\{A\} \\
\{v\} \\
\{C\}
\end{bmatrix}
= \lambda
\begin{bmatrix}
[M^*] & [0] & [0] \\
[0] & [0] & [0] \\
[0] & [0] & [M_{33}]
\end{bmatrix}
\begin{bmatrix}
\{A\} \\
\{v\} \\
\{C\}
\end{bmatrix}
$$

In these two large matrices, there are two kinds of submatrices; one group could be called behavioral matrices and the other one is the constraint matrices. For example, the submatrices K^* and M^* correspond to the stability of the panel including the flexural contribution of the stiffeners. The submatrices K_{33} and M_{33} correspond to the out-of-plane stability of the stiffeners. The submatrices K_{15}, K_{51}, K_{53}, and K_{35} correspond to the constraints on the rotation of the stiffeners. Note that the two large matrices are not symmetric.

As can be seen, it is possible to choose the level of constraining by choosing the order of the system to send to the eigenvalue solver. For example, starting from the top left of the matrices, an order

1. MN corresponds to the stability of the panel only taking into account the flexural contribution of the stiffeners : exactly as in the previous study[5].

Verification and Examples

2. $MN + IK + IK'L$ corresponds to the stability of the panel taking into account the effect of the out-of-plane bending stiffnesses of the stiffeners.

Therefore, this new analysis can be compared with the previous one in Ref. 5 by selecting an order MN system for panels with equally sized cells. The results of such runs were exactly the same as the ones in the previous study.

4.2 Convergence Study

As it is for most studies in which Fourier series are involved, there is a real need to know exactly the lowest number of terms that will give a good approximation of the solution. It should be recalled that the Fourier series approach relies on infinite sums of terms, and that the precision increases with the number of terms in the series. These terms are written in matrix form in the computer code, and the more they are the larger is the order of the system and the time to solve it; but the better is the precision of the result.

With the Lagrange multiplier technique, constraints are imposed at certain points along the length of the stiffeners. This technique results in adding as many supplementary equations as the number of constraint points. However, a large number of constraint points will increase the order of the system. For this reason, the minimum number of constraint points that are needed to obtain a reasonable solution should be determined.

If the number of constraint points corresponding to a continuous constraint is small, the system will be under restrained, and in the case of buckling response, the system will buckle in a mode that violates the constraint conditions of the actual system. This is important for the determination of

Verification and Examples

the buckling load of such a system since the determined buckling load will be lower than the actual. This leads to a conservative design.

In the case of the geodesically stiffened panel, there are 5 parameters that need to be studied:

M : number of terms for the skin deflection along the x axis.

N : number of terms for the skin deflection along the y axis.

K' : number of terms for the stiffener deflection along the η axis

L : number of terms for the stiffener deflection along the ζ axis

K : number of constraint points per stiffener.

As it was previously mentioned, it is possible to isolate different levels of constraint in the global matrix. For the sake of simplicity a name is given to each of these levels:

Level 1 : Include only the constraint corresponding to the flexural contribution of the stiffeners.

Level 2 : Include the constraints corresponding to both the flexural contribution of the stiffeners and the continuity of rotation between the skin and the stiffeners.

The aim of the following convergence study is to show the influence of the different parameters on the resulting critical load of the panel. This study is done for a panel under compression, knowing that for a shear loading the effect of the parameters is similar. Nevertheless it can be noted that a panel under shear loading requires more terms for the skin deflection. This makes sense since the mode shapes are unsymmetrical. This study was done on a 4 cell cross stiffened panel, a level 2 of constraining was applied, and an optimal panel from the previous study was studied for the following reasons. When taking a panel with very strong stiffeners only the skin buckles. Then, the number of terms in the out-of-plane deflection of the stiffeners will be meaningless since this deflection is zero. When taking a very thick skin and stiffeners with little bending stiffness, only the stiffeners are going to buckle. Then M and N would not have any effect on the buckling load. By

taking an optimum panel from the previous analysis (LMM1), both skin and stiffeners have a deflection for the buckling mode. Then all the parameters are important.

It must be noted that the number of parameters needed depends on the panel geometry and the number of cells. For example a 1 cell panel requires fewer terms for the skin deflection than a multiple cell panel. For each case, before any optimization, a convergence study is done on the baseline design, to determine the parameters needed.

4.2.1 Influence of K

This parameter controls the number of constraint points along the stiffener axes. At these constraint points, both constraints 1 and 2 are imposed. The influence of the value of K on the panel buckling load is demonstrated in Figure 17. As it can be expected, the smaller the number of constraint points (i.e., K small), the lower the buckling load. For example, it can be seen from the figure that 10 constraint points are enough to obtain a stable solution. From design to design, the minimum value for K does not change and usually it is set to 12 for the analysis of any panel.

4.2.2 Influence of M and N

The numbers M and N correspond to the number of terms in the skin deflection series, and setting them to small values artificially reduces the freedom of the skin, thereby stiffening it. By setting M to a large value and varying N the effect of N can be isolated, and vice versa. The standard parameters are $M = 20$, $N = 9$, $K = 13$, $K' = 6$, $L = 6$, when one is varying the others remain constant. The effect of the number of terms in the assumed displacement on the buckling load of panels is shown in Figures 18 and 19. In either increasing M or N, the buckling load reaches a stable
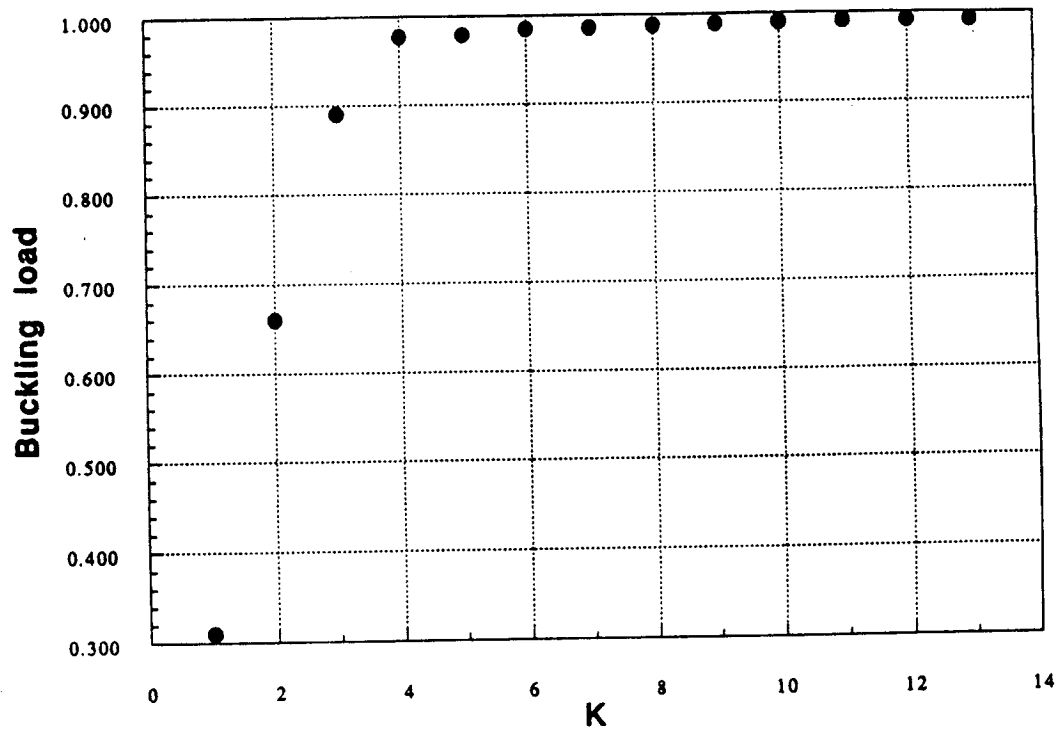
Figure 17. Influence of K on the panel buckling load

value after approximately 10 terms. If too few terms in the series are used, then the predicted buckling loads are high and lead to nonconservative designs. For the case of a small number of terms in the series the solution of the eigenvalue problem seems to be unstable, producing artificially high values for the eigenvalues.

The eigenvalue solver normilizes the eigenvectors such that their largest component is 1. For all the unstable cases, the "1" and all the large values are in the subvector corresponding to the second constraint (i.e., $\{v\}$). The other components (deflection series terms) are relatively very small (at least 10^{10} times less). Moreover, some complex eigenvalues are returned by the eigenvalue solver. It seems that for these cases, the computer is not precise enough to mix high and very low order terms. Increasing the parameters over $M = 20$ and $N = 9$ leads to a stable buckling load. The subvectors are now of comparable magnitudes, the "1" is in the subvector corresponding to skin deflection series (i.e., $\{A\}$), and all eigenvalues are real.

By reducing the number of constraints (decreasing K), over-constrained cases can become stable cases. For example, the case $M = 17$, $N = 9$, $K = 13$ is not stable while $M = 17$, $N = 9$, $K = 11$ is perfectly stable.

This problem seems to be ill-conditioning of the system in the eigenvalue solver when the number of deflection terms is insufficient. Some submatrices contain large numbers (i.e., 10^6) while some others contain very small values (i.e., 10^{-3}). In the case of a small number of deflection terms, conditioning of the matrices may be possible. By multiplying the submatrices by some appropriate constant, some over-constrained cases can become stable. In selecting the constant, the subvectors of the eigenvector are artificially set to be of the same magnitude. For example, the case $M = 1$, $N = 1$, $K = 13$ can be stabilized by multiplying the second column of the $[A]$ matrix of the system by 10^8. This has the effect of reducing the magnitude of the subvector $\{v\}$ while the other subvectors have their magnitude increased to approximately the same magnitude as $\{v\}$.
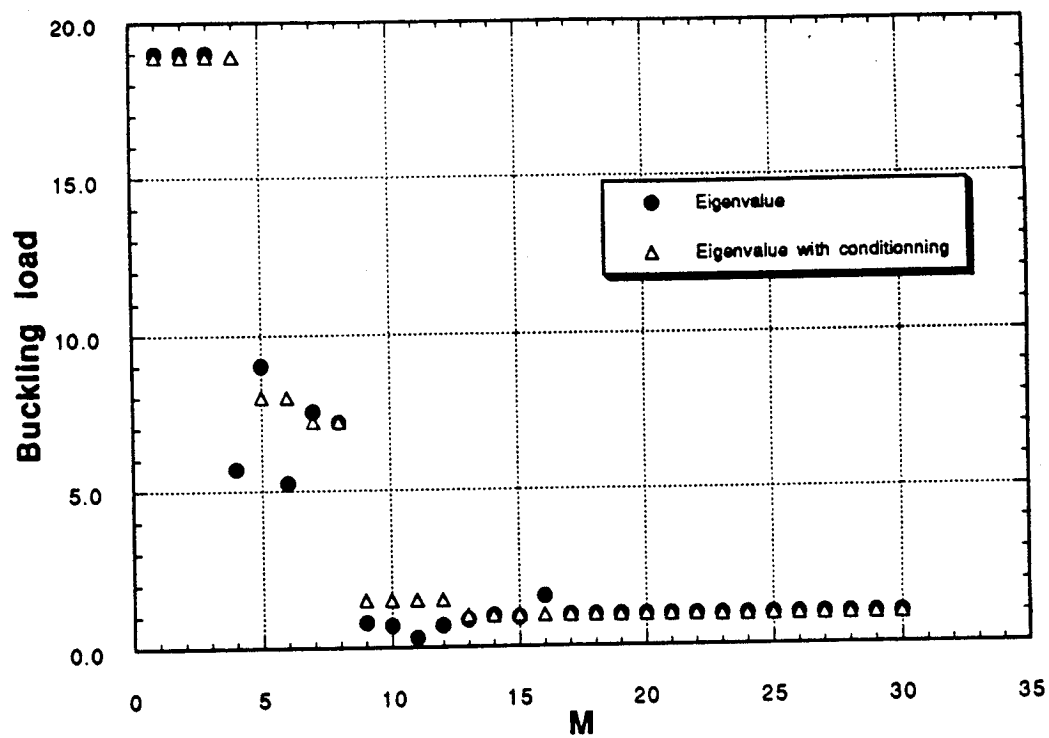
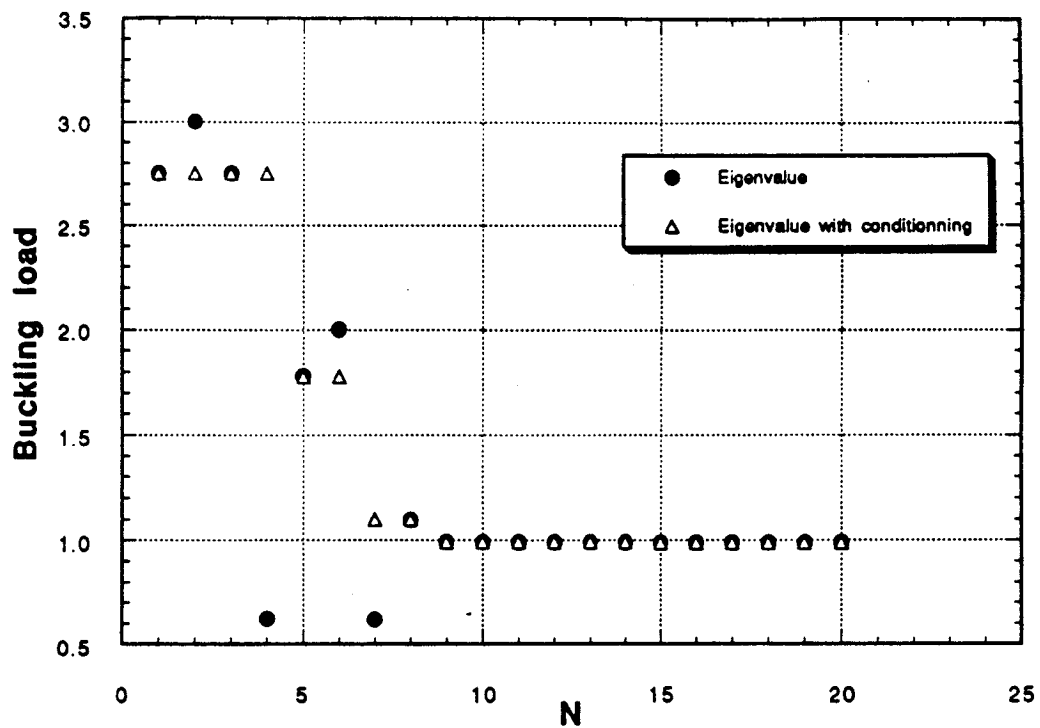Figure 18. Influence of M on the panel buckling load.

Figure 19.   Influence of N on the panel buckling load.

A practical method of setting M and N is the following. M (N) should be at least twice the number of inter-stiffener sections crossed by a line parallel to the X (Y) axis. Then M and N should be increased until a stable eigenvalue is reached. For example, a 4 cell cross-stiffened panel has 9 (3) inter-stiffener sections for the X (Y) axis. Therefore, M (N) should equal 18 (6), but a slight increase to 20 (9) is needed to obtain a stable eigenvalue.

4.2.3 Influence of K′ and L

These parameters represent the number of terms in the out-of-plane deflection of the stiffeners. As it was for the terms M and N, the larger they are, the more accurate is the solution. However, their minimum value for an acceptable solution is sought. K' and L represent, respectively, the number of terms along the η and ζ axis of the stiffener. The effects of increasing K' and L on the panel buckling load is shown in Figures 20 and 21, respectively. As can be observed from Figure 20 and Figure 21, $K' = 6, L = 1$ is a sufficient pair to describe with accuracy the out-of-plane deflection of the stiffeners. $L = 1$ means that the deflection of the stiffener is linear with ζ (see Eq. (43)).

4.2.4 Conditioning of such a problem

The problem of ill-conditioning of eigenvalue problems and generalized eigenvalue systems is often difficult to solve, particularly in the case of large systems. Ill-conditioning occurs when a small variation of one of the terms in the matrix induces a large variation in the eigenvalues and eigenvectors.

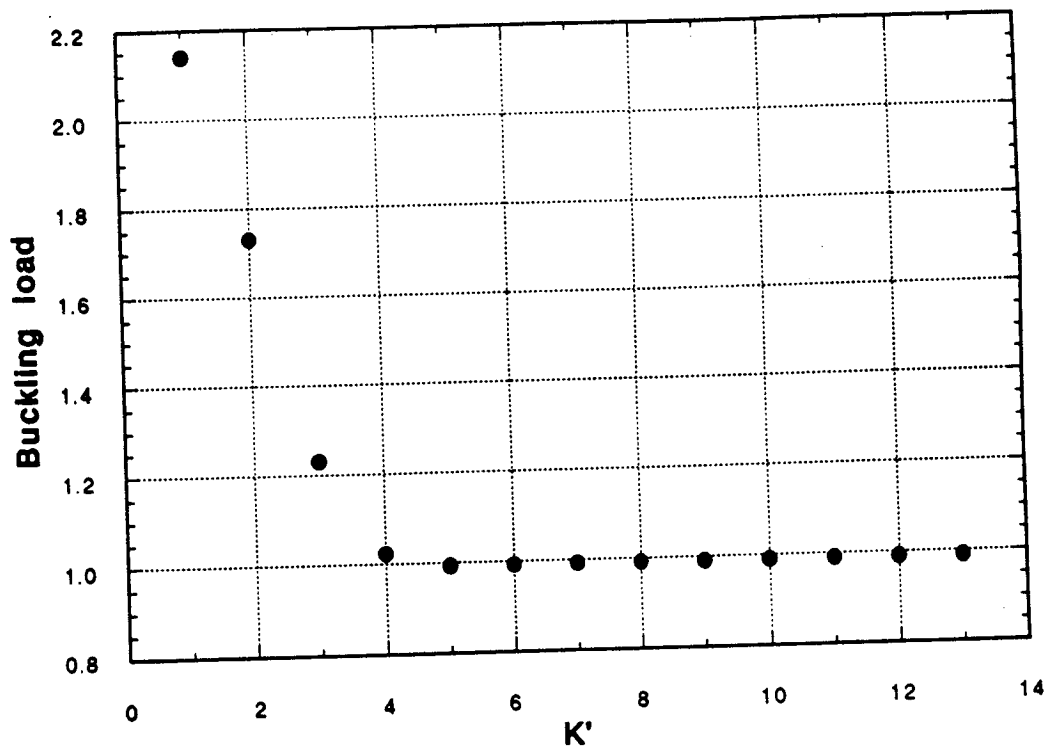As an example, let us consider the following matrix:

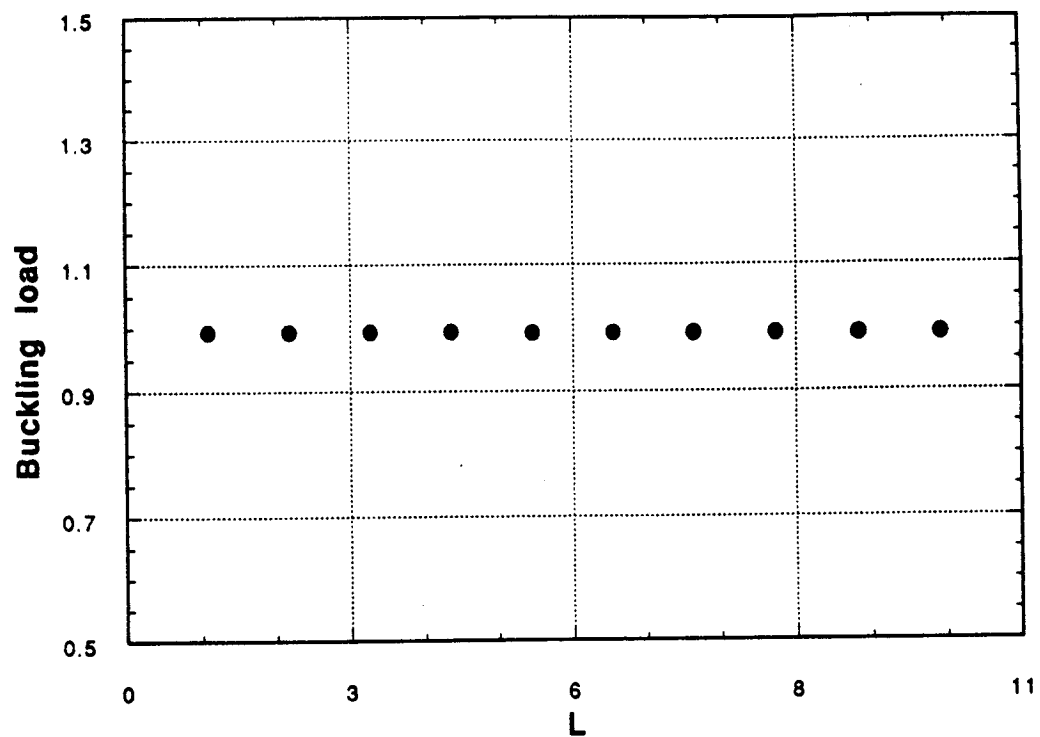Figure 20.   Influence of K' on the panel buckling load

Figure 21.   Influence of L on the panel buckling load

$$
\begin{bmatrix}
0 & & & & & & \varepsilon \\
1 & 0 & & & & & \\
 & 1 & 0 & & & & \\
 & & 1 & \cdot & & & \\
 & & & \cdot & \cdot & & \\
 & & & & \cdot & \cdot & \\
 & & & & & 1 & 0
\end{bmatrix}
\tag{66}
$$

For this example, let us set the order to 40. If $\varepsilon = 0$ all the eigenvalues are zero ($\lambda_i = 0$, $i = 1, \dots, n$). Now, if $\varepsilon = 10^{-40}$, the eigenvalues become $\lambda_i = 10^{-1}$, $i = 1, \dots, n$. During the computations of the eigenvalue solver, mistakes on the order of ε are currently made. In our example, there is a significant chance that the eigenvalue solver will replace $\varepsilon = 10^{-40}$ by 0, which would lead to erroneous results.

Noting the way the constraints are written, it can be observed that the coefficients corresponding to the Lagrange multipliers are very small when the others are quite large. In fact, some of the submatrices K_{51}, K_{53}, and K_{35} are blocks of very small numbers compared to K^*. This can have an effect similar to the effect of ε in the previous example.

Solving such a system can result in a solution for which the subvectors are very different in magnitude. As it is well known, computers can hardly handle computations involving both very small and very large numbers. To avoid this kind of a problem, it is possible to normalize the constraints by multiplying some of the submatrices by a selected constant and thereby obtain an homogeneous eigenvector.

A method that was successful in solving the conditioning problem is explained here. In this method, the system as represented by equation (62) is considered. To simplify, the notation $cond\{A\}$ is used to represent the largest number in the Λ matrix. The method is as follows;

1. The second "line" is multiplied by $cond\{K'\}/cond\{K_{s1}\}$

2. The second "column" is multiplied by $cond\{K'\}/cond\{K_{3s}\}$

3. The $[B]$ matrix is multiplied by $cond\{A\}/cond\{B\}$

4. The obtained eigenvalue is multiplied by $cond\{A\}/cond\{B\}$ to obtain the eigenvalue of the original problem.

5. The obtained eigenvector does not need to be modified.

The fifth operation is justified by the following operation:

$$[A]\{x\} = \lambda [B]\{x\} \quad \sim \quad [A]\{x\} = \left(\frac{\lambda}{\mu}\right)[\mu B]\{x\} \tag{67}$$

The eigenvalue solver used is the Fortran IMSL subroutine (DGVLRG 1990)[10].

4.3 Panel Buckling Response

In the present work a constraint ensuring the continuity of rotations between the skin and the stiffeners is used to improve the analysis and the prediction of the buckling load of the panels. This constraint also has an effect on the buckling mode shape of the panel. The aim of this section is to determine the effect of the new constraint on the buckling mode shapes and critical buckling loads of geodesically stiffened composite panels.

However, it should be recalled that the analysis was developed in the restricted field of small displacement theory. No post-buckling analysis was done and the modes are only of a qualitative interest.

As mentioned, the goal in adding the second constraint to the analysis was to improve the prediction of the solution. In order to determine if there is any improvement, we compare the new

Verification and Examples

buckling mode shape and critical load to those obtained by the previous method (LMM1) and to some results obtained with the Finite Element Method (FEM).

4.3.1 The panel buckling modes

4.3.1.1 Types of response

The following brief study is used to show the different types of response of a panel under shear or compression. A one cell cross stiffened configuration was studied. For both compression loading and shear loading, four cases were included. From one case to another only the skin thickness was varied. It should be noted that for each type of loading (compression or shear) the panels do not have the same buckling load.

Interaction between the stiffener deflection and the skin deflection is shown in Figures 22 through 29. On each figure the contour lines of the skin and stiffener buckling modes are drawn and a 3-D view of these modes is also presented. Figures 22 through 24 show the buckling mode of panels under compression loading having, respectively, a thin, medium and thick skin. Only the panel with thick skin does not participate in local inter-stiffener buckling; but in all cases the stiffeners buckle in a two half wave type mode. However, only in the case of the thin skin (see Figure 22) is this mode truly a two half wave mode. In the other two cases the mode shape of the stiffeners is distorted due to skin mode interaction. In the case of Figure 22 the skin does not present any deflection along the stiffener axis. For the other two cases (see Figures 23 and 24) the buckling modes of the stiffeners are more complicated, and the skin presents a deflection along the stiffener axis. Figure 25 shows the buckling mode for a panel having a very thick skin under compression loading. In this case the applied load is not large enough to buckle the skin. However, the load caried by the stiffeners is large enough to buckle them. It can be noted that the stiffeners buckle as if they were clamped onto the skin.
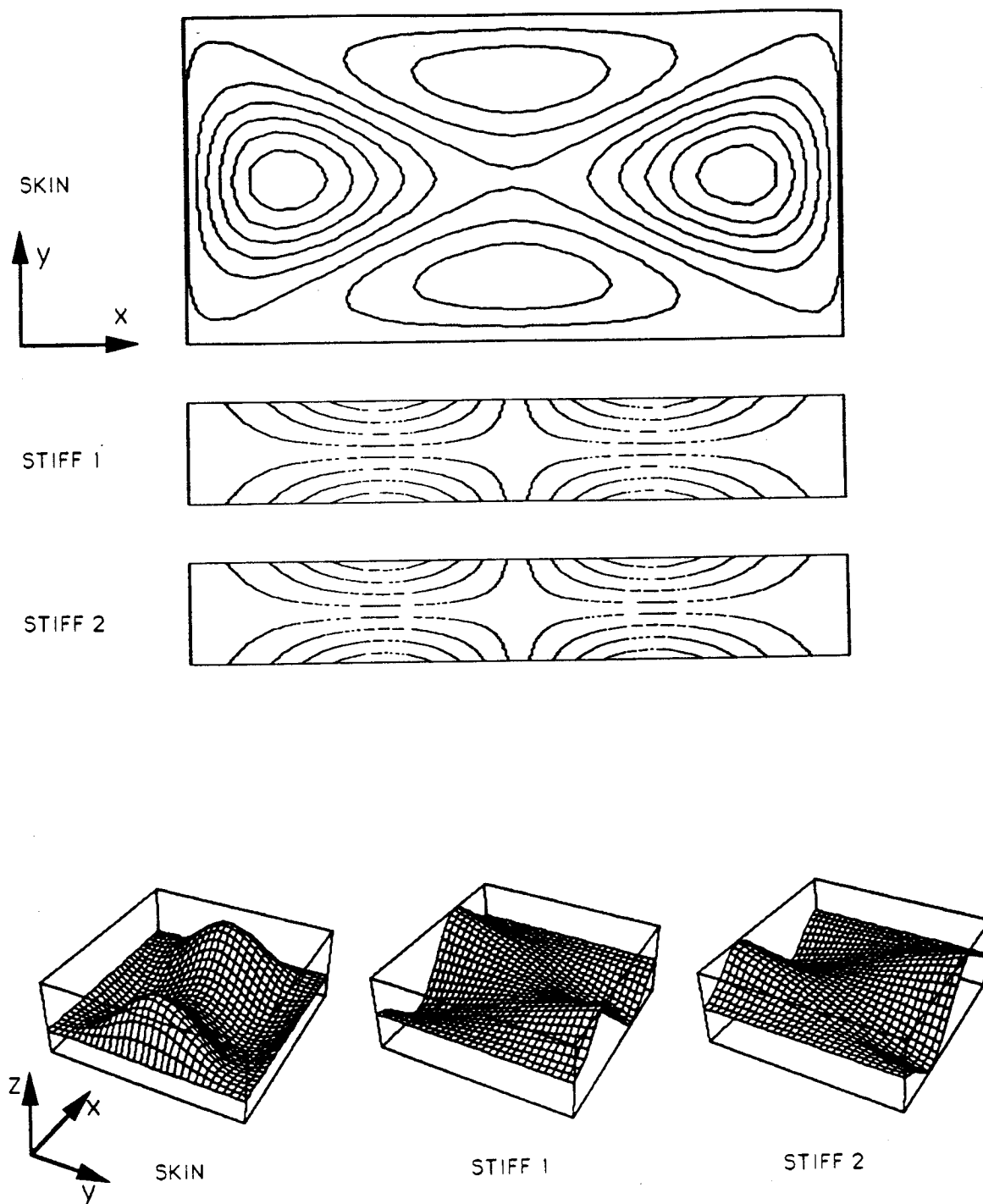
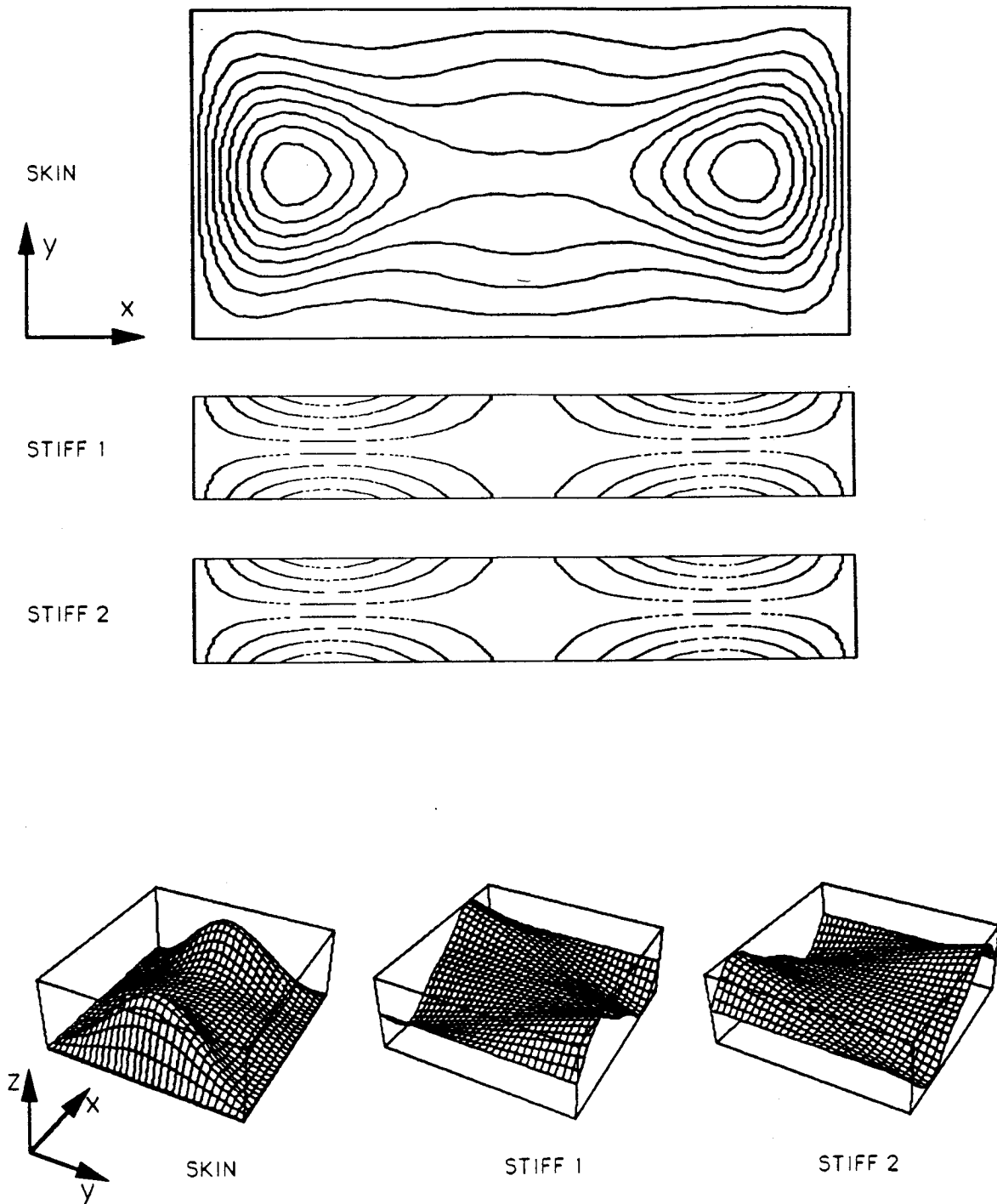Figure 22. Mode Shapes for 4C1CxS0S (H = 3.614; $\tau_r = 0.113; \tau_r = 0.08$)

Figure 23. Mode Shapes for 4C1CxS0M (H = 3.614; $\tau_r = 0.113; \tau_s = 0.256$)

Figure 24. Mode Shapes for 4C1CxS0B (H = 3.614; $\tau_r = 0.113; \tau_s = 1.0$)

SKIN

No deflection

STIFF 1

STIFF 2

the stiffener 1 (2)

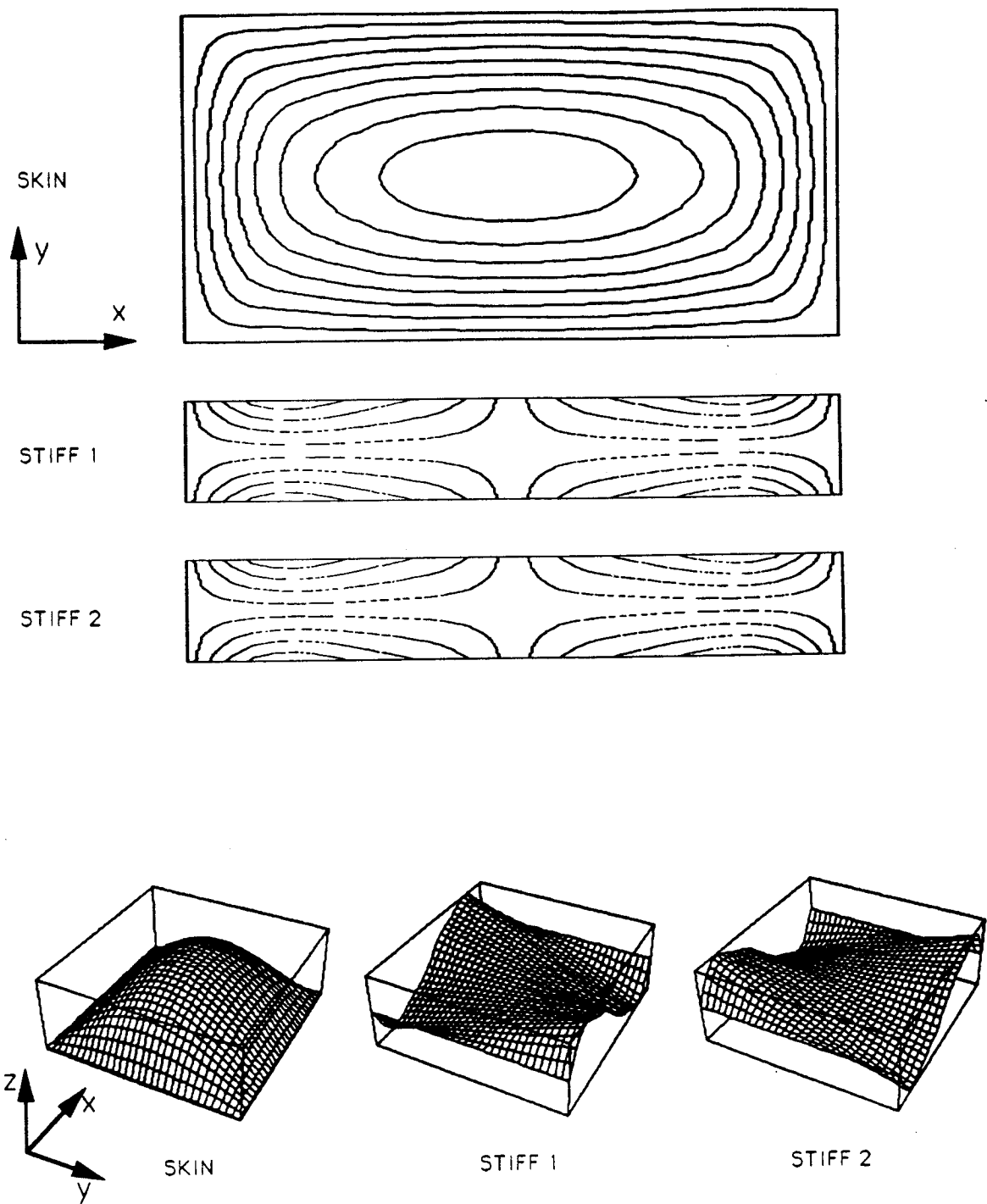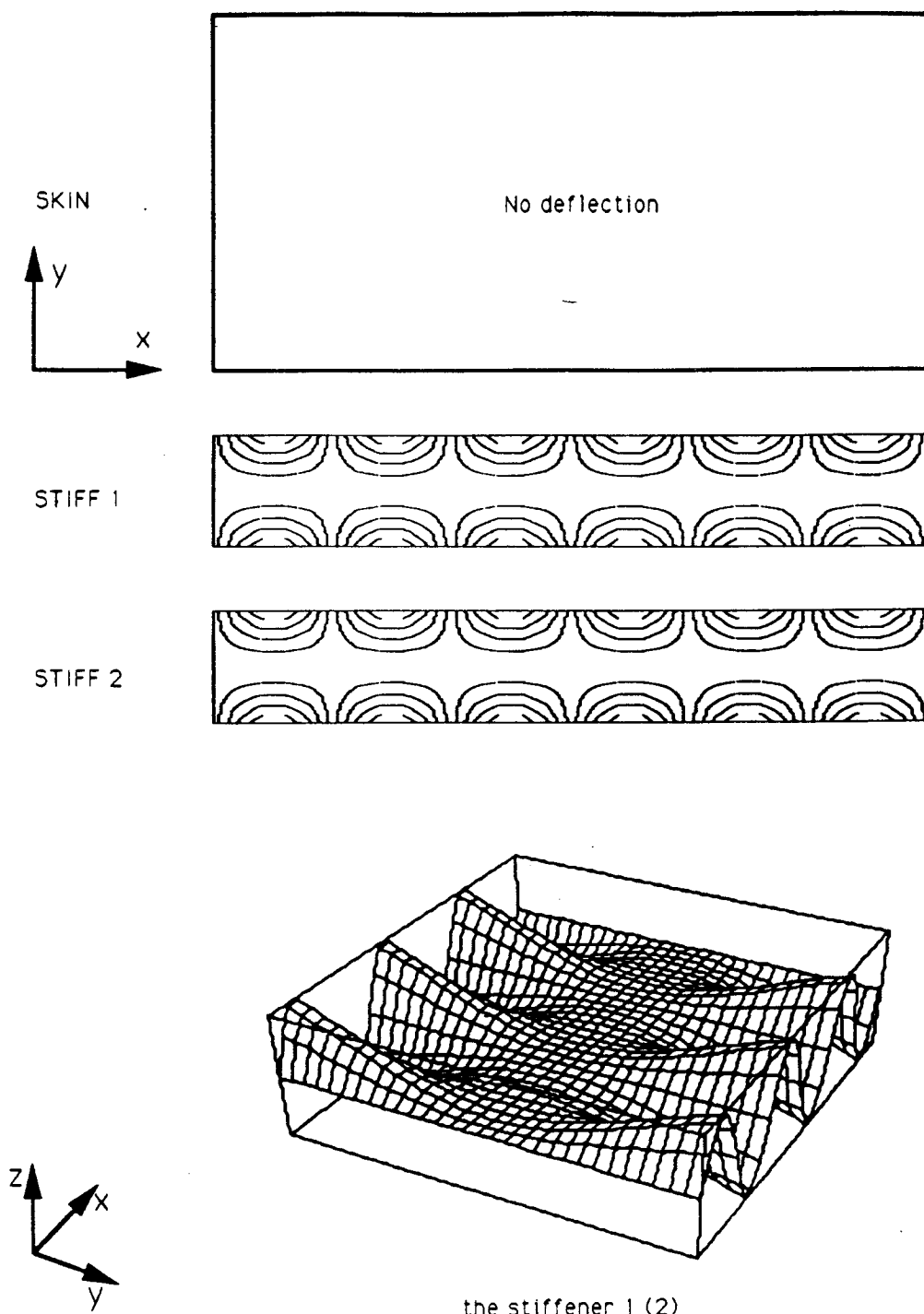Figure 25. Mode Shapes for 4C1CxS0K (H = 3.614; τ_r = 0.113; τ_r = 3.0
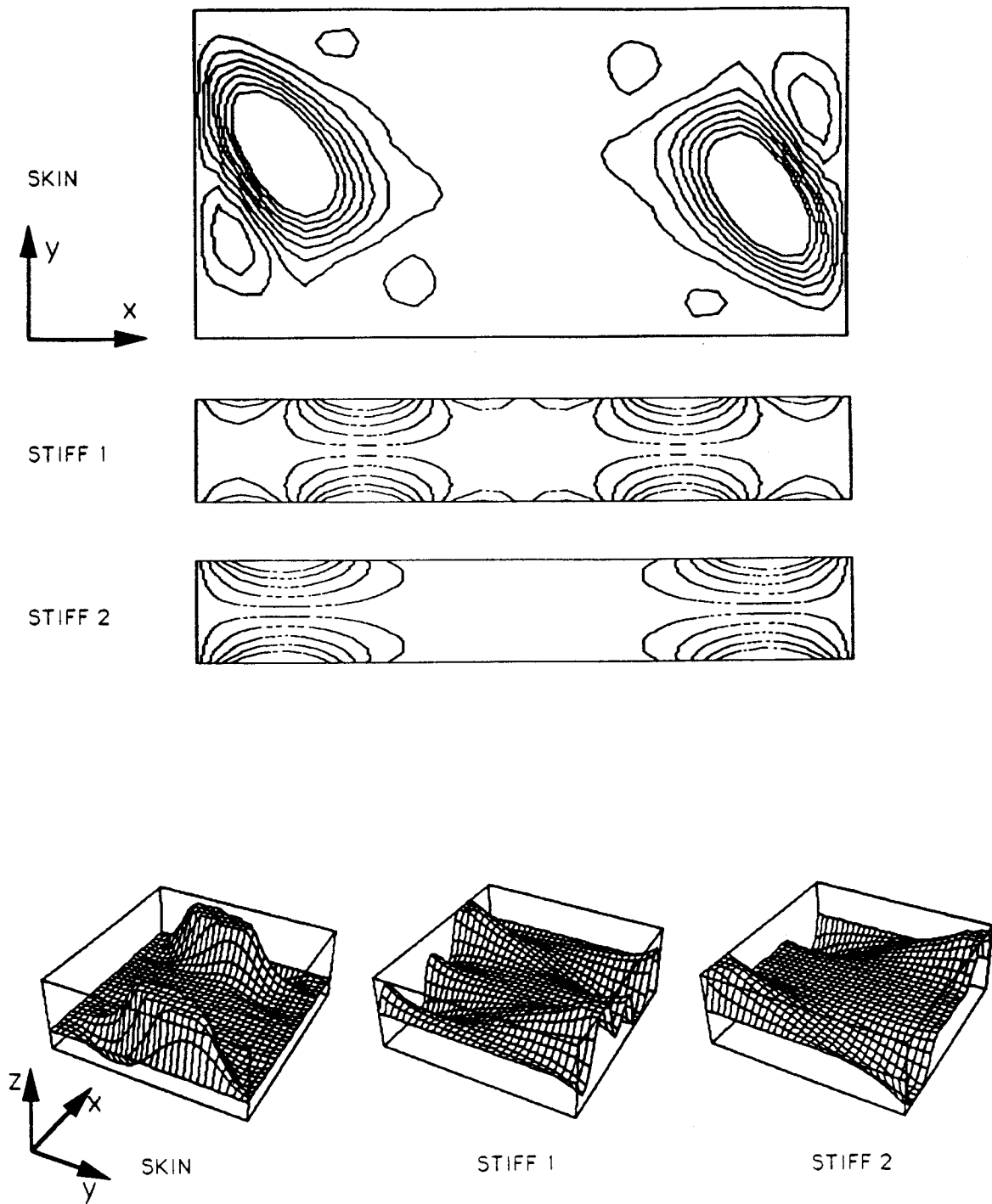
Figure 26. Mode Shapes for 4C1C0SxS (H = 1.205; $\tau_r = 0.133; \tau_s = 0.05$)
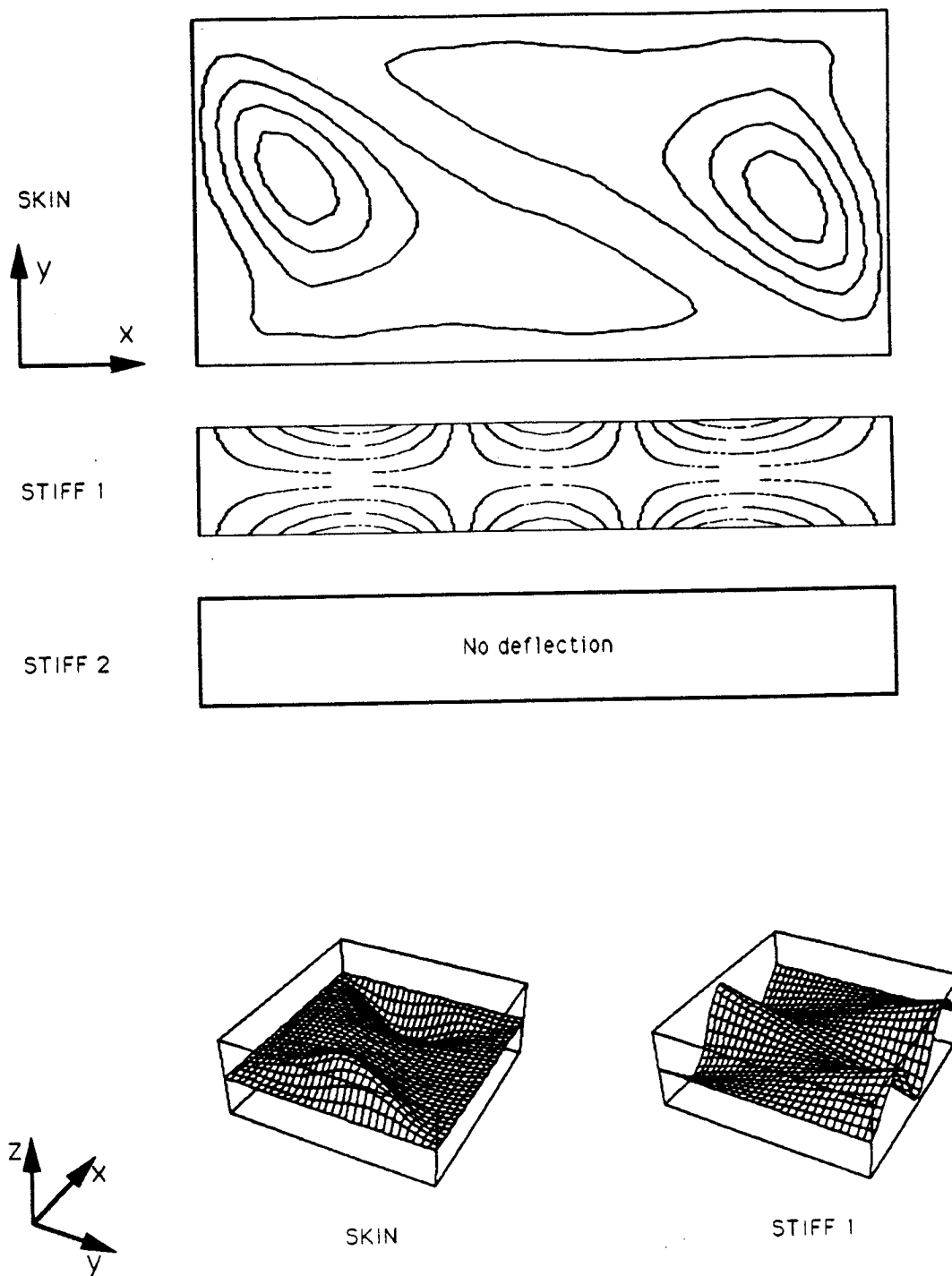
Figure 27.   Mode Shapes for 4C1C0SxM (H = 1.205; $\tau_r = 0.133; \tau_s = 0.177$)

SKIN

STIFF 1

STIFF 2

SKIN   STIFF 1   STIFF 2
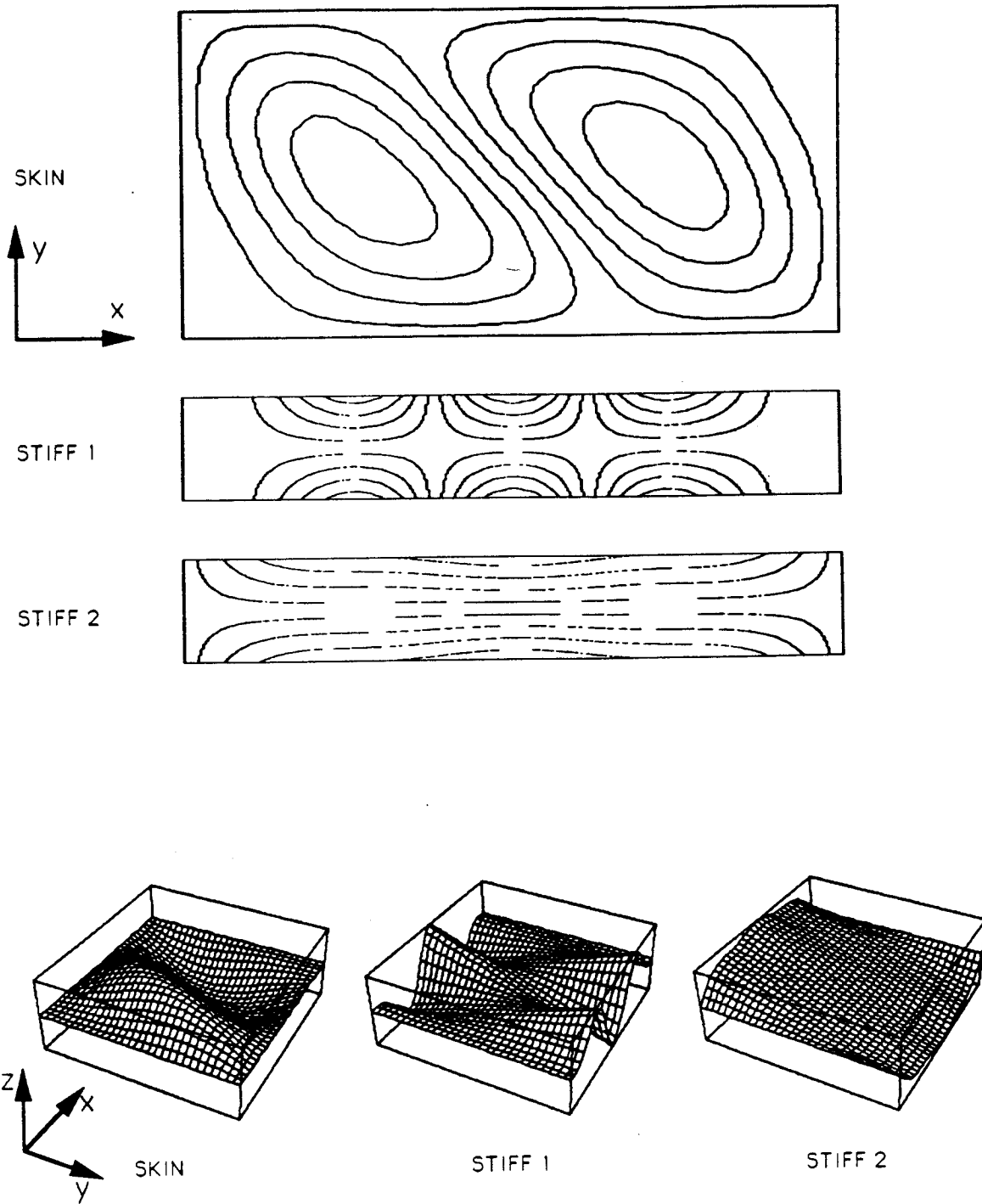
Figure 28.   Mode Shapes for 4C1C0SxB (H = 1.205; $\tau_r = 0.133; \tau_s = 0.721$)

SKIN

No deflection

STIFF 1

STIFF 2

No deflection

Figure 29. Mode Shapes for 4C1C0SxK (H = 1.205; $\tau_r = 0.133; \tau_t = 2.4$)

The buckling mode of panels under shear loading with increasing skin thickness is shown in Figures 26 through 28. All of them present local inter-stiffener buckling. For these three geometries the only stiffener under compression loading is stiffener 1. Stiffener 2 is under tensile loading but still presents nonzero deflection, this is due to the interaction between the skin and the stiffeners. Figure 29 shows the bucking mode of a panel having a very thick skin under shear loading. The load is too small to result in skin buckling but the load caried by stiffener 1 (compression load) buckles it. Stiffener 2, under tensile loading, does not participate in any deflection. For both thick skin panels (Figures 25 and 29) the stiffeners buckle in a six half wave mode. This is due to the length/height ratio of the stiffener. This would be the natural buckling mode of a clamped stiffener. When the skin buckles, the stiffener has more complicated deflections that clearly show the importance of the effect of the skin on the stiffener buckled mode.

4.3.1.2   Rotation of the skin along the stiffeners

It is important to know if the stiffeners, via their rotational effect, can significantly affect the mode shape of the skin. In order to answer this question, different configurations of panels were studied with the old method (LMM1) and the improved one (LMM2). When plotting the contours of the skin, no significant difference was found. When the plots of the rotation of the skin along the longitudinal axis of the stiffeners (where the rotational effect should be maximum) obtained by LMM1 and LMM2 were compared only some slight differences were detected. In order to illustrate this, the same 4C1CxS0 and 4C1C0Sx configurations shown in the previous section are considered in Figure 30 through Figure 35. The two thin lines represent the variation along the stiffener axis of the slope of the skin with respect to a direction perpendicular to the stiffener, as computed using LMM1. That is only including the constraint on the bending displacement of the stiffeners. The two thick lines show the slope of the skin along the stiffener axis η as computed using LMM2, including both the constraint on the bending displacement of the stiffeners and the constraint enforcing the continuity of rotation between the skin and the stiffeners. Dashed lines are used for the second

Figure 30. Skin Slope along the stiffeners for 4C1CxS0S (H = 3.614; $\tau_r = 0.113$; $\tau_t = 0.08$)

Figure 31. Skin Slope along the stiffeners for 4C1CxS0M (H = 3.614; $\tau_r = 0.113; \tau_r = 0.256$)

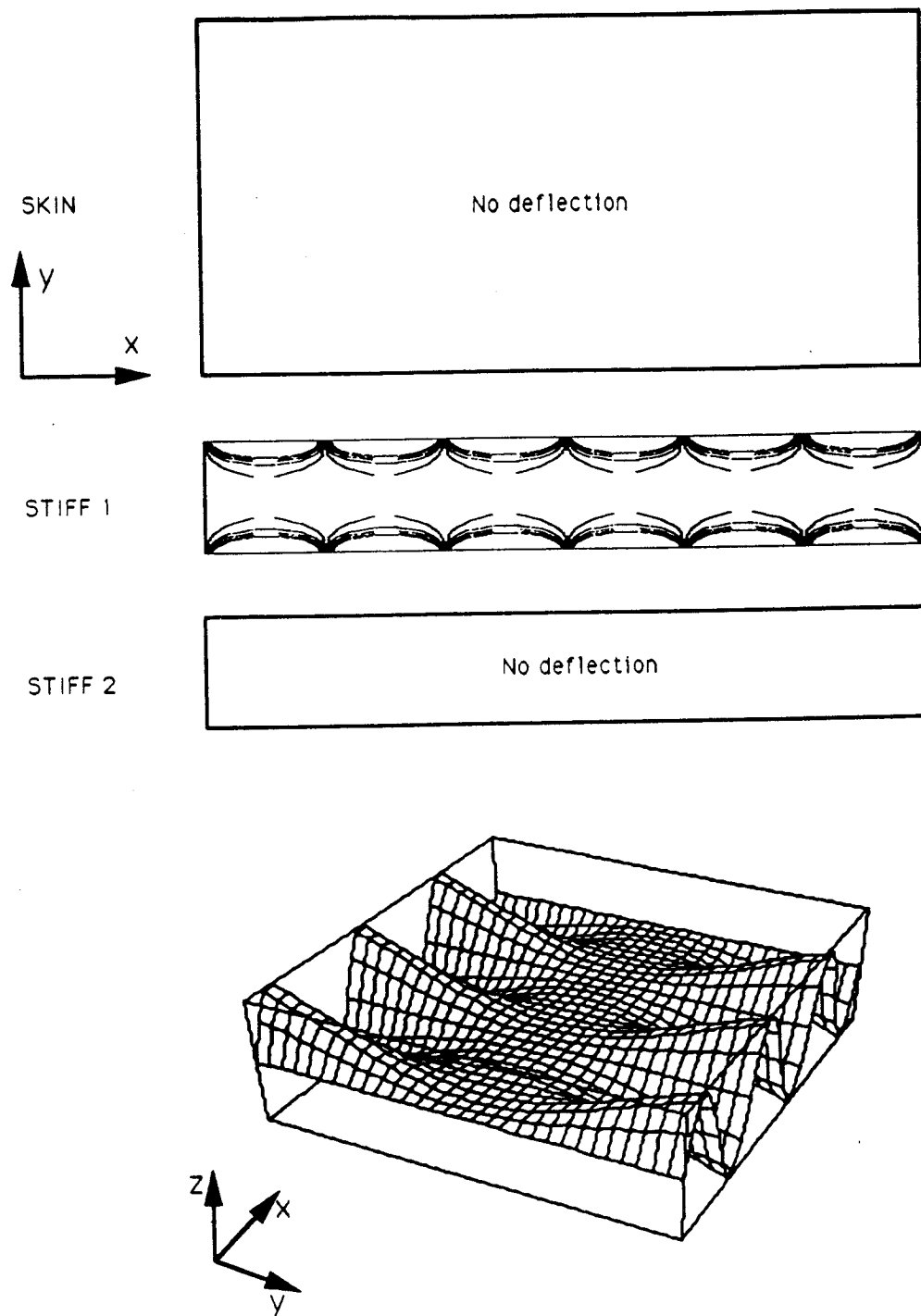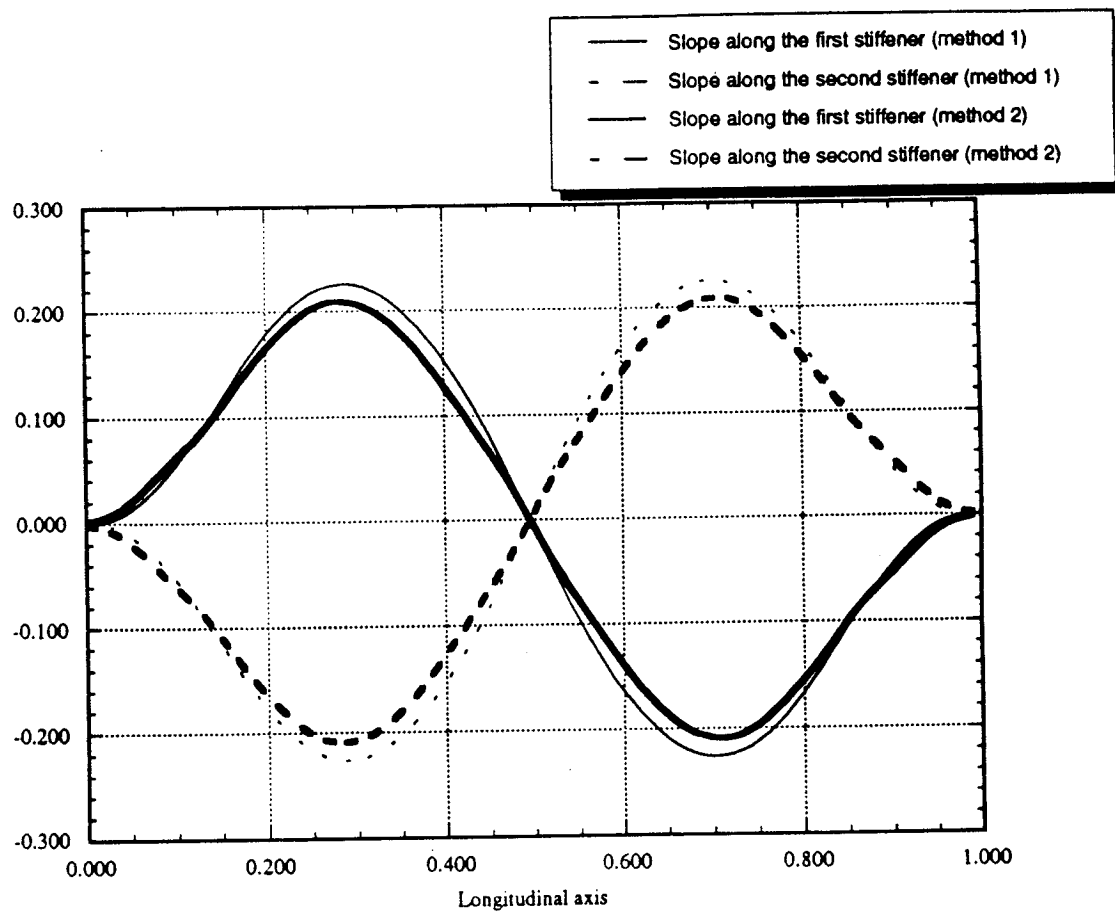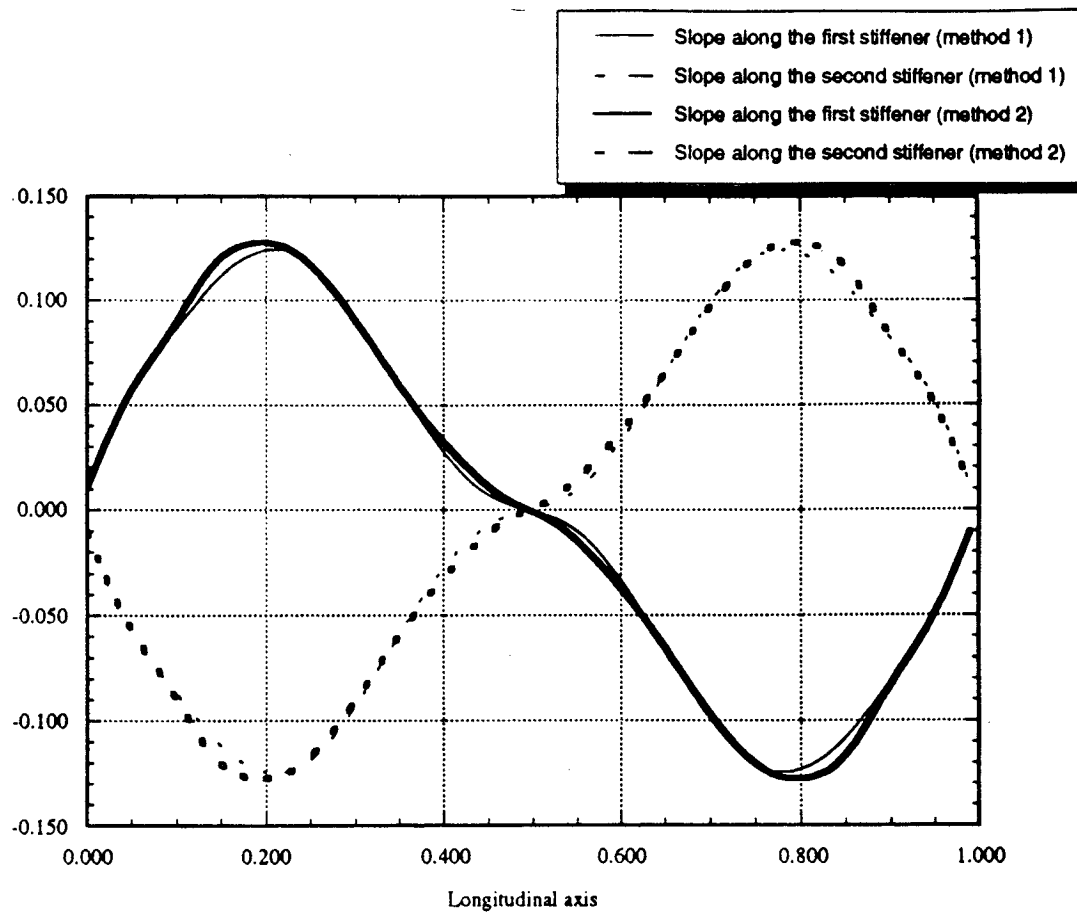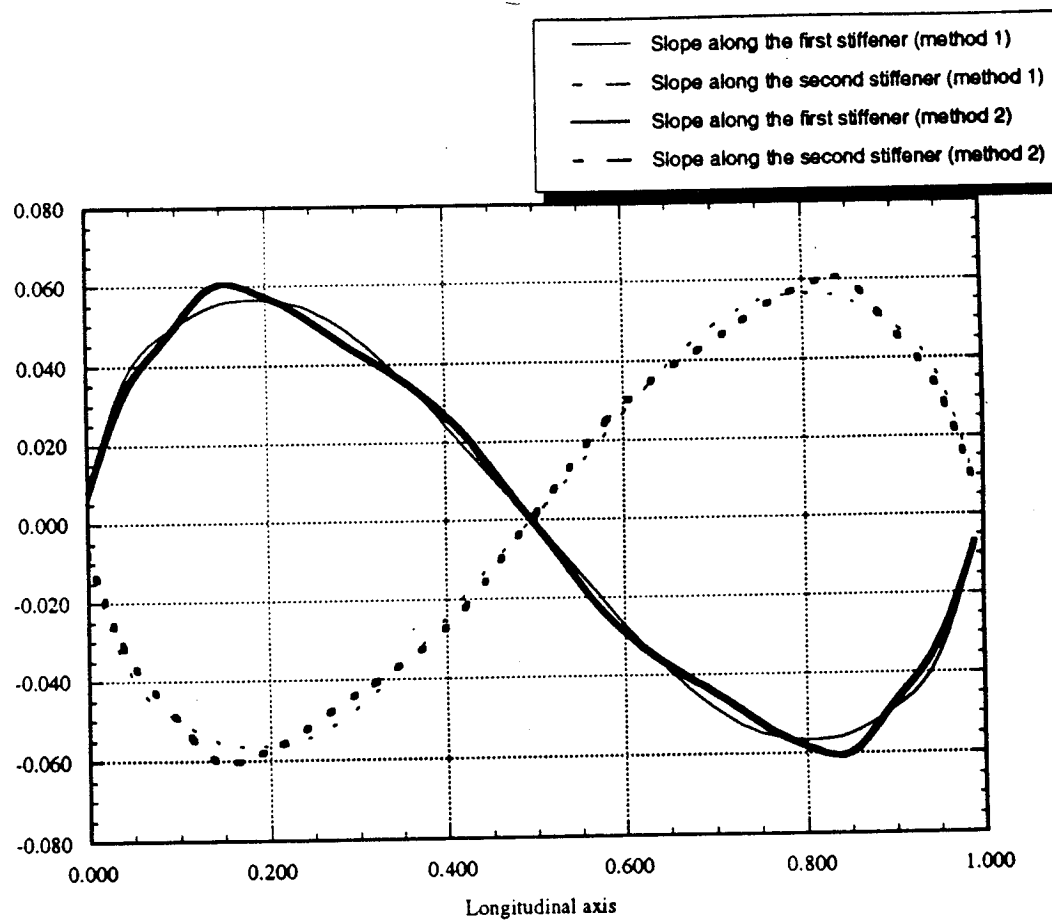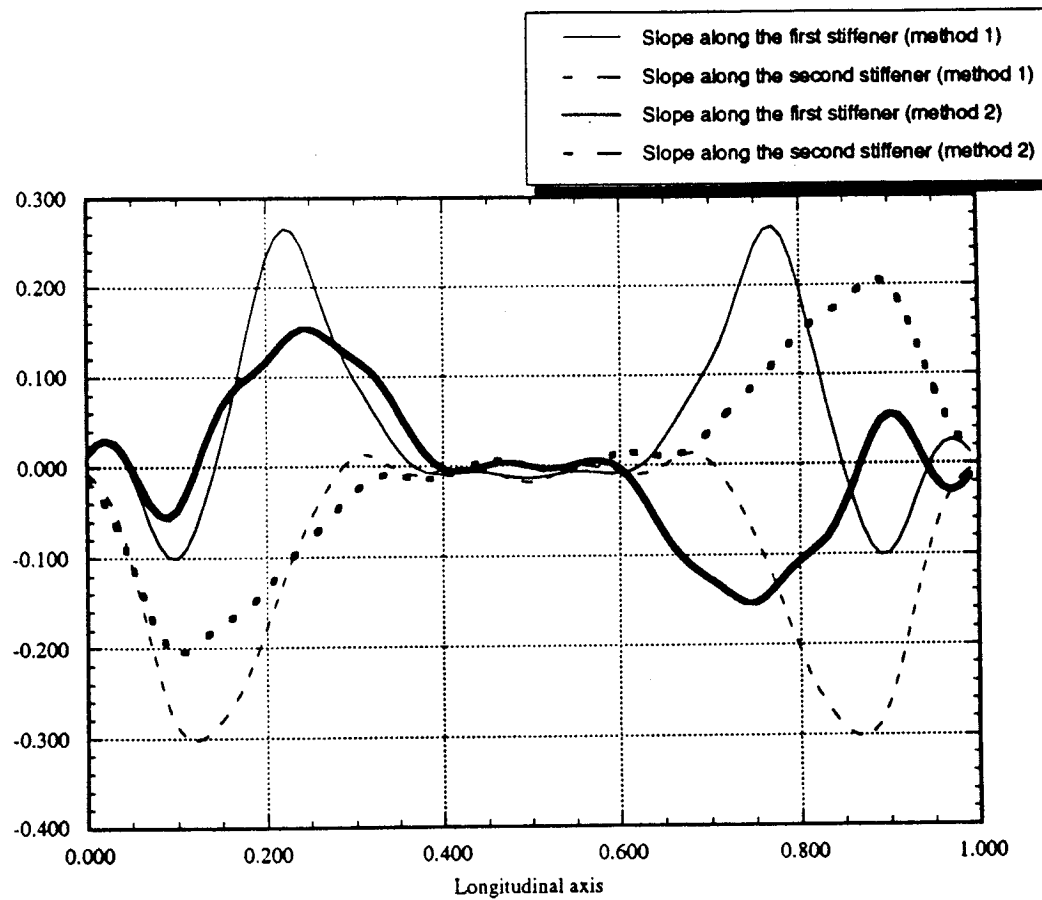Figure 32. Skin Slope along the stiffeners for 4C1CxS0B (H = 3.614; τ_r = 0.113; τ_t = 1.0)

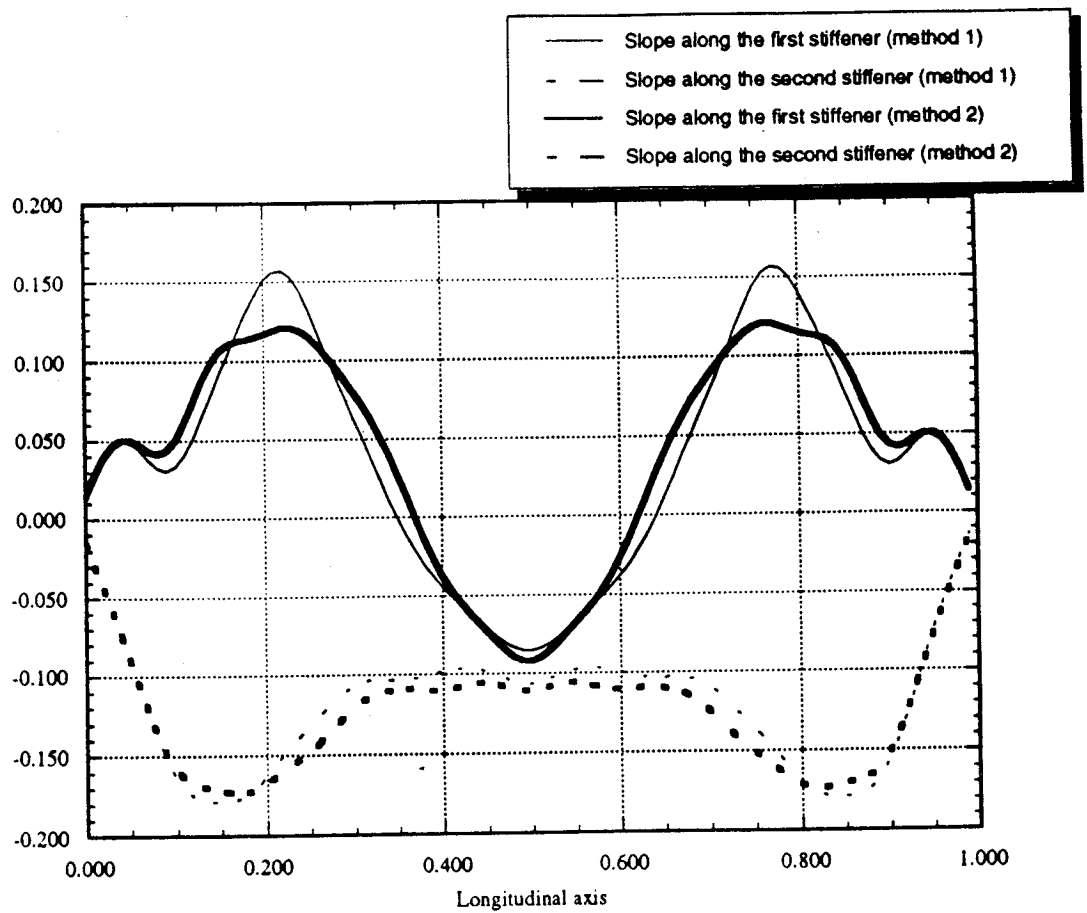Figure 33. Skin Slope along the stiffeners for 4C1C0SxS (H = 1.205; $\tau_r = 0.133$; $\tau_s = 0.05$)

Figure 34. Skin Slope along the stiffeners for 4C1C0SxM (H = 1.205; $\tau_r = 0.133; \tau_t = 0.177$)
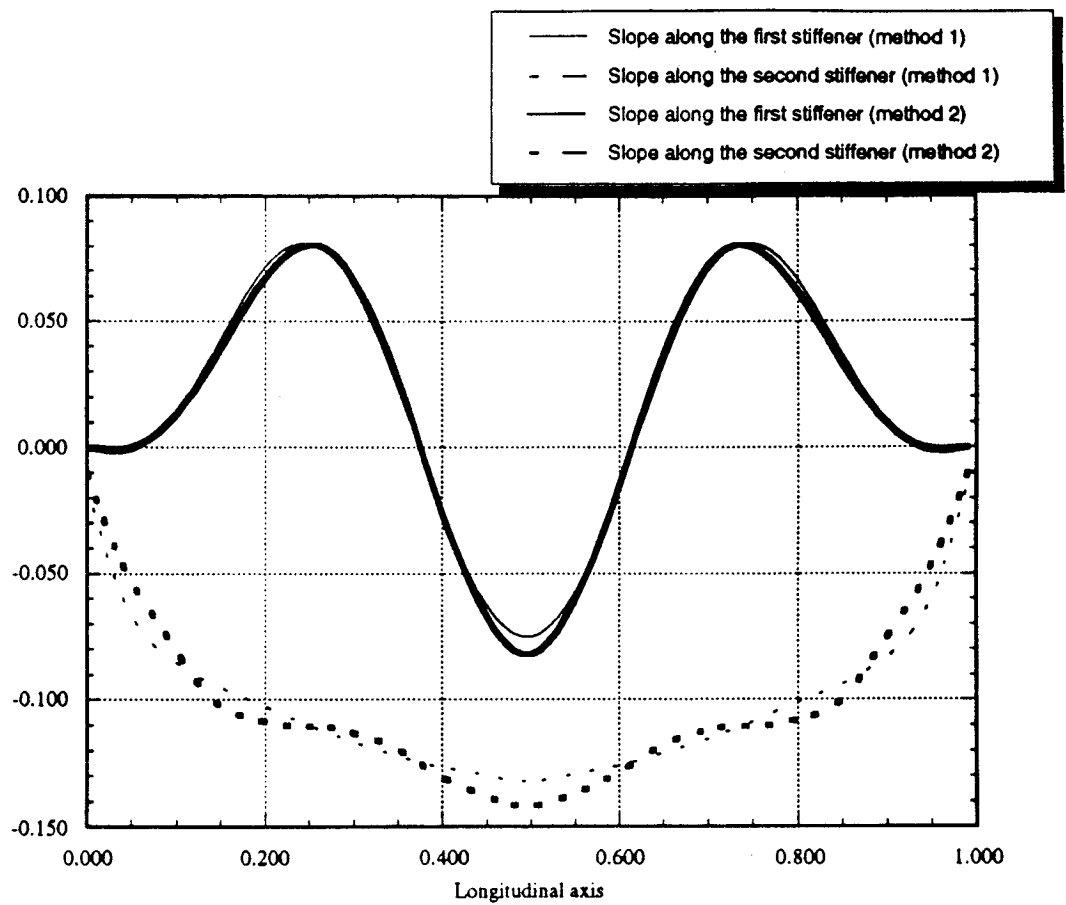
Figure 35. Skin Slope along the stiffeners for 4C1C0SxB (H = 1.205; $\tau_r = 0.133; \tau_r = 0.721$)

stiffener. As it appears on Figures 30 through 32, which corresponds to compression loading, only the thin skin buckles in a truly two half wave mode along the stiffener attachment line. For thicker skins, the mode is more complicated. Another interesting effect is shown in Figure 33 (thin skin, shear loading), where the slope of the skin along the stiffener, as calculated with LMM2, is anti-symmetric. However, for all cases, no major change in the skin buckling mode appears.

4.3.1.3 Comparison of the Buckling Mode Shapes with LMM1 and FEM

In the previous work[5], LMM1 was compared with the FEM (with the program CSM Testbed[11]) on a 3 cell cross stiffened panel (4C3CxS0). The test panel was 80 inches long by 28 inches high and had three cross-stiffened cells. The skin was 0.2 inches thick and its stacking sequence was $[-45/45/90/0]_s$. The stiffeners were made of unidirectional fibers and their thickness was 0.2 in. Four different stiffener heights of 0.5, 0.75, 1.0 and 1.25 were considered.

The new analysis was applied to the same test panels and their buckling mode shapes were drawn. The mode shapes obtained by the two methods (i.e., LMM1 and LMM2) are compared in Figure 36. The contours obtained with the FEM are shown in Figure 37 and compared with the present results. It appears that adding the second constraint to the analysis was a sensible improvement, since the prediction of the buckling modes for the cases (A) and (B) is now closer to the one obtained by the FEM.

4.3.2 The buckling load

Keeping the same panel configurations, the buckling loads obtained by the three methods are now compared in Table 3.

(A)   (A')

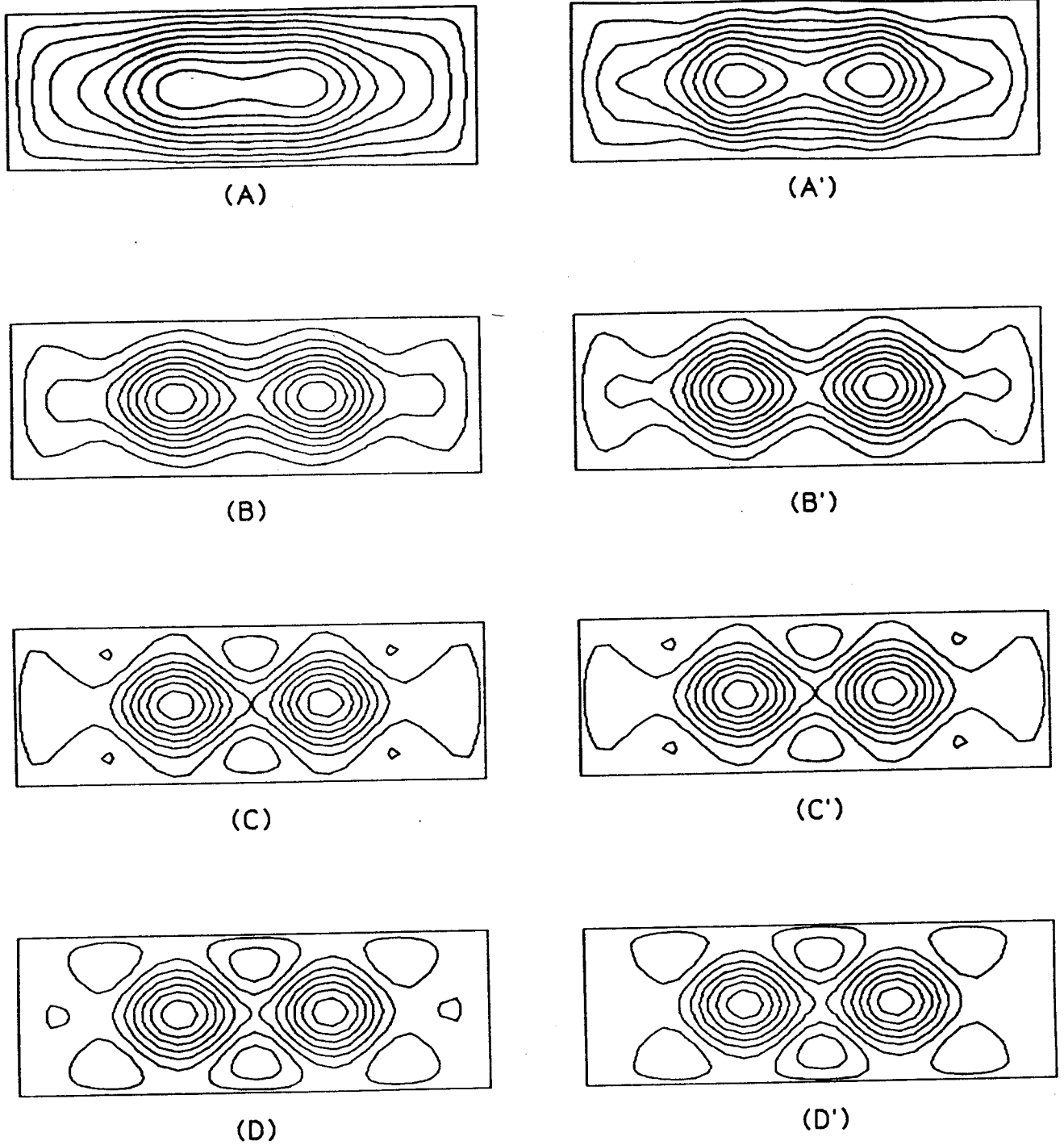(B)   (B')
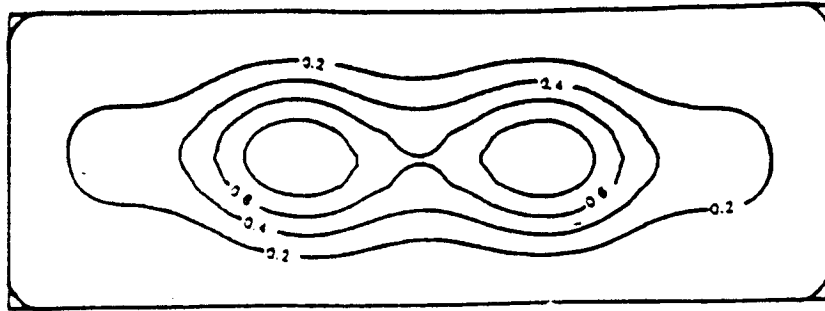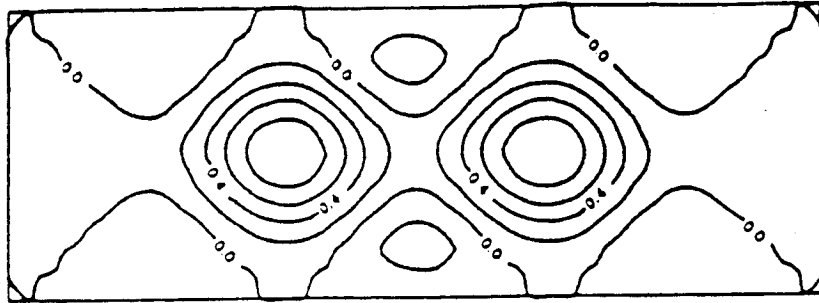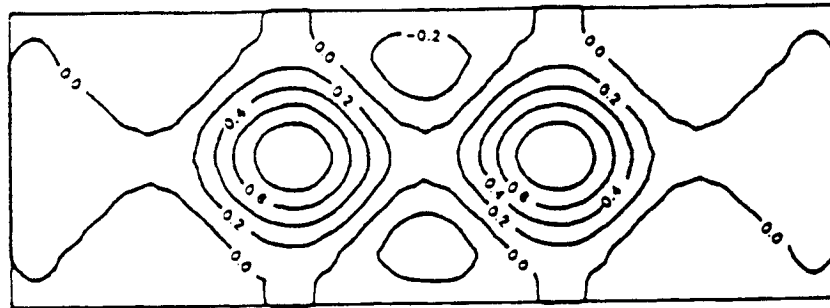
(C)   (C')

(D)   (D')

Figure 36.   Buckled Mode Shapes for geodesically Stiffened Panels, LMM1 and LMM2:   LMM1 A)H = 0.5,   B)H = 0.75,   C)H = 1.0,   D)H = 1.25   /   LMM2   A')H = 0.5,   B')H = 0.75, C')H = 1.0, D')H = 1.25
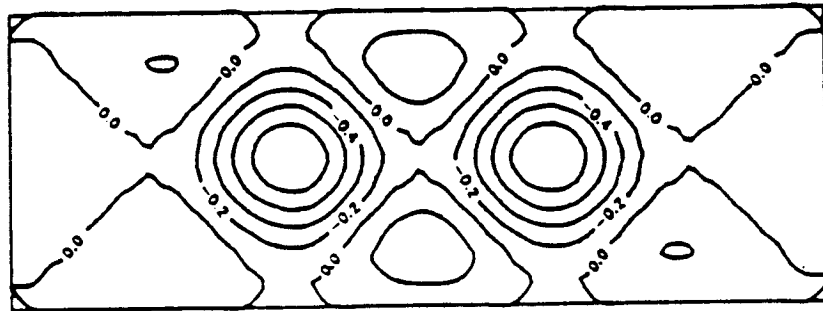
Figure 37. Buckled Mode Shapes for geodesically Stiffened Panels, FEM: A)H = 0.5 B)H = 0.75 C)H = 1.0 D)H = 1.25

C-2

Table 3. Comparison of Buckling Loads for 3-cell cross-stiffened panels, between LMM1, LMM2 and FEM.

Stiffener Height (in)	Panel Buckling Load (lbf/in)			$\dfrac{N_{LMM1}}{N_{FEM}}$	$\dfrac{N_{LMM2}}{N_{FEM}}$
	N_{FEM}	N_{LMM1}	N_{LMM2}		
0.5	573	342	471	0.596	0.823
0.75	705	613	649	0.870	0.921
1.0	748	708	727	0.946	0.972
1.25	783	743	770	0.949	0.983

As can be seen in the table (Table 3), the new method predicts buckling loads that are much closer to the finite element results than those from LMM1. This improvement confirms that the effect on the panel buckling load of the continuity of the rotations between the panel skin and the stiffeners can be significant.

4.4 Second Constraint and Buckling Load

The purpose of this section is to study the influence of the second constraint on the panel buckling load. Recall that the second constraint is used to ensure the continuity of the skin and stiffener rotations at the base of the stiffener along its axis η.

In order to study the second constraint, the following method has been used. Using an initial design and keeping the same cross-sectional area of the stiffeners ($H \times \tau_r = constant$) and the same skin thickness, the ratio H/τ_r is varied. The reason for keeping the same cross-sectional area for the stiffeners is to keep the same load distribution in the panel. It must be noted that a ratio H/τ_r smaller than 5 is not acceptable since the Classical Lamination Theory assumes the plate to be thin. The critical loads obtained by using the two levels of constraint are compared. The examples of studies on a 1 and 3 cell cross stiffened panel are shown in Figure 38 and Figure 39. These two

Figure 38. Influence of the second constraint on the panel buckling load of a 4C1CxS0 panel

Figure 39.   Influence of the second constraint on the panel buckling load of a 4C3CxS0 panel
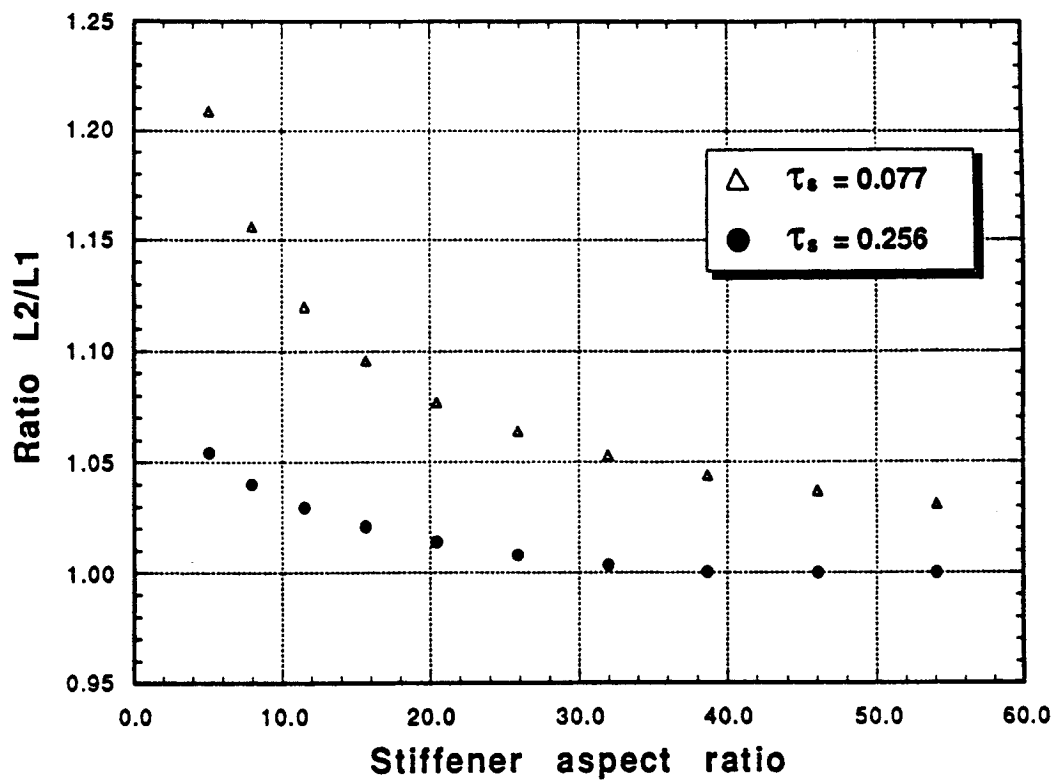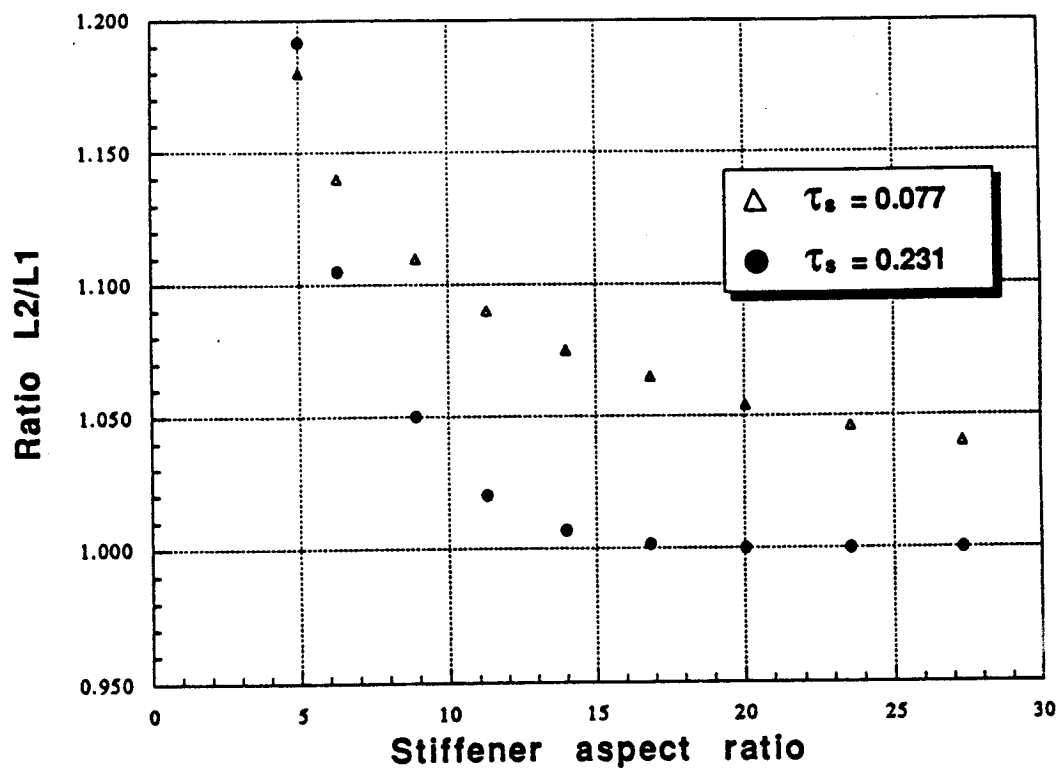
figures show the panel buckling load obtained by using LMM2 normalized by the panel buckling load obtained by LMM1 as a function of the stiffener aspect ratio, for two different skin thicknesses.

From both figures, it appears that the second constraint has a greater effect on thin skins than on thick skins regardless of the stiffener aspect ratio. Moreover, this effect decreases as the aspect ratio increases. As can be seen, in the case of thick skins, the effect of the the second constraint can be neglected for an aspect ratio larger than 20. However, for small aspect ratios and/or thin skins this constraint has to be taken into account. In addition, comparison of the results for 1 and 3 cell panels presented in Figures 38 and 39, respectively, indicates that increasing the number of stiffeners results in a larger rotational effect of low aspect ratio stiffeners for the thick skin. For an aspect ratio $H/\tau_r = 5$, the 4C4CxS0 panel (Figure 39), the rotational effect of the stiffeners corresponds to 20% of the buckling load of the panel, for any skin thickness.

The analysis reveals that the second constraint is directly related to the out-of-plane bending stiffnesses of the stiffeners. Thus, the thicker the stiffeners are, the more effective is the constraint on the continuity of rotation between the skin and the stiffener. The stiffeners behave as an infinitely large number of torsional springs placed on the skin. It is then obvious that these springs will have a larger effect on a thin skin than on a thick one.

From the first remarks about the out-of-plane bending stiffnesses of the stiffeners (D_{ij}), the concept of stiffeners made of a sandwich material is implied. A stiffener made up of a light but thick core and two skins would have the same in-plane properties (useful for its flexural contribution) and the same weight (or not very different) than a stiffener including only the two skins (glued together) but will have much higher out-of-plane bending stiffnesses. Taking again the example of the springs, a stiffener made with a sandwich composite material would increase the stiffness of the torsional springs.

To summarize this discussion about the rotational effect of the stiffeners on the panel buckling load, it can be concluded that this effect increases as the skin thickness and/or the stiffeners aspect ratio H/τ_r decreases (keeping the same cross sectional area).

5.0 Wing Rib Design

In this section a design study of wing ribs is conducted. The code written to check LMM2 is used to study new panel configurations that are likely to produce more efficient practical designs.

5.1 The Cell Distribution

As was mentioned, the parameters that control the the cell distribution can now be used as design variables. The aim is to find out if there is a nonuniform cell distribution that yields panels with higher buckling loads, or for a given load panels that are lighter.

In the first section, the sensitivity of the panel to the cell distribution is studied. Then, some optimum designs obtained by including the cell distribution in the design variables set are presented and compared to previous results.

5.1.1 Sensitivity to the cell distribution

As an example, a 3 cell cross stiffened panel under compression loading is considered. The width X of the center cell (see Figure 40) is varied and the buckling load and the weight are studied. When the code was used to find an optimum design using X as a design variable along with the skin and stiffener thicknesses and the stiffener height, the calculated optimum cell distribution corresponded to $X_{opt} = 13.66$. The effect of varying X from its optimal value on the panel buckling load and the panel weight, both normalized by their optimum values, is shown in Figure 40.

If X is increased from the optimum value, the weight decreases but the buckling load also decreases below the design load. It can be noted that the reason for the weight decrease is that its minimum is for 3 equally sized cells (i.e., X = 26.67). If X is decreased, the buckling load increases and the panel becomes safer with respect to buckling, but the objective function increases as well. This shows that the computed optimum is correct.

Another remark can be made. Increasing or decreasing X by 20% will only affect the weight by 0.3% and the buckling load by 4%. This has at least two implications. The first one is that some manufacturing errors are permitted in this range. The second is that the optimizer might have difficulties finding the actual optimum cell distribution, since the gradients of the objective function and constraint on the buckling load with respect to the cell width design variable will be small.

5.1.2 Optimization of the cell distribution

For the three geometries and three different loadings (compression, shear and combined), a group of panels was optimized by using constraint level 1 and including the cell distribution parameters in the set of design variables. It should be noted that since the second constraint is not active here,
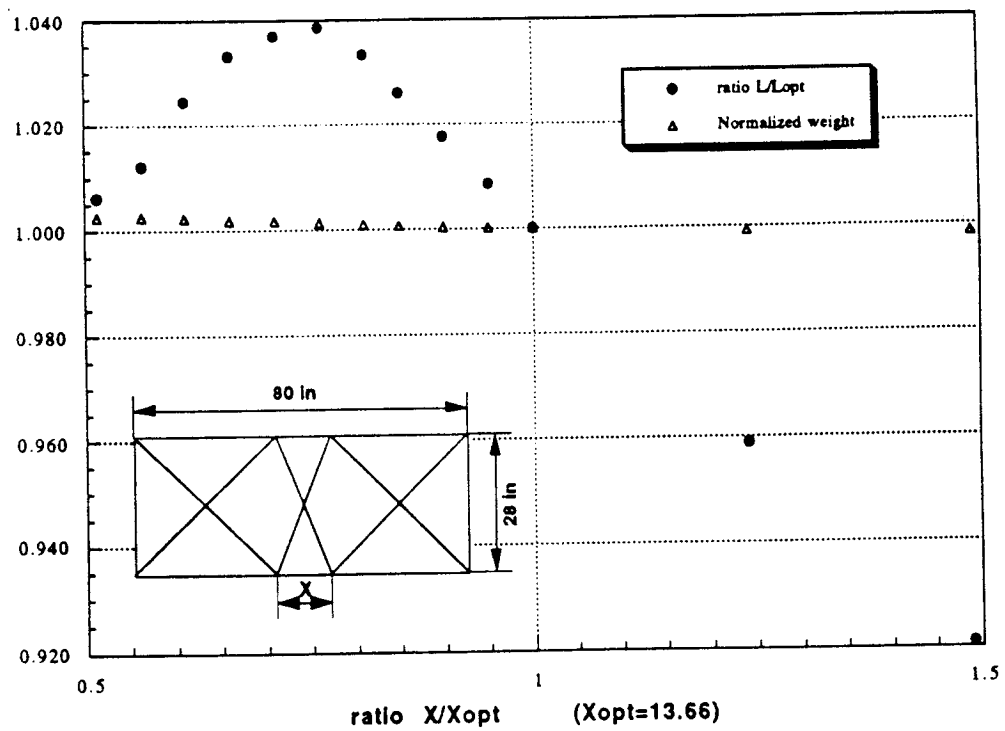
Wing Rib Design

Figure 40. Sensitivity to the cell distribution

the buckling of the stiffeners has to be studied separately as it is done in Ref.5. In fact for these design cases, LMM1 analysis is modified to include the cell width design variable. By comparing the optimum designs obtained with the modified analysis with the optimum designs found with LMM1 (with equally sized cells), it appears that a certain weight reduction can be achieved for panels having a small number of cells. However, when the the number of cells increases, the weight reduction diminishes, and is insignificant for an 8 cell panel. Since optimum design panels are those having a large number of cells for the three geometries, they also should have equally sized cells.

Some examples of the influence of cell distribution on the optimum weight for a cross stiffened panel are shown in Table 4. Panels $Nc = 3$, 4, and 5 are under an in-plane average compression loading of $N_y = 1000$ lbf/in. The eight cell panel is under a combined compression-shear average loading of $N_y = N_{xy} = 1000$ lbf/in. The weight reduction obtained by also including the cell distribution as a design variable is not significant and decreases as the number of cells increases.

Table 4. Variable Stiffening Arrangement For Optimum Cross Stiffened Panel under Compression loading

	NUMBER OF CELLS			
	Nc = 3	Nc = 4	Nc = 5	Nc = 8
Cross Stiffened Panel				
$DV(1)$ Skin Thickness (in)	0.215	0.199	0.171	0.125
$DV(2)$ Stiffener Height (in)	1.19	1.003	0.978	0.679
$DV(3)$ Stiffener Thickness (in)	0.127	0.092	0.096	0.122
$DV(4)$ Cell #1 width (in)	34.35	24.11	17.66	10.80
$DV(5)$ Cell #2 width (in)	11.30	15.87	14.62	10.38
$DV(6)$ Cell #3 width (in)	-	-	15.44	8.85
$DV(7)$ Cell #4 width (in)	-	-	-	9.96
$G(2)$ Skin Buckling	0.88E-3	0.1E-2	0.57E-5	0.2E-3
$G(3)$ Stiffener Buckling	-0.24	-0.2E-2	-0.48E-2	-0.97E-1
$G(4)$ Strength of Material	-0.93	-0.93	-0.93	-0.81
OBJ Panel Mass (lbm)	31.61	28.32	25.22	20.43
Panel Mass reduction (%)	-3.7	-2.8	-2.0	-1.0

$DV(i)$ = Design Variables, $G(i)$ = Constraints, OBJ = Objective Function
Constraints $G(i)$ are feasible when negative, range: $-1 \leq G(i) < \infty$
Skin laminate [-45/45/90/0]s, all plies equal thickness.

5.2 Stiffener Rotational Effect / Optimum Design

In the previous study[5], it was shown that the trend for the optimum design of geodesically stiffened panels is toward a large number of cells, a thinner skin, a lower aspect ratio of the stiffeners and a lower ratio τ_s/τ_r. Moreover, it was shown in the present work that the rotational effect of the stiffener is higher when the ratio τ_s/τ_r is lower. For these reasons it seems that for the optimum design of such panels, the second constraint should be included in the analysis. Nevertheless, for a large number of cells ($nc \geq 8$), the order of the system is large and, therefore, the computational time required to solve it is large. For this reason, for the study of the rotational effect of the stiffeners, only a small number of cells is considered. In fact, even with a small number of cells, a physical understanding of the nature of the interaction mechanism between the skin and stiffeners is possible.

5.2.1 Rotational effect and number of cells

In order to study the rotational effect of the stiffeners when the number of cells is varied, the following study was performed. The optimum designs obtained with LMM1 in the previous work were considered. Their buckling loads were computed with LMM2 and compared with the ones computed with LMM1. It appeared that the ratio N_{LMM2}/N_{LMM1} increases as the number of cells is increased. However, for these panels, N_{LMM2} never exceeded N_{LMM1} by more than 5%. An explanation is based on the fact that for these panels the stiffeners were too thin to have a significant bending effect; that is the ratio τ_s/τ_r was larger than 1.

ORIGINAL PAGE IS
OF POOR QUALITY

5.2.2 Lamination of the stiffener

As was previously mentioned, the rotational effect of the stiffener is directly related to its out-of-plane bending stiffnesses. Until now the code could not handle stiffeners as plates. With the modifications introduced in this work, it is now possible to investigate the effect of the laminate stacking sequence of the stiffeners on the panel buckling load. In practice, it is possible to build panels in which the stiffeners are laminated, if the additional effort to manufacture them is worthwhile.

In order to investigate the effect of stiffener stacking sequence on panel buckling, non-zero angle plies are placed on the two faces of the stiffener laminates. Nine basic configurations of a 1 cell cross stiffened panel were considered. For each of them the stiffeners were laminated in the sequence $[-\alpha/\alpha/0/0]_s$, and α was varied. The 9 basic configurations were divided in 3 main groups. The first group has a thick skin, the second one has a medium skin, and the third one has a thin skin. In each group, the cross-sectional area was kept constant (to keep the same load distribution), but the ratio τ_s/τ_r was varied.

Note that this analysis was derived for specially orthotropic stiffeners or stiffeners for which anisotropic effects due to bend-twist coupling terms can be neglected. The present stiffener laminated in the sequence $[-\alpha/\alpha/0/0]_s$ presents non-zero bending-twisting coupling terms D_{16}, D_{26}. Anisotropic effects exist but are negligible since these coupling terms are much smaller than the other bending stiffnesses D_{ij}.

The panel buckling load, normalized by $1000\ lbf/in$, as a function of α, the orientation of the stiffener outer plies, is shown in Figures 41 through 43 for three aspect ratios of the stiffener ($H/\tau_r = 5$, 16 and 32).

Figure 41. Influence of the orientation of the outer plies of the stiffeners on the buckling load of the panel: Thick skin ($H\tau_r = 0.4084$, $\tau_s = 0.256$)
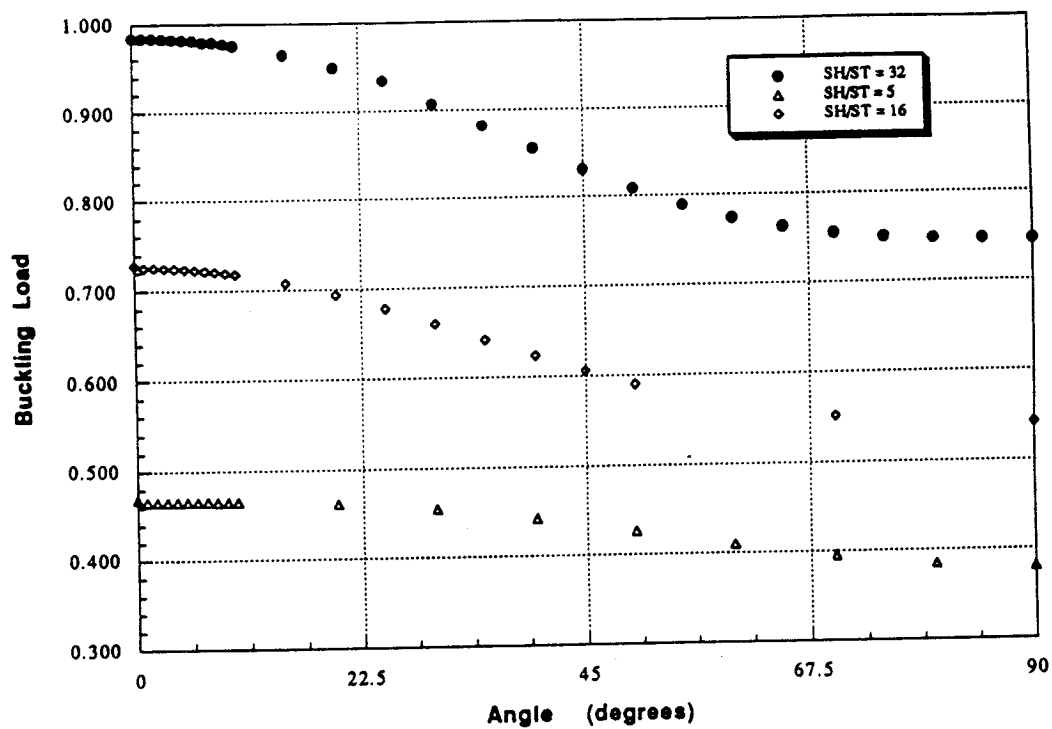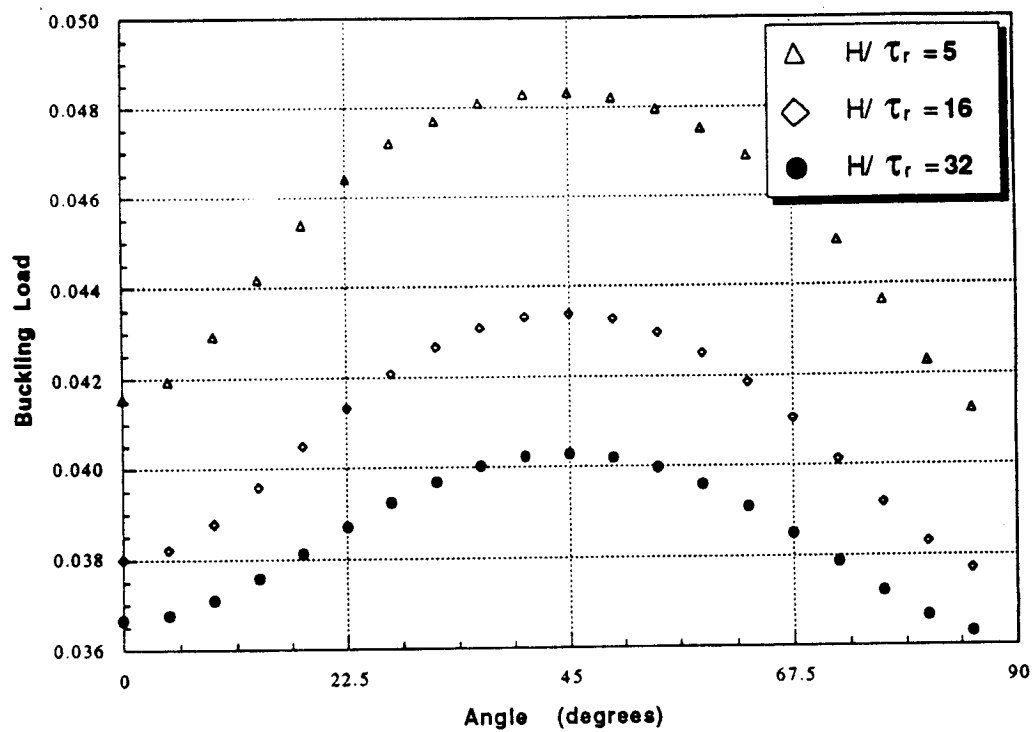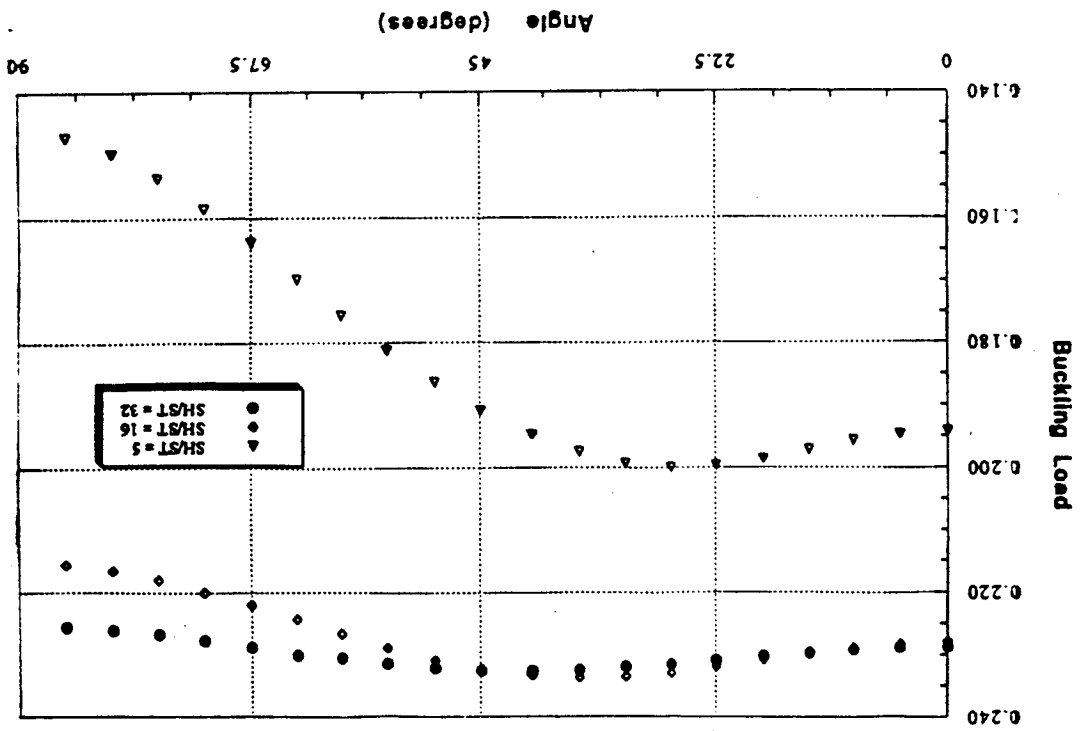
Figure 42. Influence of the orientation of the outer plies of the stiffeners on the buckling load of the panel: Thin skin ($H\tau_r = 0.4084$, $\tau_s = 0.08$)

5.2.2.1 Thick skin

From Figure 41 it appears that the best stiffener laminate, for the case of thick skin, is unidirectional fibers. In this case, the gain in out-of-plane bending stiffness for the stiffeners in not sufficient in comparison to the loss in the in-plane extension stiffnesses to maintain the buckling load at its initial level. Moreover, the higher the aspect ratio of the stiffener is, the higher is its buckling load, for any angle α.

5.2.2.2 Thin skin

For thin skin panels, see Figure 42, the effect of the stiffener aspect ratio is reversed; it appears that as the aspect ratio of a stiffener is increased, the buckling load of the panel decreases. By reducing the stiffener height but increasing its thickness, stiffener in-plane bending stiffnesses are reduced but out-of-plane bending stiffnesses are increased. In this example, for the same stiffener cross sectional area, higher buckling load panels are obtained when the stiffener aspect ratio is lower, or when the stiffener out-of-plane bending stiffnesses are higher. Since the rotational effect of the stiffener is related to its out-of-plane bending stiffnesses it appears that for thin skins this effect is important. Moreover, it is verified that the angle at which the buckling load is the largest (for any aspect ratio) is $\alpha = 45^o$.

5.2.2.3 Intermediate case

The figure for the buckling load of intermediate thickness panels (Figure 43) shows two interesting facts. First, for each aspect ratio, there is an angle α for which the buckling load is maximum. This shows that for these cases both the flexural and rotational effects are important, and that by judi-

ciously laminating the stiffeners it is possible to achieve gains in the buckling load of the panel for the same panel weight. For example, with $\alpha = 34°$ the buckling load of the panel for which $H/\tau_r = 16$ is increased by more than 5%. Secondly, the two curves on the top of the graph show that a turning point between the two first cases (Thick and Thin Skins) is reached here; the buckling load is not increased by doubling the aspect ratio of the stiffeners when $H/\tau_r = 16$ but it remains the same.

5.2.2.4 Practical aspect of laminated stiffeners

In the previous study, it was shown that the trend for the optimum design of geodesically stiffened panels is toward a large number of cells. It can be noted in the optimum designs obtained by Phillips[5] that the ratio τ_s/τ_r decreases when the number of cells is increased.

From what was presented, some non-zero angle plies in the stiffeners can increase the panel buckling load significantly when the stiffener thickness is large compared to the skin thickness. For this reason, it might be interesting to include lamination of the stiffeners in the optimum design of the panels. The analysis now permits it.

5.2.3 Sandwich stiffeners

Another way of increasing the rotational effect of the stiffeners is to use stiffeners made of sandwich material. In order to give some motivation to future work, the following study is presented. The 4C8C3S3 optimum design obtained by Phillips[5] with LMM1 is considered. The stiffener thickness is $\tau_r = 0.12\ in$. The panel buckling load computed with LMM1 is $N_{l\ MM1} = 1000\ lbf/in$ and with LMM2 is $N_{LMM2} = 1049\ lbf/in$, for a combined compression/shear loading ($N^{shear} = N^{Compression}$). Now, the following sandwich stiffener is tried. The thickness of the core is $0.12\ in$ and its density is 10 times less than the composite one; on each face of the core a skin of thickness $0.06\ in$ is placed.

This results in increasing the bending stiffnesses by a factor of 7 while keeping the same in-plane extension stiffnesses, and only increasing the weight of the whole panel by 2%. The effect of the new stiffeners on the panel buckling load is quite interesting; the buckling load is now $N_{LMM2}^{new} = 1123$ lbf/in, which is 7.1 % higher than N_{LMM2} and 12.3 % higher than N_{LMM1}.

5.2.4 Partial Conclusion

From this study it appears that the second constraint could be neglected during the optimization of geodesically stiffened panels having unidirectional fiber stiffeners and low number of cells, since their rotational effect on the panel buckling load is not significant. However, when the number of cells is increased the rotational effect of the stiffeners is significant and should be taken into account for any analysis. Moreover, the rotational effect of the stiffeners can be significantly increased by using laminated stiffeners and even more by using sandwich stiffeners.

Thick sandwich laminates are prone to adverse transverse shear effects. Since the use of sandwich stiffeners can significantly increase the buckling load of the panel due to their important rotational effect, it may be necessary to modify the analysis to include the shear effect in the stiffeners and further study the use of sandwich stiffeners for wing rib panels.

5.3   Horizontal stiffeners

By placing stiffeners at locations where the buckled skin deflection is large, it is possible to increase the panel buckling load. Starting from the buckled mode shapes obtained in Ref. 5, it can be seen that deflection maximums are aligned horizontally. For this reason it is surmised that horizontal stiffeners should be a good way to obtain more highly stable panels. Because of the assumption that

strain along the X axis of the panel is zero (i.e., $\varepsilon_x = 0$), it is further assumed that these horizontal stiffeners are not loaded in the prebuckling mode. In order to study panels with horizontal stiffeners, the design code Pansys was modified.

5.3.1 Improvement of the panel buckling load

In order to show the effect of horizontal stiffeners on the panel buckling load the following examples are given. The two optimum 3 cell cross stiffened panels for compression and shear loadings of 1000 lbf/in obtained in Ref. 5 are considered. For both panels the critical load is computed considering one, three, and seven additional horizontal stiffeners placed respectively at (1/2), (1/4,1/2,3/4), (1/8,1/4,3/8,1/2,5/8,3/4,7/8) of the panel height. The critical loads for these panels are indicated in the following table (Table 5).

Table 5. Critical load of two LMM1 optimum three cell cross-stiffened panels reinforced by horizontal stiffeners.

Horizontal stiffener location (b)	Panel Buckling Load (lbf/in)	
	Compression	Shear
1/2	1520	1350
1/4,1/2,3/4	1780	1790
1/8,1/4,3/8,1/2,5/8,3/4,7/8	2040	2310

It appears that the panel critical load can be improved by a significant amount by adding horizontal stiffeners.

5.3.2 Horizontal stiffeners and panel weight minimization

Since placing horizontal stiffeners permits a significant panel buckling load increase for some design loads, it is possible to design lighter panels than the ones obtained before. Two three cell cross-

stiffened panels reinforced by one and three additional horizontal stiffeners placed at (1/2) and (1/4,1/2,3/4) of the panel height were optimized for the loadings 1000 *lbf/in* in compression and shear. Their weight is compared with optimum three cell cross-stiffened panels for the same loadings obtained in the previous study[5]. In Ref. 5 the weight corresponding to the optimum panels was 32.81*lbs* for compression loading 1000 *lbf/in*, and 23.29*lbs* for shear loading 1000 *lbf/in*. The weight reduction obtained by reinforcing with horizontal stiffeners is given in the following table (Table 6).

Table 6. **Weight reduction obtained for optimum 3 cell cross-stiffened panels including one or three horizontal stiffeners.**

| Horizontal stiffener location (b)	Weight reduction (%)	
	Compression	Shear
1/2	−15%	−12%
1/4,1/2,3/4	−19%	−20%

5.3.3 Remarks

In order to increase the panel buckling load, horizontal stiffeners should be placed where the skin deflection is likely to be the highest. As an example the buckled mode shapes of the same 3 cell cross stiffened panel with horizontal stiffeners under compression loading are given in -- Figure id 'HOR1' unknown --. Starting from configuration (A), a horizontal stiffener is placed at $y = b/2$ where the deflection of the buckled skin is highest. Then the buckled skin shape is given by (B). Two more stiffeners are then added at $y = b/4$ and $y = 3b/4$ and the buckled skin mode is shown by (C).

For thin skin cross-stiffened panels with one horizontal stiffener at $y = b/2$, the buckling load should be the same as the one obtained for a diagonally stiffened panel with the same number of cells and thicknesses but with only half the height. This is true only for thin skin panels where the buckled
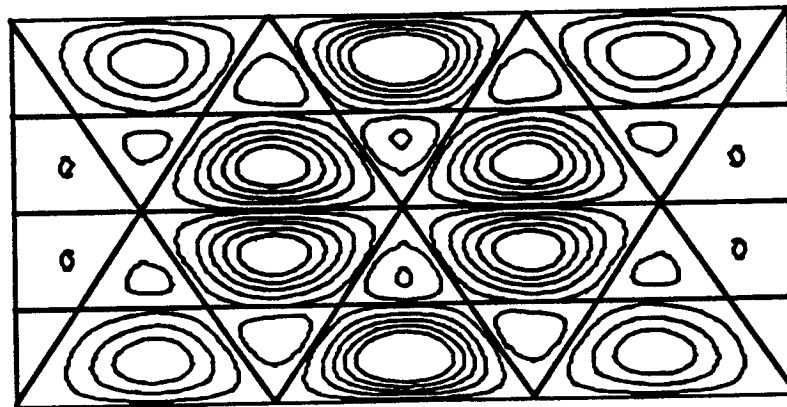
skin deflection along the horizontal stiffener is zero and the stiffener almost corresponds to a simple support edge. This was verified successfully for various numbers of cells.

Wing Rib Design
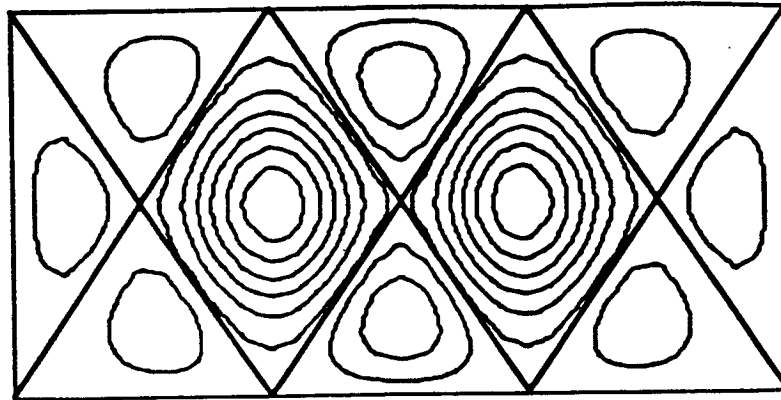
(A)
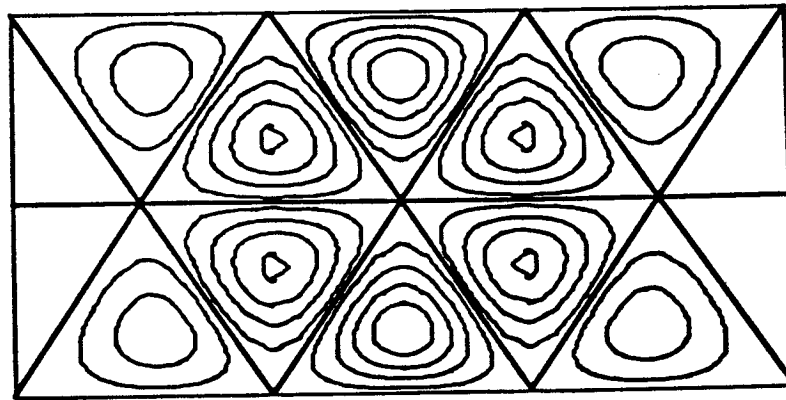
(B)

(C)

Figure 44.   Buckled mode shapes for optimum three cell cross-stiffened panels with (A) 0, (B) 1, (C) 3 horizontal stiffeners: Compression loading (1000 lbf/in)

6.0 Concluding Remarks

The aim of the present work was to improve an energy method used for the prediction of the buckling load of geodesically stiffened wing rib panels that are designed for use in large transport type aircraft. An analysis developed previously for geodesically stiffened panels assumed the stiffeners to be beam like elements and was only taking into account the flexural contribution of the stiffeners in a direction perpendicular to the skin via the Lagrange Multiplier Technique. For certain panel geometries comparison of the buckling load obtained by this analysis with the one calculated via Finite Elements showed significant discrepancy. The lack of stiffener out-of-plane bending stiffnesses (out-of-plane with respect to a plate like stiffener), which was ignored in the previous analysis, was thought to be responsible for this difference. One of the major goals of this study was to improve the capabilities of the previous analysis and design code to account for the out-of-plane bending stiffness of the stiffeners. Modifications were also sought to extend the analysis capability to handle variable geodesic grid density.

The wing rib was modeled as a rectangular panel 80 inches wide by 28 inches high. The boundary conditions were idealized to be such that the edges were simply supported and the in-plane extensional deformation in the width direction was zero. The stiffeners were considered to be symmetrically laminated and balanced plates. The grid of stiffeners was symmetrically located on both sides of a balanced, symmetrically laminated skin.

The Lagrange Multiplier Method (LMM) was modified by including the energy terms associated with the out-of-plane bending stiffness of the stiffeners. The stiffeners are assumed to be plate elements attached to the skin by using constraints (in addition to the ones that ensure the equality of the out-of-plane deflection of the skin to the stiffener deflection) in the LMM analysis. These additional constraints ensured the continuity of rotations between the skin and the stiffeners along the stiffener attachment line. The result is an analysis tool that permits the prediction of the buckling load and mode shape of a geodesically stiffened panel with orthotropic plate-like stiffeners. For the panel designs two constraints are considered, panel buckling (which includes the interactive skin stiffener buckling) and material strength failure. This new analysis routine was combined with ADS, a numerical optimizer package, in order to obtain a tool for designing wing ribs.

The results of the new LMM buckling analysis (LMM2) was compared with the results of a Finite Element Method. Results indicate that LMM2 generates a much better panel buckling prediction than LMM1 for low aspect ratios of the stiffeners The effect of stiffener out-of-plane bending stiffness was studied and it was shown that it should not be neglected in the case of thin skin and/or low aspect ratio of the stiffeners.

The analysis tool was then used to investigate new possibilities for designing optimum wing ribs. It was shown that a variable cell distribution can produce lighter designs than the uniform cell panels for a low number of cells but is less and less efficient as the number of cells is increased. The study of the effect of out-of-plane bending stiffness of the stiffeners lead to the concept of sandwich laminated stiffeners that are likely to increase the buckling load of the panel. The code was modified to maximize the buckling load of the panel by using the ply orientations and thicknesses of both the skin and the stiffeners as design variables. The panel weight minimization, using the skin ply thicknesses as design variables was shown to yield designs with significant weight reductions. It was also shown that horizontal stiffeners can improve the buckling response significantly without much weight penalty.

Concluding Remarks

7.0 References

1   Freeman, W.T., "History and Future of Large Composite Structure Fabrication," Review for Virginia Tech Center for Composite Materials and Structures, February 8, 1989.

2   Barrie, R., Biggers, S., Campion, M., and O'Brien, D., "Design Methods and Considerations for Composite Transport A/C Primary Structure," Lockheed-Georgia Company Presentation, April 1, 1987.

3   Swanson, G.D., "Structural Efficiency Study of Composite Wing Rib Structures," MS Thesis, Virginia Polytechnic Institute and State University, November 1987.

4   Gendron, G., and Gurdal, Z., "Optimal Design of Geodesically Stiffened Composite Cylindrical Shells," proceedings of AIAA/ASME/ASCE/AHS/ASC 33rd Structures, Structural Dynamics and Material Conference, April 13-15, Dallas, Texas, 1992.

5   Phillips, J.L., and Gurdal, Z., "Structural Analysis and Optimum Design of Geodesically Stiffened Composite Panels," CCMS-90-05, Virginia Polytechnic Institute, July 1990.

6   Vanderplaasts, G.N., "ADS - A Fortran Program for Automated Design Synthesis - Version 1.10," NASA, Grant NAG1-567, 1985.

7   Whitney, J.M., "Structural Analysis of Laminated Anisotropic Plates," Technomic Publishing, Inc., 1987.

8   Rivello, R.M. "Theory and Analysis of Flight Structures," McGraw-Hill Book Co., 1969.

9   Stoll, F., and Gurdal, Z., "Stiffener Failure Constraints for the Design of Isogrid-stiffened Panel s," ESM internal report, Virginia Polytechnic Institute, February 1991.

10   "IMSL MATH/LIBRARY FORTRAN Subroutines for Mathematical Applications," IMSL, Inc., 1987.

11   "Computational Structural Mechanics Testbed User's Manual," NASA Technical Memorandum No. 100644, October 1989.

BIBLIOGRAPHIC DATA SHEET	1. Report No. VPI-E-92-21; CCMS-92-24	2.	3. Recipient's Accession No.
4. Title and Subtitle Structural Analysis and Design of Geodesically Stiffened Composite Panels with Variable Stiffener Distribution			5. Report Date August 1992
			6.
7. Author(s) B. Grall and Z. Gürdal			8. Performing Organization Rept. No. VPI-E-92-21, CCMS-92-24
9. Performing Organization Name and Address Virginia Polytechnic Institute and State University Department of Engineering Science and Mechanics Blacksburg, VA 24061-0219			10. Project/Task/Work Unit No.
			11. Contract/Grant No. NAG-1-643
12. Sponsoring Organization Name and Address Aircraft Structures Branch NASA Langley Research Center Hampton, VA 23665-5225			13. Type of Report & Period Covered Sept. 90 - May 92
			14.

15. Supplementary Notes

16. Abstract

A computationally efficient analysis is developed to predict the critical buckling loads of geodesically stiffened composite panels under in-plane loading. The analysis procedure accounts for the contribution of the in-plane extensional and out-of-plane bending stiffnesses of the stiffeners through the use of Lagrange multipliers technique in an energy method solution. The analysis is used to understand the effect of various stiffener deformation modes on the buckling load and to determine skin deformation patterns of geodesically stiffened panels under various load combinations.

The analysis routines are then coupled with the numerical optimizer ADS to create a package for the design of minimum-mass stiffened panels, subject to constraints on buckling of the panel assembly and material strength failure. Material failure in the skin and stiffeners is estimated using a maximum strain criterion. The design variables that can be used for optimization include thickness of the skin laminate, stiffener thickness and height, and positions of straight stiffeners. Applied loads are uniaxial compression, pure shear, and combined compression-shear.

17. Key Words and Document Analysis.   17a. Descriptors

Optimization, composite panels, geodesic stiffeners, grid stiffeners, buckling of stiffened panels, design of panels, plates

17b. Identifiers/Open-Ended Terms

17c. COSATI Field/Group

18. Availability Statement	19. Security Class (This Report) UNCLASSIFIED	21. No. of Pages 121
	20. Security Class (This Page UNCLASSIFIED	22. Price